Assessment, Planning and Control of Voltage and Reactive Power in Active Distribution Networks

by

Hany Essa Zidan Farag

A thesis
presented to the University of Waterloo
in fulfillment of the
thesis requirement for the degree of
Doctor of Philosophy
in
Electrical and Computer Engineering

Waterloo, Ontario, Canada, 2013

AUTHOR'S DECLARATION

I hereby declare that I am the sole author of this thesis. This is a true copy of the thesis, including any required final revisions, as accepted by my examiners.

I understand that my thesis may be made electronically available to the public.

Abstract

Driven by economic, technical and environmental factors, the energy sector is currently undergoing a profound paradigm shift towards a smarter grid setup. Increased intake of Distributed and Renewable Generation (DG) units is one of the Smart Grid (SG) pillars that will lead to numerous advantages among which lower electricity losses, increased reliability and reduced greenhouse gas emissions are the most salient.

The increase of DG units' penetration will cause changes to the characteristics of distribution networks from being passive with unidirectional power flow towards Active Distribution Networks (ADNs) with multi-direction power flow. However, such changes in the current distribution systems structure and design will halt the seamless DG integration due to various technical issues that may arise. Voltage and reactive power control is one of the most significant issues that limit increasing DG penetration into distribution systems. On the other hand, the term microgrid has been created to be the building block of ADNs. A microgrid should be able to operate in two modes of operation, grid-connected or islanded. The successful implementation of the microgrid concept demands a proper definition of the regulations governing its integration in distribution systems. In order to define such regulations, an accurate evaluation of the benefits that microgrids will bring to customers and utilities is needed. Therefore, there is a need for careful consideration of microgrids in the assessment, operation, planning and design aspects of ADNs. Moreover, SG offers new digital technologies to be combined with the existing utility grids to substantially improve the overall efficiency and reliability of the network. Advanced network monitoring, two ways communication acts and intelligent control methods represent the main features of SG. Thus it is required to properly apply these features to facilitate a seamless integration of DG units in ADNs considering microgrids.

Motivated by voltage and reactive power control issues in ADNs, the concept of microgrids, and SG technologies, three consequent stages are presented in this thesis. In the first stage, the issues of voltage and reactive power control in traditional distribution systems are addressed and assessed in order to shed the light on the potential conflicts that are expected with high DG penetration. A simple, yet efficient and generic three phase power flow algorithm is developed to facilitate the assessment. The results show that utility voltage and reactive power control devices can no longer use conventional control techniques and there is a necessity for the evolution of voltage and reactive power control from traditional to smart control schemes. Furthermore, a probabilistic approach for assessing the impacts of voltage and reactive

power constraints on the probability of successful operation of islanded microgrids and its impacts on the anticipated improvement in the system and customer reliability indices is developed. The assessment approach takes into account: 1) the stochastic nature of DG units and loads variability, 2) the special philosophy of operation for islanded microgrids, 3) the different configurations of microgrids in ADNs, and 4) the microgrids dynamic stability. The results show that voltage and reactive power aspects cannot be excluded from the assessment of islanded microgrids successful operation.

The assessment studies described in the first stage should be followed by new voltage and reactive power planning approaches that take into account the characteristics of ADNs and the successful operation of islanded microgrids. Feeders shunt capacitors are the main reactive power sources in distribution networks that are typically planned to be located or reallocated in order to provide voltage support and reduce the energy losses. Thus, in the second stage, the problem of capacitor planning in distribution network has been reformulated to consider microgrids in islanded mode. The genetic algorithm technique (GA) is utilized to solve the new formulation. The simulation results show that the new formulation for the problem of capacitor planning will facilitate a successful implementation of ADNs considering islanded microgrids.

In the third stage, the SG technologies are applied to construct a two ways communication-based distributed control that has the capability to provide proper voltage and reactive power control in ADNs. The proposed control scheme is defined according to the concept of multiagent technology, where each voltage and reactive power control device or DG unit is considered as a control agent. An intelligent Belief-Desire-Intention (BDI) model is proposed for the interior structure of each control agent. The Foundation for Intelligent Physical Agents (FIPA) performatives are used as communication acts between the control agents. First, the distributed control scheme is applied for voltage regulation in distribution feeders at which load tap changer (LTC) or step voltage regulators are installed at the begging of the feeder. In this case, the proposed control aims to modify the local estimation of the line drop compensation circuit via communication. Second, the control scheme is modified to take into consideration the case of multiple feeders having a substation LTC and unbalanced load diversity. To verify the effectiveness and robustness of the proposed control structure, a multiagent simulation model is proposed. The simulation results show that distributed control structure has the capability to mitigate the interferences between DG units and utility voltage and reactive power control devices.

Acknowledgements

Praise be to Allah, the Cherisher and Sustainer of the worlds, whose countless bounties enabled me to accomplish this thesis successfully.

I then would like to express my sincere gratitude to my supervisor Prof. Ehab El-Saadany for his professional guidance, valuable advice, continual support and encouragement.

Lastly, I would like to thank my parents and my wife for their understanding, continuous support, and encouragement.

Dedication

This thesis is dedicated to my wife, my son, my daughter and my parents.

Table of Contents

List of Figures

List of Tables

List of Acronyms

ACL	Agent Communication Language
ADN	Active Distribution Network
ANSI	American National Standard Institute
BCBV	Branch-Current to Bus-Voltage Matrix
BDI	Belief-Desire-Intention
BIBC	Bus-Injection to Branch-Current Matrix
CPU	Central Processing Unit
CRC	Cyclic Redundancy Check
CNP	Contract Net Protocol
CFP	Call for Proposal
DB	Dead Band
DFIG	Doubly-Fed Induction Generator
DG	Distributed Generation
DNO	Distribution Network Operator
DMS	Distribution Management System
DM	Decision Maker
DRIS	Distributed Resources Islanded Systems
EMS	Energy Management System
EPS	Electric Power System
FSC	Feeder Switched Capacitor
FIPA	Foundation of Intelligent Physical Agent
GA	Genetic Algorithm
GLR	Generation Load Ratio

IEEE	Institute of Electric and Electronic Engineers
IID	Island Interconnection Device
JADE	Java Agent Development Framework
KSE	Knowledge Sharing Effort
KIF	Knowledge Interchange Format
KQML	Knowledge Query and Manipulation Language
LDC	Line Drop Compensator
LTC	Load Tap Changer
LVR	Line Voltage Regulator
MAS	Multiagent Systems
MCS	Monte-Carlo Simulation
MGCC	Microgrid Central Controller
MT	Micro-Turbine
MPPT	Maximum Power Point Tracking
PDF	Probability Density Function
PI	Proportional Integrator
PV	Voltage controlled bus/ Photovoltaic
PQ	Constant Active and Reactive Power controlled bus
PLC	Power Line Communication
SAIDI	System Average Interruption Duration Index
SAIFI	System Average Interruption Frequency Index
SCADA	System Control and Data Acquisition
SE	State Estimator
SG	Smart Grid

S_G	Synchronous Generator
SC	Shunt Capacitor
SCDF	Sector Customer Damage Function
SL	Semantic Language
SVR	Step Voltage Regulator

Chapter 1
Introduction

1.1 Background

Smart grid (SG) means the modernization and automation of the current power delivery systems, both transmission and distribution. SG initiatives are based on several pillars; among which improving system reliability and efficiency, as well as promoting a high penetration level of renewable and distributed generation (DG), are the most salient [1-3] .

From a design perspective, SG aims to incorporate elements of traditional and advanced power engineering, sophisticated sensing and monitoring technology, information technology and two ways communication links. SG technology aims to provide better grid performance and support a wide array of additional services to customers and the economy. Therefore, many of the current research and development activities related to SG share a common vision as to desired functionality. Some of these desired functionalities include [2]:

1- Accommodating a wide variety of DG and storage options
2- Increasing system reliability and improving power quality
3- Optimizing asset utilization
4- Self-healing
5- Minimizing operations and maintenance expenses

On the other hand, conventional distribution systems are characterized by their passive structure with unidirectional power flow. However, in response to the SG initiatives, distribution systems are expected to undergo major transition towards being Active Distribution Networks (ADNs) [4]. Those ADNs are characterized by high DG penetration along with multi-direction power flow. ADNs will be distributed into set of layers; these layers are based on the microgrid concept [5]. A typical microgrid configuration is formed of a cluster of loads and DG units connected to a distribution network [6].

Facilitating a high penetration of a wide variety of DG units as well as the successful implementation of the microgrid concept in ADNs will bring multiple benefits to customers and utilities [7]. Such benefits include maintaining the customer's service in emergency situations, voltage support, loss reduction, transmission systems and distribution systems capacity release and improved utility system reliability [8, 9].

1.2 Research Motivations

Distribution systems are generally designed to operate without any imbedded generation whether on the distribution system or at the customer site. Therefore, the introduction of DG units on distribution systems can significantly impact the flow of power and voltage conditions at customer and utility equipment. Based on the distribution system operating characteristics and the DG characteristics, these impacts may be positive by supporting the system or negative by causing technical issues. Positive impacts include voltage support, loss reduction and capacity release. Yet, to achieve these positive impacts, DG units must be reliable, dispatchable, and of a proper locations and size. As most of the DG units are not utility owned and are characterized by being intermittent energy sources like wind and solar, there is no guarantee that these positive impacts are fully achieved. In contrast, with the high degree of complexity and uncertainty that are accompanied with the integration of DG units, conventional voltage and reactive power control strategies in distribution systems are expected to face numerous challenges. When DG units are interconnected to a distribution system, they can significantly change the system voltage profile and interfere with the conventional local control strategies of load tap changers (LTC), step voltage regulators (SVR) and shunt capacitors (SC). This interference leads to overvoltage, undervoltage, increasing in system losses and excessive wear and tear of voltage control devices. Therefore, to mitigate voltage and reactive power control issues and facilitate a seamless integration for large penetration of distributed generation, DG units need to coordinate with traditional utility voltage and reactive power control devices.

On the other hand, the concept of microgrids will be able to offer multiple benefits. The most salient among those benefits, is improving the microgrids customers' reliability by transition to islanded mode during outage of the upstream network. Therefore, one of the most important issues in SG is to quantitatively evaluate the possibility of successful implementation of microgrids. Assessing the implementation in a proper way will give rise to an accurate evaluation of the benefits that microgrids may bring to customers, DG owners and utilities. Therefore, there is a need for an accurate evaluation of the probability of successful operation of islanded microgrids and consequently its effects on individual and system reliability. Such evaluation needs to take into account the special features and philosophy of operation during islanded condition. Voltage and reactive power constraints are part of the operational characteristics that cannot be excluded from the evaluation of the successful operation of islanded microgrids.

Once an accurate assessment of voltage and reactive power aspects in ADNs considering islanded microgrids is done, new planning and control schemes that take into account the structure of ADNs, microgrids concept and SG technologies need to be defined.

1.3 Research Objectives

This research aims broadly to develop new assessment, planning and control algorithms for voltage and reactive power in ADNs with high penetration of DG units considering islanded microgrids and SG technologies.

To be fulfilled, the above objective needs to evolve and builds upon a number of tasks. Key tasks are:

1- Development of a generic three-phase power flow algorithm for ADNs.

2- Using the developed power flow algorithm to accurately assess the impacts of high penetration of DG units on the conventional voltage and reactive power control schemes in distribution systems.

3- Development of an accurate algorithm for assessing the successful implementation of islanded microgrids considering the impacts of voltage and reactive power constraints.

4- Development of a new capacitor planning algorithm in ADNs considering islanded microgrids.

5- Development of new control schemes for voltage and reactive power in ADNs using SG technologies.

1.4 Thesis Layout

The remainder of this thesis is structured as follows:

Chapter 2 presents the state-of-the-art and a critical literature survey on voltage and reactive power in ADNs.

Chapter 3 is divided into two phases. In the first phase, a comprehensive three phase power flow algorithm for active distribution systems is presented. Using the power flow algorithm, the second phase addresses the drawbacks of conventional voltage and reactive power control schemes and the necessities of their evolution in future distribution systems.

Chapter 4 presents a probabilistic technique to evaluate the impacts of voltage and reactive power constraints on the success of islanded microgrids taking the special features and operational characteristics of both dispatchable and non-dispatchable DG units into consideration. Supply

adequacy and reliability indices have been modified to account for the effect of voltage and reactive power constraints in the assessment of islanded microgrids.

Chapter 5 presents a probabilistic formulation for the problem of capacitor planning in ADNs taking into considering the special features and philosophy of operations of islanded microgrids combined with the probabilistic models of DG units and the load variability.

Chapter 6 presents an active control scheme that has the capability to provide proper voltage regulation in active distribution feeders. The proposed control scheme formulates the problem of voltage regulation based on a distributed or multi-agent control structure, where each device is considered as a control agent.

Chapter 7 is an extension for the multiagent control scheme presented in chapter 6 to: 1) mitigate the interference between LTC and DG operation and guarantee a proper voltage regulation in all operating conditions, 2) relieve the stress on tap operation of LTC, 3) avoid unnecessary DG active power curtailment, and 4) prevent the increase in system losses due to the reactive power control of DG units, in case of multiple feeders having a substation LTC, unbalanced load diversity and high DG penetration.

Chapter 8 presents the thesis summary, contributions, and directions for future work.

Chapter 2

Background and Literature Survey

2.1 Introduction

This chapter presents a brief background on the problem of voltage and reactive power control in ADNs.

2.2 Conventional Voltage and Reactive Power Control in Distribution Systems

Voltage and reactive power control in distribution systems is very important. Improper voltage regulation can cause many problems for end users. Sustained overvoltages or undervoltages can cause unsafe or less-efficient equipment operation and tripping of sensitive loads. While undervoltages can cause overheating of induction motors, overvoltages can cause equipment damage or failure and higher no-load losses in transformers. Further, improper control of reactive power flow can cause significant increase in the total system losses. In contrast, a proper voltage regulation will improve the voltage profile, reduce system losses, and increase system efficiency [10].

Delivering voltage to customers within a suitable range is one of the utility's core responsibilities. Most regulatory bodies and most utilities in North America follow the ANSI voltage standards (ANSI C84.1-1995) which have been revised in 2006 [11]. ANSI C84.1 standard defines three voltage classes: low voltage (1 kV or less), medium voltage (greater than 1 kV and less than 100 kV), and high voltage HV (greater than or equal to 100 kV). Within these classes, ANSI defines two ranges of voltage; they are:

1- *Range A —Normal Operating Conditions*; most service voltages are within these limits, and utilities should design electric systems to provide service voltages within these limits.
2- *Range B — Upnormal Operating Conditions;* these requirements are more relaxed than Range A limits. According to the standard: "Although such conditions are a part of practical operations, they shall be limited in extent, frequency, and duration. When they occur, corrective measures shall be undertaken within a reasonable time to improve voltages to meet *Range A* requirements." Utilization equipment should give acceptable performance when operating within the *Range B* utilization limits, according to the standard.

For low voltage systems, ANSI C84.1 gives limits of -5% and +5% for *Range A* and -8.3% and +5.8% for *Range B*. For medium voltage systems, ANSI C84.1 gives tighter limits for *Ranges A* and *B*. *Range A* is –2.5 to +5%, and *Range B* is –5 to +5.8%.

In general, there are three different types of control devices that are widely employed to control voltage magnitude and reactive power flow in a distribution system; those are LTC, SVR and SC [12]. LTC is installed at the main transformer to keep the secondary voltage close to a specified value under changing load conditions. SC is installed at the secondary bus of the substation to adjust the reactive power flow through the main transformer to keep the system operating at a high power factor. On each feeder, there are also some SVR and SC that have been commonly employed to provide voltage regulation and reactive power compensation to improve the voltage profile along the feeder.

The purpose of voltage and reactive power control in distribution systems is to find an optimal scheduling of LTC and SVR positions and SC status in order to achieve certain objective functions and practical constraints such as:

1- Keep the voltage profile at all load nodes within a certain specified limit.
2- Minimize the total daily power loss.
3- Take into consideration the distribution feeder capacity limits.
4- Limit the total switching operations of LTC, SVR and SC due to the limit of their life expectation.

Many conventional control schemes have been reported for voltage and reactive power control in a distribution system. As shown in Figure 2.1, these control schemes could be classified as follows:

2.2.1 Local voltage and reactive power control

Local control is mainly based on local information. The control set-points alteration for voltage and reactive power control devices is very rare, on seasonal basis for example [12, 13]. The main advantage of the local control is that it is autonomous i.e. receiving local information from the system, somehow selecting an action to perform, and performing that action. Therefore, it has the flexibility to respond to load fluctuations. The main drawbacks of the local control are that the power losses are not guaranteed to be minimized and a proper coordination among devices is required to avoid conflicts [10]. Some of the traditional local control techniques for voltage and reactive power control devices are listed as follows:

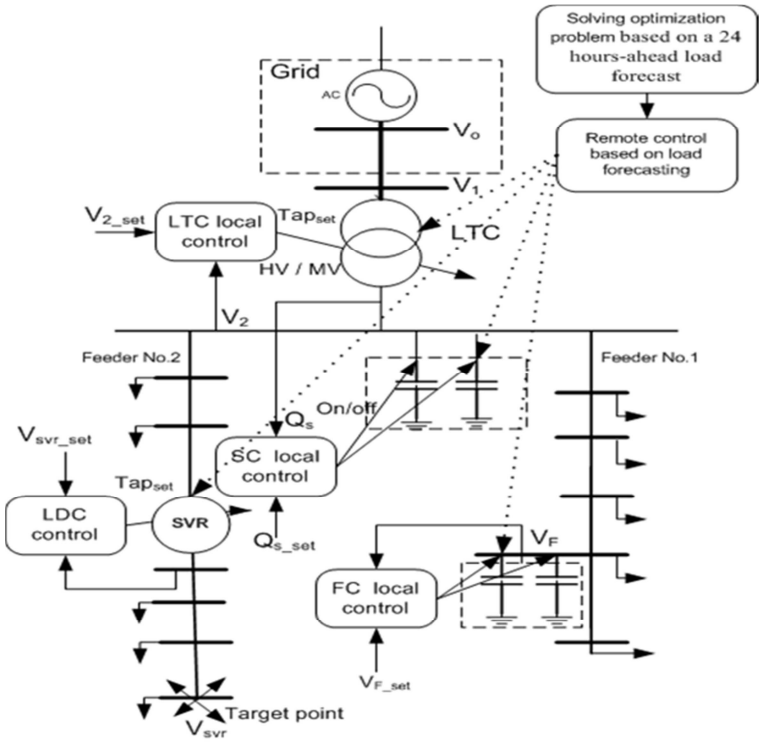

Figure 2.1: Conventional voltage and reactive power control in distribution systems.

2.2.1.1 Local control of LTC and SVR:

Both LTCs and SVRs keep consumer voltage magnitudes within standards. LTC keeps the secondary bus voltage close to a specified value under changing load conditions as given in (2.1).

$$V_{2\_LB} \leq V_2 \leq V_{2\_UB} \tag{2.1}$$

where,

$V_{2\_LB} = V_{2\_set} - 0.5\,DB$ lower boundary voltage;

$V_{2\_UB} = V_{2\_set} + 0.5\,DB$ upper boundary voltage;

V_{2_set} is the LTC set point voltage and *DB* is the dead-band (The band where no actions occurs to prevent oscillations and repeated activation-deactivation cycles “hunting”).

The line drop compensation (LDC) feature shown in Figure 2.2, which is an integral part of the SVR control, estimates the line voltage drop ΔV and performs voltage corrections based on the LDC current I_{comp}, R_{set} and X_{set} equivalent LDC parameters and LDC load side voltage V_{reg}.

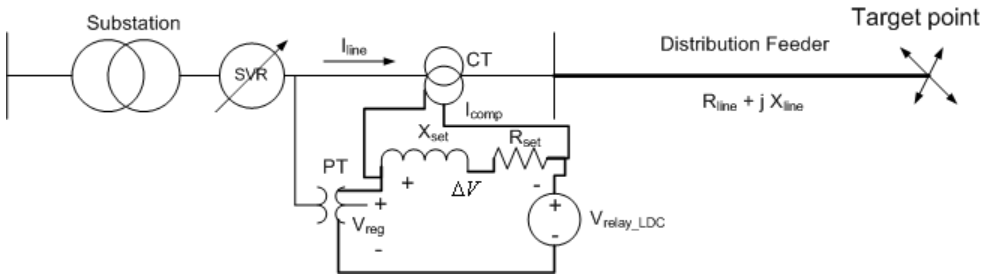

Figure 2.2: Line drop compensator circuit

Equations (2.2)-(2.6) show the LDC calculations based on its local measurements [14].

$$\Delta V = I_{comp}(R_{set} + jX_{set}) \tag{2.2}$$

$$V_{relay\_LDC} = V_{reg} - \Delta V \tag{2.3}$$

The number of required taps Tap_i at each time *i* can be calculated as follows:

$$Tap_i = Tap_{i-1} \qquad if \quad V_{svr\_LB} \leq V_{relay\_LDC} \leq V_{svr\_UB} \tag{2.4}$$

$$Tap_i = Tap_{i-1} + round\left(\frac{V_{svr\_set} - V_{relay\_LDC}}{0.75}\right) \qquad if\ V_{relay\_LDC} < V_{svr\_LB} \tag{2.5}$$

$$Tap_i = Tap_{i-1} - round\left(\frac{V_{relay\_LDC} - V_{svr\_set}}{0.75}\right) \qquad if \quad V_{relay\_LDC} > V_{svr\_UB} \tag{2.6}$$

where V_{relay_LDC} is the LDC relay voltage, V_{svr_set} is the reference voltage of the regulating point, V_{svr_LB} is the lower boundary voltage and V_{svr_UB} is the upper boundary voltage.

2.2.1.2 Local control of substation and feeders shunt capacitors:

Shunt capacitors are installed at the secondary bus of the substation to improve its power factor. Usually, substation capacitors use a local VAR controller to control their switching operation. Feeder switched capacitors (FSC) can be controlled by different methods of local controls, such as voltage, current, reactive power, time and intelligent controls. Voltage controlled FSC are most appropriate when the main role of capacitors is voltage regulation. Current control works well if the power factor of the load is fairly constant. To minimize the reactive power flow, reactive power controlled capacitors are most appropriate. If feeders have typical load profiles in a long term, time controlled capacitors could be effective [15]. To

mitigate short comings of single input control, intelligent control uses multiple inputs in the capacitor switching algorithm.

2.2.2 Remote voltage and reactive power control

Remote control needs to achieve better performance by solving the problem of voltage and reactive power control in distribution systems as an optimization problem for the 24 hours of the day before the dispatch day. Where the LTC and SCs are remotely dispatched every hour, by using an automated schedule, which is defined based on a 24 hours-ahead load forecast [16, 17]. The objective of the optimization problem is to minimize the daily system losses, while limiting the number of LTC and capacitor bank hourly switching operation [18-20]. Mathematically, the voltage and reactive power optimization problem can be expressed as follows:

$$\min \sum_{i=1}^{24} P_{loss,i} \tag{2.7}$$

subject to:

$$f\left(x_{1(i)}, x_{2(i)}, x_{3(i)}\right) = 0 \tag{2.8}$$

$$x_{1(i)min} \leq x_{1(i)} \leq x_{1(i)max} \tag{2.9}$$

$$x_{2(i)min} \leq x_{2(i)} \leq x_{2(i)max} \tag{2.10}$$

$$\sum_{i=1}^{24} |Tap_i - Tap_{i-1}| \leq KT \tag{2.11}$$

$$\sum_{i=1}^{24} |C_i - C_{i-1}| \leq KC \tag{2.12}$$

where

$P_{loss,i}$ real power loss at each time step *i*

f non-linear power flow equations

$x_{1(i)}$ discrete control variables, i.e. transformer tap settings and capacitor bank

$x_{2(i)}$ Injected reactive power at the slack bus and bus voltage magnitudes.

$x_{3(i)}$ Injected active powers at the slack bus and bus voltage angles.

KT Maximum allowable number of switching operations for LTC.

KC Maximum allowable number of switching operations for shunt capacitor banks.

As shown in (2.7)-(2.12), the reactive power and voltage control optimization problem is basically a non-deterministic, non-convex, mixed-integer nonlinear programming problem. Solving this optimization problem is not an easy task due to the load variation, the discrete nature of the LTC and capacitor bank switching, as well as the nonlinear power flow constraints. Due to load variations, even though the LTC tap position and capacitors ON/OFF configuration are optimum during their dispatching times, there is no guarantee that these configurations continue to be optimal until the next scheduled dispatch is executed. Moreover, remote control doesn't have the capability to adapt automatically to load changes that deviate from the forecasted one.

2.2.3 Combined local and remote voltage and reactive power control:

As most of the distribution systems have the characteristics of being radial in topology, the voltage and reactive power control problem can be simplified by breaking it down into two parts. One is dealing with the substation controls and the other with control of the feeders. The authors in [21] used remote control to find the optimal LTC tap positions and shunt capacitors on/off configuration on the substation side based on a 24 hours-ahead load forecast; while fuzzy systems were used to determine the states of FSC based on local information.

2.3 Smart Grid, Active Distribution Networks and Microgrids

The electric energy sector is currently moving towards the SG era [3]. The main goals of the SG paradigm are 1) transform the power system from the centralized scheme to a deregulated structure, 2) facilitate the interaction between customers, network operators and power producers, and 3) increase the system reliability and efficiency [2].

The distribution substation provides the connection between the transmission system, where most generation is currently interconnected, and the distribution system. The distribution system consists of distribution circuits used to distribute power from the distribution substations to numerous transformers serving individual or small groups of customers. Pre-interconnection of DG units, most area Electric Power Systems (EPS') are radial and have only one source of power i.e. the distribution substation. The

SG setup will evolve the distribution networks from their conventional passive structure into ADNs with high penetration of DG.

As the number of DG units increases; local and/or area electric power systems (EPS) with sufficient generation to meet all or most of its loads can be formed. These local and/or area EPS are known as microgrids or Distributed Resources Islanded Systems (DRIS). Typical microgrid's characteristics are: 1) formed of a cluster of loads and DG units, 2) intentionally planned, and 3) able to disconnect from and parallel with the area EPS (they are able to operate in normal parallel (grid-connected) and island modes.

The concept of microgrid may offer multiple potential benefits such as [22]:

1- Improving the microgrid customers' reliability by supplying the islanded portion during an area EPS outage or disturbance.

2- Relieving area EPS overloading issues by allowing the microgrid to be intentionally islanded. In this case, the microgrid load is removed from the rest of the area EPS thus this benefit is for both island and normal parallel operation.

3- Isolating the microgrid from area EPS power quality issues such as (voltage distortion, voltage sag and flicker).

4- Mitigating power-quality issues by reducing total harmonic distortion (THD) at the load points.

5- Allowing for system maintenance on the area EPS while keeping microgrid customers in service.

Various operating configurations can be initiated for islanded microgrids. Basically, the configurations can be identified based on the zone of the devices that allow separation of a microgrid from the EPS. These devices are called Island Interconnection Devices (IIDs) [22]; they might be circuit breakers or automatic reclosers. Figure 2.3 shows examples of microgrids configurations in a distribution network. As shown in the figure, the distribution network is configured into set of microgrids. Each microgrid is basically a group of components (e.g. lines, DG units, loads and protection devices) with an IID at its entry. The figure shows three types of island configurations; microgrid # 1 is a lateral island, microgrid # 2 is a circuit island and microgrid # 3 is a substation

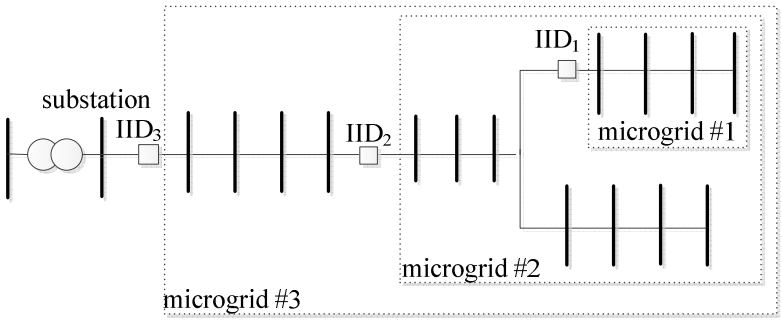

Figure 2.3: The structure of ADNs considering microgrid

island [22]. As shown in the figure, the microgrid configurations include the local EPS and may include portions of the area EPS.

2.4 Evaluating the Impacts of DG Integration on Conventional Voltage and Reactive Power Control:

The integration of DG units with distribution networks can significantly change the system voltage profile and the total system losses and interfere with conventional voltage and reactive power control schemes due to:

1- The applied voltage and reactive power control techniques are derived under the strong assumption of unidirectional power flow and they are being optimized for a passive use of distribution networks.
2- Many DG units are not utility owned and characterized by high degree of uncertainty such as solar and wind.
3- Unlike small number of power plants, a large number of small DG units are required to be controlled.

The impacts of DG units depend on the DG size, type and location, feeder parameters and loading conditions. The negative impacts of DG units could be summarized as follows:

2.4.1 Voltage rise issue and the change of the voltage profile when a DG is connected downstream LTCs [23, 24]:

The two bus system shown in Figure 2.4 has been selected to demonstrate how DG units cause voltage rise. Let us first, consider that the DG is disconnected. In this case, the voltage at the end of the feeder V_r is dependent on the secondary substation voltage V_s, the feeder parameters (R_{line} and X_{line}), the load active

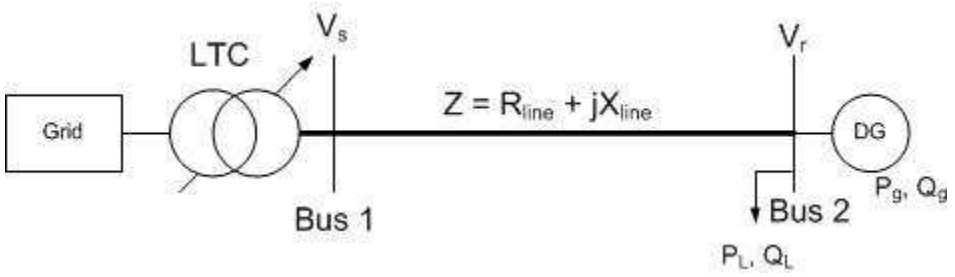

Figure 2.4: One line diagram of a two bus system

power P_L and the load reactive power Q_L as shown in (2.13). To maintain V_r within permitted limits, Distribution Network Operator (DNO) often maintains V_s close to the maximum in order to guarantee that voltages are above the minimum at the end of long feeders. As shown in (2.14), when a DG is connected at the end of the feeder, the incremental flow of DG real power P_g, interacting with the feeder resistance, may tend to cause voltage rise at the DG location.

$$V_r = V_s - \frac{X_{line}Q_L + R_{line}P_L}{V_r} \tag{2.13}$$

$$V_r = V_s - \frac{X_{line}(Q_L \mp Q_g) + R_{line}(P_L - Pg)}{V_r} \tag{2.14}$$

2.4.2 Interaction with voltage regulators, which are using LDC control:

When a DG unit is applied just downstream of LTC or SVR that is using considerable LDC, the DG may confuse the regulator in setting a lower or higher number of taps than necessary. This improper action could cause excessively low or high voltages towards the feeder end. To simplify the analysis, the distribution feeder shown in Figure 2.5 has been considered. The real voltage at the target point consists of two terms, as shown in (2.15). The first term is seen by the LDC local measurements and the second term, due to the installed DG, is unseen by the LDC. This means that the estimated relay voltage based on the LDC local measurements will be inaccurate when DG units are installed [25].

$$V_{real} = V_{relay\_LDC} - \Delta V_{error} \tag{2.15}$$

Figure 2.6 shows another type of interaction between DG units and SVR when the DG is connected after the SVR regulating point and the DG real power generation exceeds the customer demand

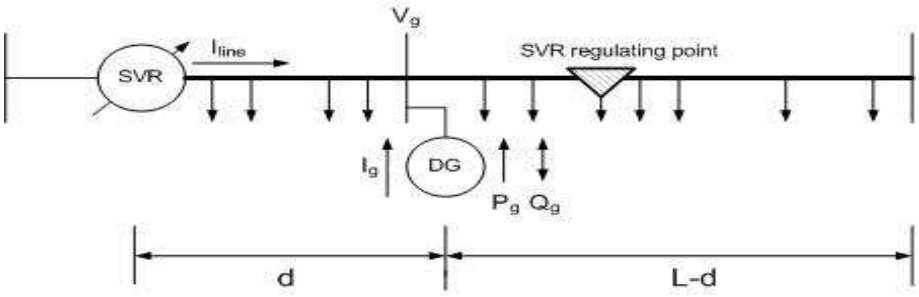

Figure 2.5: A DG unit connected between SVR and its regulating point

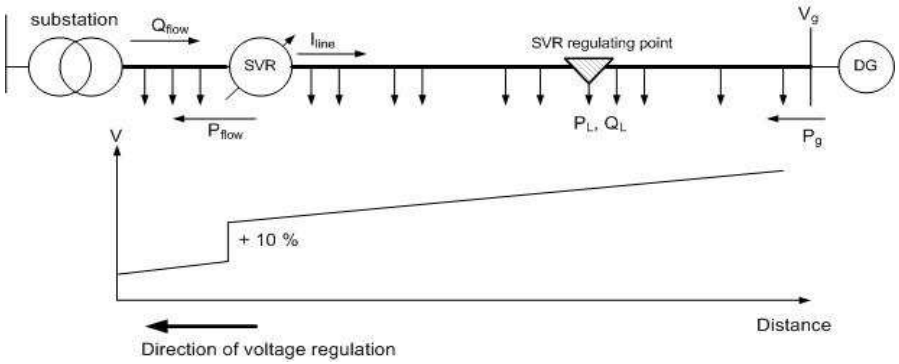

Figure 2.6: SVR operation in case of normal bidirectional reverse mode

between the SVR and the DG. In this scenario, the real power flow through the SVR is from DG to substation and the regulator will operate in reverse mode and regulate the voltage on the substation. The conflict appears when the substation side voltage is greater than the SVR set-point voltage. In this case, the SVR will tap down in an attempt to lower the voltage. Since the substation voltage is fixed the net effect is to raise the voltage on the DG side. This sequence will continue until the regulator taps to minimum tap, resulting in a 10% overvoltage on the DG side of the SVR [26-28].

Moreover, If DG units are characterized by being fluctuating power sources such as wind or solar, they may cause excessive operation for voltage regulators, which in consequence cause a great wear for this device and therefore, an increase in the maintenance cost. Further, when multiple voltage regulators are used on a distribution feeder, it is necessary to coordinate the timing of the voltage regulators. DG output changes may disrupt this timing and contribute to excessive tap changes.

2.4.3 Interaction with the local control of shunt capacitors

The impacts of DG units on the operation of shunt capacitors depend on the local control of capacitor switching. Voltage controlled capacitor banks could be impacted by the DG if the DG causes overvoltage. DG can impact capacitor switching when line current control is applied, since it can offset the line current when the DG is connected downstream the capacitor. If a DG is operating in constant power factor mode and it is installed downstream of the reactive power controlled capacitor, a high feeder-end voltage may occur. The impact of a DG on the feeder-end voltage will increase further when it operates at a constant power factor other than unity. Both temperature and time controls can also be affected by a DG. An overvoltage may occur when capacitor bank is switched on while a local DG is operating [15].

2.4.4 Voltage unbalance

Single-phase DG units generate power on only one phase. By injecting power on only one phase, the voltage balance between the three phase voltages can be lost. The voltage change created by the DG may combine with existing unbalanced voltage on the distribution systems to create unacceptable high degree of unbalance [8]. This high unbalance can exist even though the phase voltages may be within the limits of ANSI C84.1.

2.4.5 Impacts of DG on remote voltage and reactive power control

In Europe several countries such as Germany, Denmark and Spain has high renewable power penetration (up to 20%) and the same growth is expected to continue in Europe and USA. With such high degree of intermittent power sources, a question of system reliability and optimum operation of the power systems arises. Remote voltage and reactive power control would not be valid unless accurate short term forecast of power generation over one day ahead is found. The increase of uncertainties such as contingencies and the achievement of “plug and play” property will make the use of the conventional remote voltage and reactive power control difficult [25].

2.5 Evaluating the Successful Operation of Islanded Microgrids

Unlike conventional power generation power resources; which are almost exclusively based on 50/60 Hz synchronous machines, the majority of DG units are interfaced via dc-ac power electronic inverter systems [29-31]. In grid-connected operation, given the relatively small sizes of the DG units, they are controlled as PV or PQ buses and conventional voltage and reactive power control devices are dedicated for proper voltage regulation. On the other hand, in islanded microgrids, the DG units are dedicated to

achieve appropriate sharing of the load demands and to control the islanded microgrid voltage magnitude and frequency levels. To achieve such functionalities in the islanded microgrid systems, two operating schemes have been proposed in the literature.

Centralized control schemes are based on the availability of a communication infrastructure. In most cases, such schemes are found to be both costly and unreliable [29-31]. To overcome these limitations decentralized droop control schemes have been proposed. This control structure minimizes the communication bandwidth required and provides robust operation against any communication delay [29, 30]. The main tasks of the droop controlled DG controllers in islanded microgrids are: 1) to appropriately share the load demands among the DG units, 2) to prevent the rise of circulating currents between the parallel DG units, and 3) to control the DG unit output voltage magnitude and frequency. Droop control realizes active power sharing by introducing droop characteristics to the frequency of the DG unit output voltage. On the other hand, the reactive power sharing between the DG units is not exact and depends on the system parameters i.e. mismatches in the power line impedances [32].

The evaluation of the successful operation of islanded microgrids and its impacts on the anticipated improvement in system and customer reliability indices has been recently discussed in the literature. The authors in [9] considered the effects of allowing islands downstream of faults on the system average interruption frequency index (SAIFI) and the system average interruption duration index (SAIDI). However, the study in [9] did not consider the importance of ensuring system generation adequacy in its assessment. The work in [33] discussed the effect of islanded microgrid active power generation-load-ratio (GLR) on the improvement in both system and customer reliability indices. Nonetheless, the work in [9] and [33] did not consider the intermittent nature of the renewable DG units. The authors in [34] proposed a Monte-Carlo simulation (MCS) analysis to evaluate the benefits of microgrid integration on the system supply adequacy indices considering various penetrations level of different DG technologies. Given the high computational burdens of MCS, the work in [35]-[36] proposed a probabilistic analytical approach to evaluate the impacts of microgrid islanded operation on the supply adequacy and customers' reliability indices. The studies in [35]-[36] showed the superior performance of the proposed approach. It was also shown that there are no significant differences between the results obtained using this analytical approach and those obtained using MCS.

Yet all previous works calculated the probability of microgrid islanding success using the supply adequacy assessment techniques adopted in conventional power systems. These techniques depend only

on the GLR and do not consider the impacts of the special philosophy of microgrid operation including the microgrid stability as well as voltage and reactive power constraints might have on its assessment.

Although some previous research have been done in conventional power systems to investigate the important aspects of voltage and reactive power constraints in the reliability assessment [37, 38], still the usual practice is to treat the shortage in reactive power sources and the violation of voltage constraints separately using: 1) operational corrective actions, and/or 2) volt/var planning [39]. On the other hand, given the special philosophy of islanded microgrid operation, the shortage in reactive power and the violation of the voltage constraints cannot be excluded from the evaluation of the probability of microgrid islanding success due to the following reasons:

1- Unlike the conventional distribution systems where volt/var control devices can be used to treat any shortage in the reactive power and to correct any expected voltage constraints violations, in the case of islanded microgrid such devices will either not be available to achieve the required functionality due to the microgrid isolation or will face serious operational challenges due to their interaction with the DG units operation.

2- Caution should be taken to ensure that there are no line voltage regulators online in the island that would have power flow reversed from the normal direction. As such, most line voltage regulators will be deactivated in islanded microgrids [22].

3- Some DG units that are in microgrids will not participate in voltage and reactive power control because they are not under control of islanded microgrids operations (such DG units are called non-participating DG units).

4- Even if the DG units have enough active and reactive power capacities to meet the demand of the islanded microgrid; still a voltage violation might occur at some load points due to the voltage drops along the feeders.

2.6 VAR Planning in ADNs:

Feeder shunt capacitors are the main reactive power sources that are typically installed in distribution networks to reduce the power losses and to regulate the voltage supplied to the customer [40]. Identifying the type (switching or fixed), size and locations of shunt capacitors in distribution networks using different optimization techniques was a point of interest during the last few decades [40-47]. Such optimization techniques aim to equilibrium two types of utility costs in the planning and design process; they are the cost of power and energy losses and the cost of the capital investment and maintenance of the

installed capacitors. However, the previous research in capacitor placement did not take into account the new structure of ADNs, under the SG paradigm. Therefore, the formulation of the problem of capacitor planning need to be revised to consider the following features in ADNs:

1- Load characteristics and requirements for proper operation,

2- Characteristics of both dispatchable and renewable energy sources,

3- The possible microgrids configurations in ADN,

4- The special features and operational characteristics of islanded microgrids, and

5- The shortage in reactive power and the problems of voltage regulation during island operation.

2.7 Voltage and Reactive Power Control Schemes in ADNs:

Various control schemes have been proposed in the literature to mitigate the impacts of DG integration on the voltage profile during normal parallel mode of operation. Based on the control structure and communication links, the proposed control schemes are classified into five categories; they are 1) local control, 2) remote control, 3) combined local and remote control, 4) centralized control and 5) distributed (multi-agent or peer-peer) control.

Local control schemes, decentralized control structure, aims to propose new strategies for either the available voltage control devices or DG units based on local information without communication links. Voltage control using voltage regulators with both line rise and line drop compensators (LRC/LDC) has been proposed in [48]. The authors in [49] proposed a local coordination scheme of LTC and shunt capacitors in the presence of synchronous machine DG units based on the time delay operation.

Alternatively, different local control strategies have been proposed for DG units to mitigate their impacts on the voltage profile without modifying the conventional control of the available voltage and reactive power control devices. Traditionally, most of DNOs require all DG units connected to a distribution network to operate in constant power factor control (PFC) mode [50]. The authors in [51] proposed a decentralized reactive power control (QC) approach for voltage rise mitigation in distribution networks with DG units. In this approach, each DG that is connected on a feeder absorbs a reactive power to compensate the effect of its injected active power on the voltage rise. In [52], the authors discussed the use of droop-based active power curtailment (PC) techniques for overvoltage prevention in radial low voltage feeders. Two intelligent local control schemes have been proposed in [53] to mitigate the impacts of DG on the voltage profile in weak distribution networks. The first control scheme is a deterministic

system that uses a set of rules to switch between PFC and voltage control (VC) modes, while the second scheme is based on a fuzzy inference system that adjusts the reference setting of the power factor controller in response to the terminal voltage. A local VC scheme for multiple DG units in a distribution feeder has been proposed in [54]. The drawbacks of local control methods are in general 1) high stress on the voltage control devices, especially in case of intermittent power sources, 2) the interference between the operation of voltage control devices and DG units, 3) the increase of feeder's power losses, and 4) the energy capture from DG units is not maximized.

In some distribution systems, local control of LTC and capacitor operations have been replaced with a remote control, where LTCs and capacitors are remotely dispatched every hour, based on a one-day-ahead load and generation forecast [55]. However, such control scheme will no longer be valid due to the uncertainty of load and generation profile in ADNs.

The authors in [13] proposed a combined local and remote voltage and reactive power control based on automated remote adjustment to the local control in order to minimize the losses. The LTC and substation capacitors are assumed to be remotely controllable, while the feeder capacitors are not (partial communication links). Nonetheless, the high stress on the voltage and reactive power control devices has not been taken in consideration.

Various approaches have been proposed in the literature for advanced centralized Distribution Management System (DMS), one way communication, in ADNs. In [56] a centralized control technique has been proposed to provide optimal control of LTCs for multiple feeders. The authors in [56] formulated the problem as an optimization problem to solve for the optimal sending end voltage and hence, the desired tap position. The authors in [57] proposed a two-stage scheduling centralized DMS for voltage and reactive power control in ADNs with high penetration of variable power sources. The first stage is a day-ahead schedule for the optimization of the DG production during the following day. The second stage is an intra-day schedule that adjusts the scheduling every 15 minutes to achieve the system constraints. The main drawbacks of the centralized DMS methods can be summarized as follow: 1) they require communication links at each node, which is not practical. 2) They require a power flow solution at each time step, which might cause a large computation burden and numerical stability issues when X/R ratio is low. 3) They cannot consider the daily high stress on the voltage control devices. 4) Undesirable properties with respect to reliability (single point of failure) and scalability.

2.8 Multiagent Control: A Promising Control Scheme

A multiagent system is simply defined as a system comprising two or more agents [58]. Multiagent Systems (MAS) have been mentioned recently as a potential technology for many fields of power system applications such as to perform power system restoration, power system secondary voltage control and power system visualization [59-61].

The authors in [62] gave a good insight into the strategies, requirements, technical problems and benefits of multi-agent systems application in power systems. The authors discussed the work done in the field and potential applications of multi-agent systems in power systems. Moreover, in [62] the design strategies that could be incorporated for multi-agent systems design and implementation in power systems were discussed.

Possible structure of MAS application in the future network has been presented in [63]. The high level transport system formed by active network is presented as central agent that combines three different functional agents. They are control agents for controlling physical units directly, management agent for managing and taking decisions, and ancillary agent for supporting network services.

In [64, 65] a multilayer control hierarchy based on distributed agent technology and high speed fiber communications has been proposed for ADNs. This multilayer control allows both the inclusion of low voltage DG units into cells and the aggregation of multiple cells into larger cells. The DNO supervision over multiple cells is achieved through embedding a high level agent in the DNO System Control and Data Acquisition (SCADA) system.

In [66], authors mentioned multi-agent system architecture for microgrid management. The goal of the system is to perform tasks such as measurement data acquisition, DMS functions for load shifting, load curtailment and generation scheduling. A multiagent system was presented in [66] as a control framework for microgrids, and a scalable multiagent system for microgrids was discussed in [67]. In [68] a multi-agent system has been developed for a microgrid following standard development techniques and agent communication protocols. Functionalities of islanded microgrid and securing critical loads have been incorporated into the system.

Distributed control, multi-agent with two ways communication, has been proposed recently to tackle the drawbacks of local and centralized control schemes in the problem of voltage control in ADN. The authors in [69] proposed a distributed dispatching scheme of DG units for voltage support in distribution feeders. However, the authors did not take the main voltage and reactive power control devices in

consideration. In [70], a distributed state estimation algorithm for voltage regulation in multiple feeders based on placing remote terminal units at each DG and feeder capacitor has been proposed. Nonetheless, the authors assumed that the LTC is the only responsible device for voltage control. Therefore, the daily stress of the voltage control devices has not been considered.

Although some efforts have been done to show how MAS can be implemented in power system applications in general and ADNs in particular [60-71], the following points are not clearly covered:

1- The number of control agents and the suitable organization paradigm that should be applied in MAS based ADNs.
2- The interior control structure and operation mechanism that should be implemented in each control agent.
3- The coordination and communication protocols among control agents.
4- Simulation results or verification for MAS (from theory to practice).

2.9 Power Flow Studies in ADNs:

Distribution system represents the final link between the bulk power system and the consumers; therefore, it is crucial to have an accurate analysis for such systems. Power flow programs are typically used in both operational and planning stages. There are different applications (i.e. distribution automation, network optimization, Var. planning, and state estimation) that require power flow analysis [71, 72]. The distribution system has some distinct characteristics that are different from the transmission system due to the following [73]:

1- It works in radial or weakly meshed topology.
2- Distribution lines usually have high R/X ratio.
3- Significant unbalance may be found.

Many power flow algorithms have been proposed for distribution systems. In general, these methods are categorized as node based and branch based methods [74]. In node based methods (e.g. network equivalence method, Z-bus method, Newton-Raphson algorithm and Fast decouple algorithm), node voltage or current injections are used as state variables to solve the power flow problem [75-77]. However, in branch based methods (sweep based and loop impedance methods) branch currents or powers are used as state variables to solve the power flow problem [78-80]. Teng [71] proposed a network topology based three-phase distribution power flow algorithm. The algorithm developed two matrices, namely bus-injection to branch-current matrix (BIBC) and branch-current to bus-voltage matrix

(BCBV); in order to obtain the power flow solution. The advantage of this method is that it doesn't need matrix decomposition, forward/backward substitution of the Jacobian matrix or the Y admittance matrix as in other methods. In [81] an approach for three-phase power flow for large scale distribution systems is presented. The method is based on the implicit Z-bus and the modified Gauss-Seidel method. The factorization only needs to be done once for the sub-admittance matrix (YAA, YBB and YCC) in the solution procedure which reduces the CPU execution time.

The realization of the SG functionalities in ADNs requires different studies and operational controls e.g. state estimation, self-healing, network optimization, real-time management, etc. Furthermore, such functionalities can be extended in islanded microgrids to include 1) assessing the feasibility of islanded operation in terms of the system operational constraints. 2) Energy Management System (EMS) and power sharing. 3) Microgrid stability assessment.

Once again, the first requirement for any planning, operation, control, protection, or management of ADNs is the availability of an accurate power flow analysis tool. Thus, the problem of power flow analysis in ADNs has been addressed recently in the literature. In [82] a helpful list of the various types of DG units and their connection to the grid as well as their suitable models for power flow studies (PV and PQ or negative load) were offered. The model of DG units as PV or PQ depends on its operational mode and control characteristics [83]. In [84, 85] various distribution system equipment models for distribution power flow (i.e. DG units and voltage regulators) were presented. DG units were modeled as PQ (i.e. negative load) or as PV bus using fictitious node with impedance. Teng [86] proposed three mathematical models with equations of DG units for power flow analysis. The models are: 1) constant power factor model, 2) variable reactive power model and 3) constant voltage model. Without SVR modeling, the authors in [87] studied the impact of DG models on the voltage profile and power losses for the IEEE 37 bus test feeder.

The previously proposed algorithms for power flow analysis in ADNs do not provide a mean for incorporating the line voltage regulators in the power flow formulation. Line voltage regulators (LVR) are the workhorse of the distribution feeders and are mainly required to maintain the customers' voltages within the specified operating limits [14]. Even though the LVR model is well known, it is not clear in the literature how to incorporate these models in distribution systems power flow formulation. It is remarkable that most of the IEEE radial distribution test systems that in particular include LVR such as the IEEE 34 and 123-bus systems, are rarely used in the literature. Even in most of the work that used these test feeders, LVR are always neglected for simplicity. Moreover most of the proposed three phase

power flow studies fall short in comparing their results with the published results of such IEEE test feeders [88].

In addition, the previous power flow methods could face serious challenges in multiple source distribution networks i.e. microgrids. Such challenges will be even inflated in the case of islanded microgrids where the system is operating with a different ideology and it is usually preferred to operate the DG units with decentralized droop control.

Conventional power flow formulations in ADNs are not applicable in most of the islanded microgrid operation cases due to: 1) in the conventional power flow formulations, the representation of a DG unit as slack bus means that this DG unit is treated as an infinite bus capable of holding the system frequency and its local bus voltage constant. This representation does not reflect the microgrid configuration where an islanded microgrid system is typically fed from a group of DG units of small and comparable sizes and there is no one generation unit capable of performing the slack bus function. 2) In conventional power flow formulations, the representation of the DG units as PV/PQ buses, assumes that the required active power generation and/or local voltage at each DG unit are pre-specified. However, this representation does not reflect the reality of the decentralized droop control based microgrid operation, where both the generated active power and the local voltage at each DG unit are determined locally based on the droop characteristics. Accordingly, for studying the power flow in an islanded microgrid, there is a need for new power flow algorithms.

2.10 Discussion

In this chapter, the conventional schemes of voltage and reactive power control in distribution systems have been reviewed. The challenges of such conventional control schemes in ADNs have been presented. A critic literature survey on the proposed control schemes to mitigate these challenges has been presented. The survey shows that new schemes for voltage and reactive power control in ADNs using the SG technologies are required. A brief overview, of the special features, operational characteristics and the methods of evaluation of microgrids in islanded condition is described. The overview shows that the research has not paid the attention of the importance of voltage and reactive power constraints on the successful operation of islanded microgrids. Also the survey shows that conventional capacitor planning methods have not been revisited to consider the features of ADNs considering microgrids in islanded conditions. It can be concluded in this chapter that the assessment, planning and control of voltage and reactive power in distribution systems are becoming important issues especially with the high penetration

of DG and renewable sources and the concept of microgrids. The first step of such studies is to develop accurate power flow models.

Chapter 3

The Necessity for the Evolution of Voltage and Reactive Power Control in ADNs

3.1 Introduction

This chapter is divided into two phases. The first phase is directed towards developing a comprehensive three-phase power flow algorithm for ADNs. Three-phase overhead or underground primary feeders and double-phase or single-phase line sections near the end of the feeder laterals have been considered. Unbalanced loads with different types including constant power, constant current and constant impedance are modeled at the system buses. Substation and line voltage regulators consisting of three single phase units connected in wye or two single-phase units connected in open delta are modeled to satisfy the desired voltage level along the feeder. The mathematical model of DG units connected as PQ and PV buses are integrated into the power flow program to simulate the penetration of DGs in the distribution systems. The proposed method has been tested and compared with different IEEE test feeders result.

In the second phase, the developed power flow algorithm has been used to study the impacts of high DG penetration on the voltage profile, system losses and their interference with the operation of utility voltage regulators. The drawbacks of conventional voltage and reactive power control schemes and the necessities of their evolution in ADNs have been addressed.

3.2 A Generic Power Flow Algorithm for ADNs

This section presents the proposed generic power flow algorithm [89]. In section 3.2.1, the power flow model of distribution system components has been reviewed. In section 3.2.2, the power flow problem in ADNs has been formulated and the solution algorithm has been presented. Section 3.2.3 presents a comparison between the results of the proposed power flow algorithm and the IEEE test systems results given in [88].

3.2.1 Distribution System Modeling

3.2.1.1 Feeders modeling

For transmission system, the three phase currents are balanced and transposition of the conductors pretty much eliminates the variation in the line parameters. However, distribution systems do not have these two characteristics. Balancing the loads on the three phases of a distribution system is almost next to

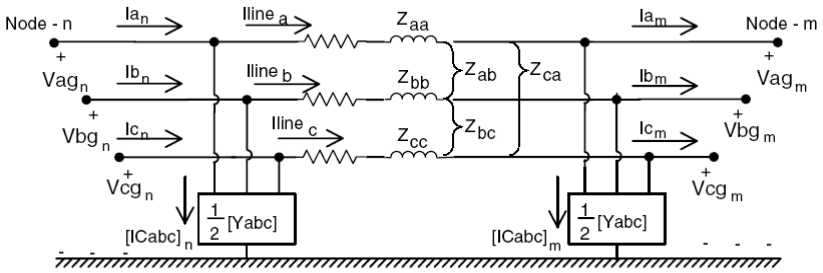

Figure 3.1: Three phase feeder model

impossible leading to three phase currents that are typically away from the balanced condition. Distribution lines are seldom transposed nor can it be assumed that the conductor configuration is an equilateral triangle. When these two characteristics are dominant, it is necessary to introduce a more accurate method for calculating the line impedance.

In this work, Carson's equations of a three-phase grounded four-wire system are used. Carson's equations allow the computation of conductor self-impedance and the mutual impedance between any number of conductors above ground. Figure 3.1 shows a three-phase line section between bus *n* and *m* [14]. A 4 × 4 matrix, which takes into account the self and mutual coupling terms, can be expressed as shown in (3.1). For a well-grounded distribution system, V_N and V_n are assumed to be zero, and Kron's reduction can be applied in (3.1). Equation (3.2) is designed to include the effects of the neutral or ground wire and to be used in the unbalanced power flow calculation [71, 88].

$$[Z_{abcn}] = \begin{bmatrix} Z_{aa} & Z_{ab} & Z_{ac} & Z_{an} \\ Z_{ba} & Z_{bb} & Z_{bc} & Z_{bn} \\ Z_{ca} & Z_{cb} & Z_{cc} & Z_{cn} \\ Z_{na} & Z_{nb} & Z_{nc} & Z_{nn} \end{bmatrix} \tag{3.1}$$

$$[Z_{abc}] = \begin{bmatrix} Z_{aa-n} & Z_{ab-n} & Z_{ac-n} \\ Z_{ba-n} & Z_{bb-n} & Z_{bc-n} \\ Z_{ca-n} & Z_{cb-n} & Z_{cc-n} \end{bmatrix} \tag{3.2}$$

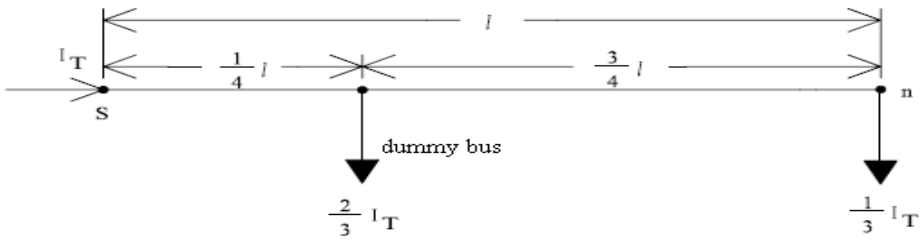

Figure 3.2: Exact lumped load model

The relation between the bus voltages and branch currents in Figure 3.1 can be expressed as shown in (3.3). The feeder shunt capacitive current in each bus can be calculated using (3.4).

$$\begin{bmatrix} V_m^a \\ V_m^b \\ V_m^c \end{bmatrix} = \begin{bmatrix} V_n^a \\ V_n^b \\ V_n^c \end{bmatrix} - \begin{bmatrix} Z_{aa-n} & Z_{ab-n} & Z_{ac-n} \\ Z_{ba-n} & Z_{bb-n} & Z_{bc-n} \\ Z_{ca-n} & Z_{cb-n} & Z_{cc-n} \end{bmatrix} \begin{bmatrix} I_{line}^a \\ I_{line}^b \\ I_{line}^c \end{bmatrix} \tag{3.3}$$

$$\begin{bmatrix} I_{sh}^a \\ I_{sh}^b \\ I_{sh}^c \end{bmatrix} = \frac{1}{2} \begin{bmatrix} Y_{aa} & Y_{ab} & Y_{ac} \\ Y_{ba} & Y_{bb} & Y_{bc} \\ Y_{ca} & Y_{cb} & Y_{cc} \end{bmatrix} \begin{bmatrix} V_{bus}^a \\ V_{bus}^b \\ V_{bus}^c \end{bmatrix} \tag{3.4}$$

3.2.1.2 Uniformly distributed load lumped model:

Figure 3.2 shows the general configuration of the exact model of uniformly distributed loads [88]. In this work, the node at one-fourth of the way from the source end has been presented as a dummy bus.

3.2.1.3 Load modeling:

The behavior of different residential, commercial and industrial loads is represented in the power flow formulation by modeling the changes in the load's active and reactive power requirements due to changes in system voltages [90]. The voltage dependency of load characteristics is represented by the exponential load model expressed as:

$$P_{Li}^{ph} = P_{oi}^{ph} \, |V_i^{ph}|^{\alpha} \tag{3.5}$$

$$Q_{Li}^{ph} = Q_{oi}^{ph} \, |V_i^{ph}|^{\beta} \tag{3.6}$$

where *ph* = *a, b,* or *c* corresponding to the three phases involved, P_{oi}^{ph} and Q_{oi}^{ph} are the load's nominal active and reactive power for phase (*ph*) at bus *i*, P_{Li}^{ph} and Q_{Li}^{ph} are the load's active and reactive power demand for phase (*ph*) at bus *i*, $\left|V_i^{ph}\right|$ is the voltage magnitude for phase (*ph*) at bus *i*, and α and β are the load's active and reactive power exponents.

3.2.1.4 Step voltage regulator modeling SVR [91]:

Step voltage regulator consists of an autotransformer and a load tap changing mechanism. The voltage change can be obtained by changing the taps of the autotransformer series winding by LDC control circuit shown in Figure 2.2. A SVR model for power flow programs is required to achieve the effective regulator ratio given by (3.7)-(3.8):

$$\begin{bmatrix} V_{an} \\ V_{bn} \\ V_{cn} \end{bmatrix} = \begin{bmatrix} aR_a & 0 & 0 \\ 0 & aR_b & 0 \\ 0 & 0 & aR_c \end{bmatrix} \begin{bmatrix} V_{An} \\ V_{Bn} \\ V_{Cn} \end{bmatrix} \tag{3.7}$$

$$\begin{bmatrix} I_{branch\_an} \\ I_{branch\_bn} \\ I_{branch\_cn} \end{bmatrix} = \begin{bmatrix} \frac{1}{aR_a} & 0 & 0 \\ 0 & \frac{1}{aR_b} & 0 \\ 0 & 0 & \frac{1}{aR_c} \end{bmatrix} \begin{bmatrix} I_{branch\_An} \\ I_{branch\_Bn} \\ I_{branch\_Cn} \end{bmatrix} \tag{3.8}$$

where aR_a, aR_b, aR_c are the effective turns ratios for the three single phase regulators and:

$$aR_{a,b,c} = 1 + Tap_{a,b,c}\Delta T \tag{3.9}$$

where ΔT is the step of tap change and it equals 0.00625 p.u. In this work, the number of required taps in each phase Tap *a,b* or *c* has been calculated using LDC control circuit (2.2)-(2.6) after load flow convergence.

If the voltage regulator is connected at the substation, (3.7) could be applied to find the receiving-end voltage of the regulator with respect to the substation voltage. This receiving-end voltage is used as a slack-bus in the power flow program. In this case, there is no need to apply (3.8). However, when the voltage regulator is connected between two nodes in the feeder (LVR), both (3.7) and (3.8) should be considered in the power flow modeling of the voltage regulator. Some previous works tackled this issue by representing the voltage regulator with the π model of the LTCs. However, this representation in most of the cases is not appropriate because the series impedance value of step

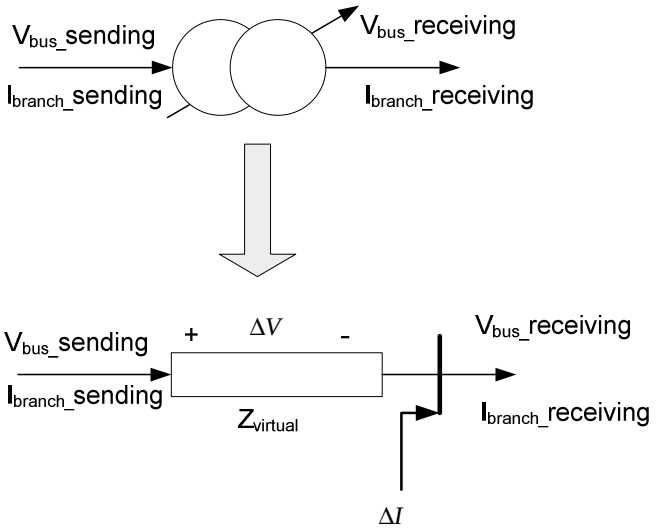

Figure 3.3: The power flow model of LVR

voltage regulators is so small and it is always being neglected and usually it is not mentioned in the manufacturer sheets. Furthermore, selecting a value of the series impedance haphazard can lead to severe convergence problems. The authors in [92] proposed a line regulator model that can be incorporated in a single equation power flow algorithm. This model is not generalized and it can be used only for branch-based power flow algorithm. In this work, a LVR power flow model is proposed to be incorporated in any power flow algorithm. Figure 3.3 shows the proposed power flow model of the voltage regulator for each phase of the distribution feeder. As shown in the figure virtual branch impedance has been connected between the sending-end and the receiving-end of the voltage regulator. This virtual impedance represents the tap ratio of the voltages. Consider the voltage drop on the virtual impedance is ΔV. Thus ΔV can be calculated using:

$$\begin{bmatrix}\Delta V_{Aa}\\ \Delta V_{Bb}\\ \Delta V_{Cc}\end{bmatrix} = \begin{bmatrix}(1-aR_a)V_{An}\\ (1-aR_b)V_{Bn}\\ (1-aR_{ac})V_{Cn}\end{bmatrix} \tag{3.10}$$

The relation between the voltage drops and the branch currents gives the value of the virtual impedance shown in (3.11). The value of the virtual impedance is updated in each iteration of the power flow program based on the changes of the sending-end voltages and currents. The above equation guarantees a proper update for the relation between the sending-end voltage and the receiving-end voltage of the voltage regulator. To achieve (3.8) an injection current ΔI has been connected at the receiving-end of the

voltage regulator. This injection current guarantees a proper update for the relation between the sending-end current and the receiving-end current of the voltage regulator. The injection current ΔI is given as shown in (3.12).

$$Z_{virtual} = \begin{bmatrix} \Delta V_{Aa}/I_{branch\_An} & 0 & 0 \\ 0 & \Delta V_{Bb}/I_{branch\_Bn} & 0 \\ 0 & 0 & \Delta V_{Cc}/I_{branch\_Cn} \end{bmatrix} \tag{3.11}$$

$$\begin{bmatrix} \Delta I_{an} \\ \Delta I_{bn} \\ \Delta I_{cn} \end{bmatrix} = \begin{bmatrix} \left(1 - \frac{1}{aR_a}\right) I_{branch\_An} \\ \left(1 - \frac{1}{aR_b}\right) I_{branch\_Bn} \\ \left(1 - \frac{1}{aR_c}\right) I_{branch\_Cn} \end{bmatrix} \tag{3.12}$$

3.2.1.5 Distributed Generator DG Modeling:

DG units can be modeled in ADNs for power flow studies as PQ or PV. When the DG operates in PQ mode, the DG unit injects pre-specified quantities of active and reactive powers, irrespective of the voltage at the DG point of common coupling (PCC). In this work, DG units are represented by PV node using a dummy node and dummy branch which inject reactive power to the specified node to maintain the specified voltage value [85] as shown Figure 3.4. The dummy reactive power injection value for each PV node at iteration *i* is calculated as follows:

$$Q_{spec,i}^{ph} = |V_i^{ph}| \left(\frac{V_{dum,i}^{ph} - |V_i^{ph}|}{\beta} \right) \tag{3.13}$$

where V_i^{ph} is the calculated voltage of PV specified node at phase ph; $V_{dum,i}^{ph}$ is the voltage of the dummy node of PV specified node at phase ph; β is the sensitivity reactance; it depends on feeder parameters, DG size and loads. The dummy node voltage is updated in each iteration *i* as follows:

$$\Delta V_{dum,i}^{ph} = V_{spec,i} - \left| V_i^{ph} \right| \tag{3.14}$$

$$V_{dum,i+1}^{ph} = V_{dum,i}^{ph} + \Delta V_{dum,i}^{ph} \tag{3.15}$$

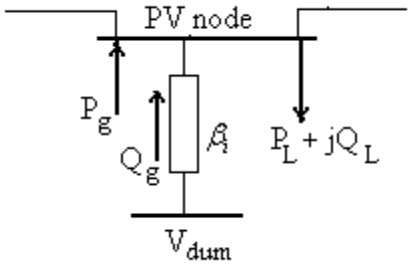

Figure 3.4: PV node model using a dummy branch

As the system is unbalance, if the DG is a synchronous machine then the positive sequence voltage has been considered as a reference ($V_{spec,i}$). If the DG is inverter-based, both positive sequence voltage and phase voltages can be taken as a reference.

To take the DG reactive power limits into consideration, the calculated DG reactive power is compared with minimum and maximum limits. If the calculated reactive power violates the upper or lower limits, the DG switch from PV to PQ mode and the reactive power is kept at its limits.

3.2.2 Problem Formulation

The proposed method is based on the relation between bus-injected currents and branch currents of radial distribution networks. For an *N* bus radial distribution network; there are only *N-1* lines (elements) and branch currents that can be expressed in terms of bus currents [93]. For an element *ij* connecting nodes '*i*' and '*j*', the bus current of node *j* can be expressed as a linear equation:

$$I_j = I_{ij} - \sum I_{jk(j)} \tag{3.16}$$

where *k(j)* is the set of nodes connected to node *j*. For the slack bus the power is not specified so it is excluded and the relationship between bus currents and branch currents are derived as a non-singular square matrix.

$$I_{bus} = K\ I_{branch} \tag{3.17}$$

The matrix *K* is the element incidence matrix. It is a non-singular square matrix of order *(N-1)*.The elemental incidence matrix is constructed in a simple way, same as the bus incidence matrix. In this

matrix *K*, each row is describing the element incidences. The elements are numbered in a conventional way *i.e.* the number of element '*ij*' is *j-1*. where:

1- The diagonal elements of matrix *K* are ones. The variable *j* is denoting the element number *K(j, j) =1*.
2- For each j^{th} element let m *(j)* is the set of element numbers connected at its receiving end *K(j, m(j)) = -1*.
3- All the remaining elements are zeros. It can be observed that all the elements of matrix *K* below the diagonal are zeros.

By using (3.17) and after the construction of the element incidence matrix *K*, the branch currents with respect to the injection bus currents can be given as:

$$I_{branch} = k^{-1} I_{bus} \tag{3.18}$$

The idea of the bus incidence matrix has been applied in this work for the case of unbalanced radial distribution systems. Figure 3.5 shows the flowchart of the proposed algorithm. Detailed explanations of this algorithm are discussed in the following steps:

step 1 : Take initial values for the magnitude of all bus voltages equal to 1.0 p.u (flat start). For any phase which fails to present, set the value of its voltage equal to zero.

step 2 : Construct the element incidence matrices K_a, K_b and K_c for phases *a*, *b* and *c* respectively. Note that the size of matrix K_a is $(N_a\text{-}1) \times (N_a\text{-}1)$, the size of matrix K_b is $(N_b\text{-}1) \times (N_b\text{-}1)$ and the size of matrix K_c is $(N_c\text{-}1) \times (N_c\text{-}1)$, where N_a, N_b and N_c are the total number of buses at which phases *a*, *b* and *c* exist respectively.

step 3 : Using the initial bus voltages, the specified load powers, the feeder shunt admittance matrix and the specified DG power, calculate the bus currents at each phase.

$$I_{bus}^{ph} = I_L^{ph} + I_{sh}^{ph} - I_G^{ph} \tag{3.19}$$

where I_L^{ph} is the load current in each phase and it can be calculated using (3.20). Note that *n* is the load exponent. It equals zero for constant power, one for constant current and two for constant impedance load.

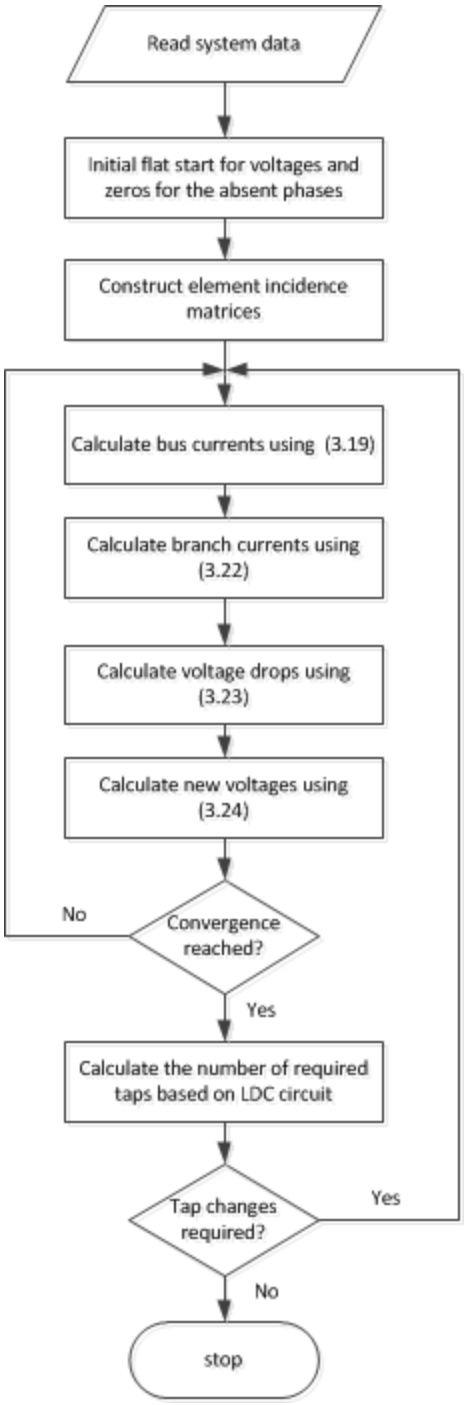

Figure 3.5: A flowchart of the proposed power flow algorithm

$$I_L^{ph} = \frac{abs(V_{bus}^{ph})^n \times conj(S_{L,spec}^{ph})}{conj(V_{bus}^{ph})} \tag{3.20}$$

where, I_{sh}^{ph} is the feeder shunt capacitive current and it can be calculated using (3.4). I_G^{ph} is the distributed generator current and it can be calculated using (3.21). $Q_{g,spec}^{ph}$ is fixed when a DG is represented as PQ and it is updated in each iteration when the DG operates in PV mode.

$$I_G^{ph} = \frac{(P_{g,spec}^{ph} - jQ_{g,spec}^{ph})}{conj(V_{bus}^{ph})} \tag{3.21}$$

step 4 : The branch currents in each phase can be expressed as:

$$I_{branch}^{ph} = K_{ph}^{-1} I_{bus}^{ph} \tag{3.22}$$

step 5 : The voltage drop at each branch (*i*) in each phase can be expressed by:

$$\begin{bmatrix} V_{branch\_i}^{a} \\ V_{branch\_i}^{b} \\ V_{branch\_i}^{c} \end{bmatrix} = \begin{bmatrix} Z_{aa\_i} & Z_{ab\_i} & Z_{ac\_i} \\ Z_{ba\_i} & Z_{bb\_i} & Z_{bc\_i} \\ Z_{ca\_i} & Z_{cb\_i} & Z_{cc\_i} \end{bmatrix} \begin{bmatrix} I_{branch\_i}^{a} \\ I_{branch\_i}^{b} \\ I_{branch\_i}^{c} \end{bmatrix} \tag{3.23}$$

step 6 : Calculate the voltages of the receiving ends with respect to the voltages of the sending end using the backward sweep, subject to the phase at bus *j* is found.

$$\begin{bmatrix} V_{bus\_j}^{a} \\ V_{bus\_j}^{b} \\ V_{bus\_j}^{c} \end{bmatrix} = \begin{bmatrix} V_{bus\_i}^{a} \\ V_{bus\_i}^{b} \\ V_{bus\_i}^{c} \end{bmatrix} - \begin{bmatrix} V_{branch\_i}^{a} \\ V_{branch\_i}^{b} \\ V_{branch\_i}^{c} \end{bmatrix} \tag{3.24}$$

step 7 : The absolute difference between the new bus voltages and the initial bus voltages gives the mismatch which represents the convergence factor. In addition, if a DG operates in PV mode, the absolute difference between the specified positive sequence voltage and the calculated one must be taken in the mismatch. Furthermore, it is possible to calculate the mismatch by comparing the specified and the calculated injected active and reactive power at each bus.

step 8 : Repeat the process from *step* 3 to *step* 7 until convergence is achieved based on the required mismatch.

3.2.3 Base Case Studies

The IEEE 13 and 37 bus unbalanced distribution test feeders shown in Appendix A, Figure A.1 and Figure A.2 respectively, have been chosen to test the effectiveness of the proposed algorithm. The two test feeders contain three phase feeder model, different load modeling, different load types (1-phase, 2-phase and 3-phase), and substation voltage regulators model with LDC control technique. The set voltage of the regulator target point is 1.015 p.u. The regulator contains a switch with 32 taps. The SVR dead-band DB equals to ±1% of the set voltage (between 1.025 p.u. and 1.005 p.u). Although the IEEE 13-bus test feeder is short, it is a comprehensive feeder. It contains overhead and underground lines with variety of phasing, shunt capacitor banks and unbalanced spots and distributed loads. In another side, the IEEE 37-bus test feeder is a three-wire delta operating with very unbalanced loading. In this feeder, all loads are spot loads, all line segments are underground and the SVR consisting of two single-phase units connected in open delta. The complete test feeders data and power flow results are available in [88, 94]. The proposed power flow algorithm has been coded in MATLAB.

3.2.3.1 Base case for IEEE 13 bus test feeder

After convergence of the program, the numbers of taps that are required to maintain the voltages within the specified standard limits have been calculated using LDC technique. It has been found that those taps are 10, 8, and 11 for phases a, b, and c respectively. The program was converged after 5 iterations. Figure 3.6 shows the voltage profile along the feeder of phase c, the most loaded phase, at different loading conditions without the interconnection of DG units. The figure shows that the voltage at the regulating point is within the specified *DB* of the set point. Table 3.1 shows the results of the proposed algorithm compared with the results in [88, 94]. The table shows that the proposed algorithm results are approximately the same, which indicate the effectiveness of the proposed algorithm.

3.2.3.2 Base case for IEEE 37 bus test feeder

In this section, the proposed method has been compared with the IEEE results and the developed algorithm in reference [71]. The algorithm developed in [71] consists of two matrices; they are bus- BIBC and BCBV. Figure 3.7 shows the voltage profile of the line voltages in the test feeder for the proposed method, IEEE results and the developed algorithm in [71]. As shown in the figure, the results are almost the same. Table 3.2 shows the radial flow summary of the test feeder.

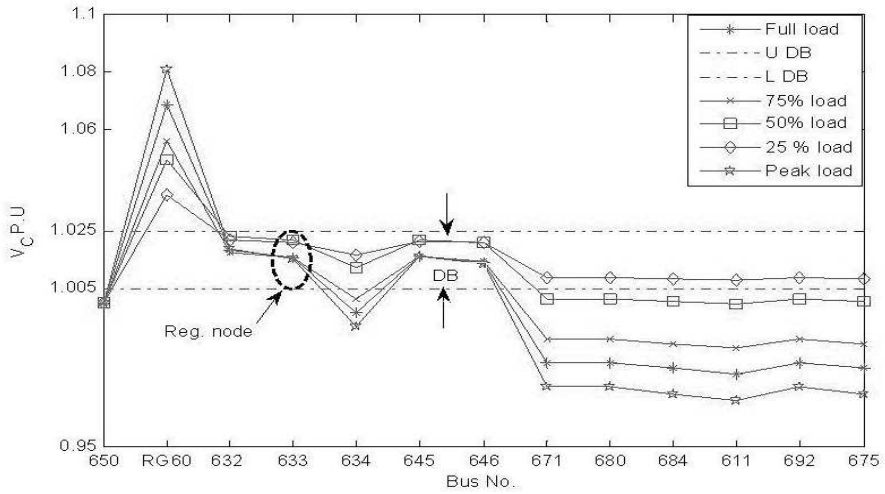

Figure 3.6: Voltage profile for phase c at different loading conditions without DG integration

Table 3.1: IEEE 13-bus power flow results of the proposed algorithm compared with IEEE results

Node	V_{A-N}				V_{B-N}				V_{C-N}			
	Test results		IEEE results		Test results		IEEE results		Test results		IEEE results	
	Mag.	Ang.			Mag.	Ang.	Mag.	Ang.	Mag.	Ang.	Mag.	Ang.
650	1.000	0.0	1.000	0.0	1.000	-120	1.000	-120	1.00	120	1.00	120
RG60	1.0625	0.0	1.0625	0.0	1.050	-120	1.050	-120	1.0687	120	1.0687	120
632	1.0220	-2.47	1.0210	-2.49	1.0402	-121.70	1.042	-121.72	1.0182	117.78	1.0174	117.83
633	1.0190	-2.54	1.018	-2.56	1.0390	-121.74	1.0401	-121.77	1.0152	117.77	1.0148	117.82
634	0.9948	-3.20	0.9941	-3.23	1.021	-122.20	1.0218	-122.22	0.9963	117.30	0.9960	117.34
645	-	-	-	-	1.0319	-121.87	1.0329	-121.9	1.0160	117.81	1.0155	117.86
646	-	-	-	-	1.030	-121.95	1.0311	-121.98	1.0141	117.85	1.0134	117.9
671	0.9909	-5.28	0.9900	-5.30	1.0515	-122.31	1.0529	-122.34	0.9780	115.97	0.9778	116.02
680	0.9909	-5.28	0.9900	-5.30	1.0515	-122.31	1.0529	-122.34	0.9780	115.97	0.9778	116.02
684	0.9900	-5.30	0.9881	-5.32	-	-	-	-	0.9763	115.85	0.9758	115.92
611	-	-	-	-	-	-	-	-	0.9744	115.73	0.9738	115.78
652	0.9834	-5.22	0.9825	-5.25	-	-	-	-	-	-	-	-
692	0.9909	-5.28	0.9900	-5.31	1.0515	-122.31	1.0529	-122.34	0.9780	115.97	0.9777	116.02
675	0.9846	-5.53	0.9835	-5.56	1.0545	-122.47	1.0553	-122.52	0.9763	115.95	0.9758	116.03

Total	KW		KVAR	
	Test results	IEEE results	Test results	IEEE results
Load	3466.352	3466.128	1400.6	1400.119
Substation power	3577.2	3577.191	1725.10	1724.772
Losses	110.848	111.063	324.5	324.653

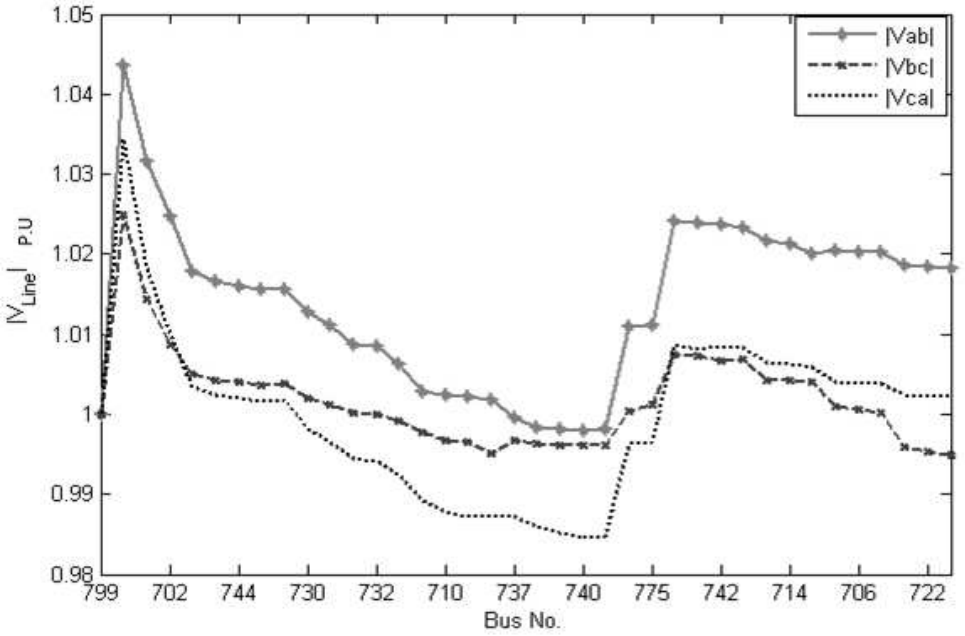

Figure 3.7: Line voltages in per unit for the base case of the IEEE 37 bus test feeder

Table 3.2: Radial power flow summary for the IEEE 37-bus test feeder

	A-B			B-C			C-A		
	IEEE results	Proposed	Ref [71]	IEEE results	Proposed	Ref [71]	IEEE results	Proposed	Ref [71]
Load									
KW	732.331	732.306	732.349	638.824	638.77	638.83	1090.1	1090.1	1090.099
KVAR	359.538	359.525	359.54	313.874	313.848	313.875	529.558	529.553	529.558
Losses									
KW	26.671	26.671	26.63	13.804	13.804	13.735	20.088	20.088	19.893
KVAR	18.769	18.995	21.283	9.953	9.952	12.239	17.733	17.961	19.854

Total	KW			KVAR		
	IEEE results	Proposed	Ref [11]	IEEE results	Proposed	Ref [11]
System input	2521.827	2521.725	2521.64	1249.435	1250.073	1256.39
Load	2461.255	2461.63	2461.28	1202.970	1202.93	1202.973
Losses	60.563	60.563	60.2582	46.455	46.908	53.3765

	Proposed	Ref [71]
Iterations	6	9
Time elapsed	0.0193s	0.02099s

As shown in the table, the number of iterations in the proposed method is 6 and the number of iterations for the developed algorithm in [71] is 9 iterations. These results show that the proposed method has good convergence characteristics in large scale distribution feeders. In addition, the total reactive power loss based on the developed algorithm in [71] is not accurate due to neglecting lines shunt capacitance.

3.3 Impacts of DG Integration on Conventional Voltage and Reactive Power Control:

3.3.1 Interferences between DG units and voltage control devices (studies are carried out on the IEEE 13-bus test feeder)

3.3.1.1 When DG units are interconnected between SVR and its regulating point:

To show the interference between DG units and SVR, a DG with 5 MVA rating is installed between SVR and its target point (633). This DG has the capability to operate at different power factors with a limit of 0.9 power factor capacitive or inductive. Figure 3.8 shows the voltage profile of phase *c* at peak load conditions, when the DG injects 4.5 MW at unity power factor, and is installed at different distances between the SVR and the target point. As shown in the figure, undervoltages occur at the end of the feeder due to the error of the estimated voltage drop in the LDC local measurements [91].

When the DG changes its power factor, a reactive power will be delivered from or absorbed by the DG. This reactive power affects the deviation of the relay voltage and the number of required taps that is calculated by LDC depending on the location of the DG. When DG operates at capacitive power factor and close to SVR, a decrease in the number of required taps for the SVR is observed. In consequence the voltage profile over the feeder will reduce, if it is compared with the voltage profile when DG operates at unity power factor. Figure 3.9 and Figure 3.10 show that the majority of the node voltages at phases c and a, are suffering from undervoltages. The reason behind that is when DG operates at capacitive power factor; it injects reactive power to the feeder. Yet, this reactive power will reduce the line current that is observed by SVR. Therefore, an improper action will be taken by LDC due to the improper current that is observed [25, 91].

In contrast, when DG operates at inductive power factor, it causes increase in the number of required taps for SVR, if it is compared with unity power factor. As shown in Figure 3.10, the increase of the taps may be beneficial when it causes compensation for the unseen voltage drop due to the injected real power. On the other hand, it may cause an overvoltage in case of lightly loaded phases. As shown in Figure 3.11, the operation of the DG at inductive power factor mode causes an overvoltage at phase b, the lowest loaded phase. This overvoltage may cause interference on the operation of the three phase capacitor that is installed at bus 675, in case it operates with local voltage control. A situation like this, will cause improper trip out for the capacitor and hence an increase in the total system loss.

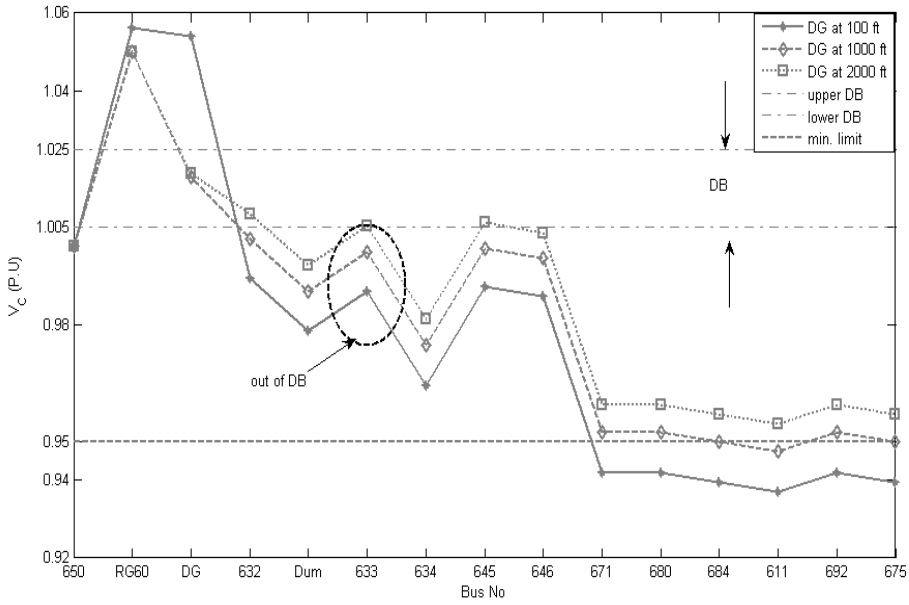

Figure 3.8: Voltage profile for phase c at peak load when a DG is installed at different distances between SVR and its target point.

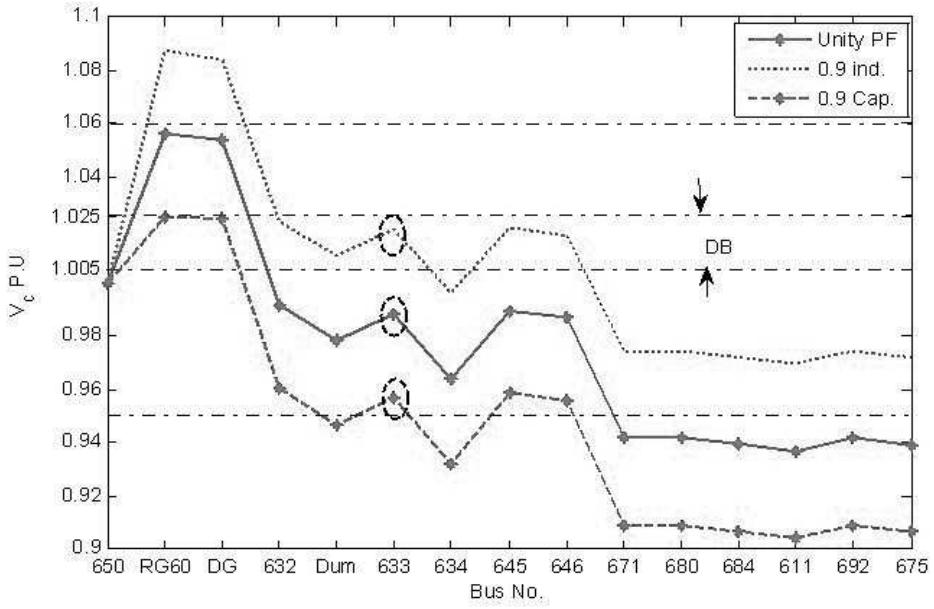

Figure 3.9: The impacts of DG's power factor on the voltage profile of phase c, the highest loaded phase, when it is installed close to SVR at peak load.

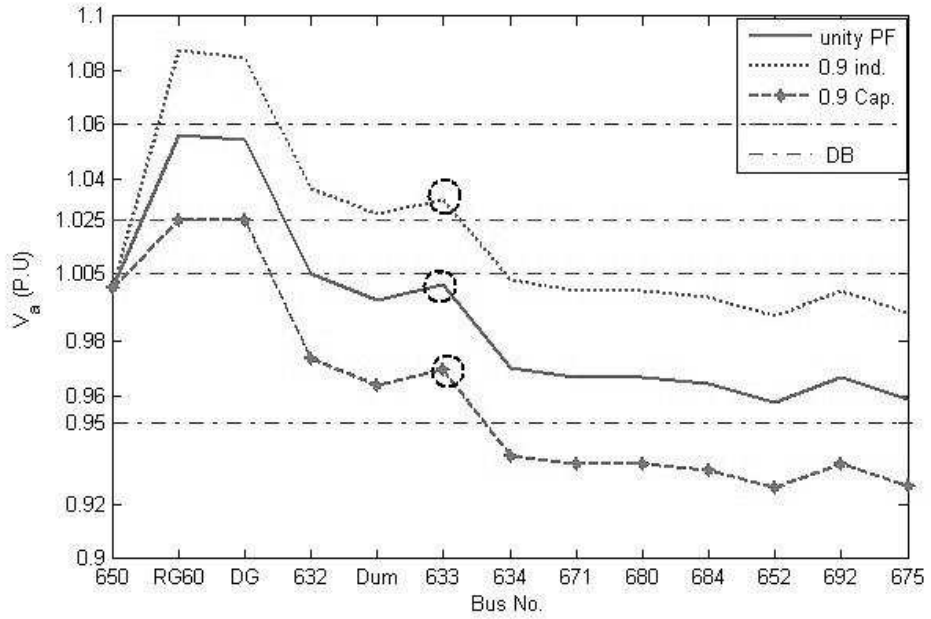

Figure 3.10: The impacts of DG's power factor on the voltage profile of phase a, the medium loaded phase, when it is installed close to SVR at peak load.

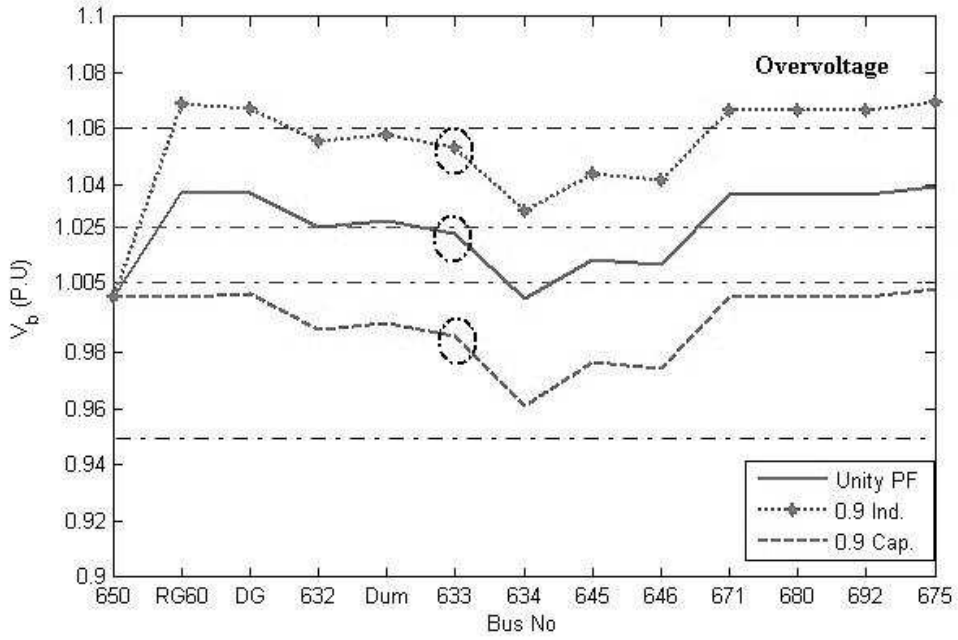

Figure 3.11: The impacts of DG's power factor on the voltage profile of phase b, the lowest loaded phase, when it is installed close to SVR at peak load.

3.3.1.2 Voltage rise issue when DG units are interconnected downstream the SVR regulating point:

Assume that the SVR target point is not at the end of the feeder and a DG is installed downstream this point. In this scenario it is expected that there will be no error in the estimation of the relay voltage using LDC local measurements. Figure 3.12 shows the voltage along the feeder at phase c, when the same DG size is installed at different buses downstream the SVR target point. As shown in the figure, the voltage of SVR target point is kept within the specified dead-band. Nonetheless, an overvoltage may occur at the end of the feeder due to the reverse power flow. Figure 3.13 shows the voltages at phase b at 2/3 load condition when the DG is connected at bus 680 and operates at different real power and unity power factor. Yet, in weak distribution networks an overvoltage is expected even if the loading is high and the DG power is low.

3.3.1.3 Interference with shunt capacitors and voltage unbalance when a single phase DG is installed:

Suppose that a single phase DG with 500 KW rating is connected at phase b of node 675. As shown in Figure 3.14, the injected real power from the DG unit in phase b caused overvoltage in some nodes during full load condition. This overvoltage may cause interaction for the operation of the three phase shunt capacitor which is connected at node 675 if this capacitor uses local voltage control. In this case the capacitor will trip out. This improper action during full load condition will cause a reduction or even undervoltages in the voltage profile of other phases. As shown in Figure 3.15, undervoltages occurs in phase c at the end of the feeder due to the interaction between the single phase DG and the three phase shunt capacitor at bus 675. Furthermore, the integration of single phase DG units might increase the voltage unbalance of the distribution feeders. In this scenario and based on the IEEE standard definition, the percentage of voltage unbalance increased from 1.8% to 3%, which violates the standards.

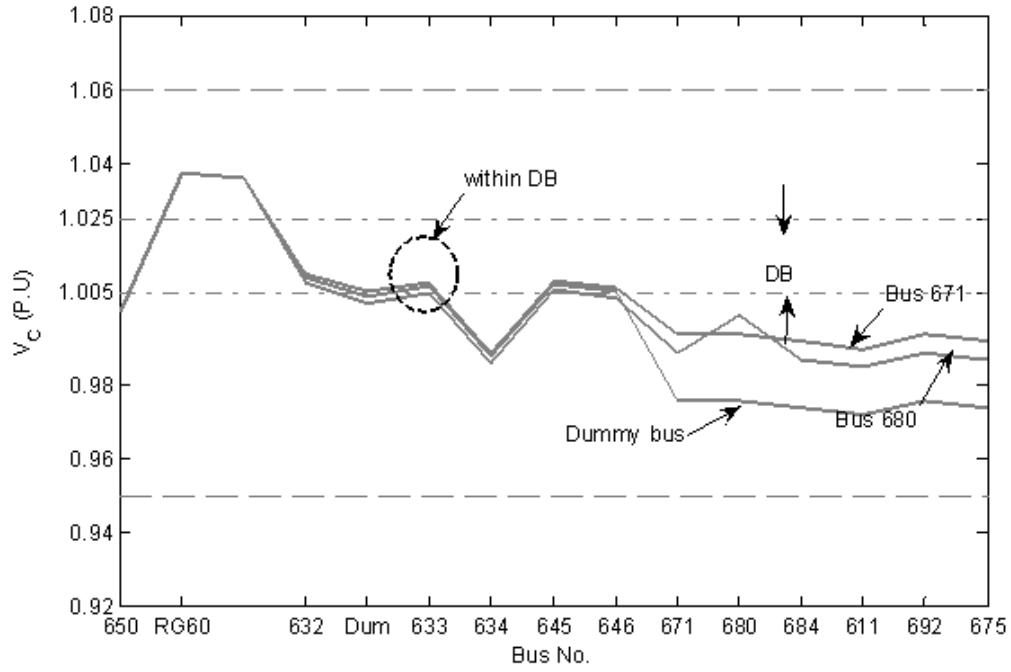

Figure 3.12: The voltage profile for phase c at peak load, when a DG is connected downstream the SVR target point and operates at unity PF.

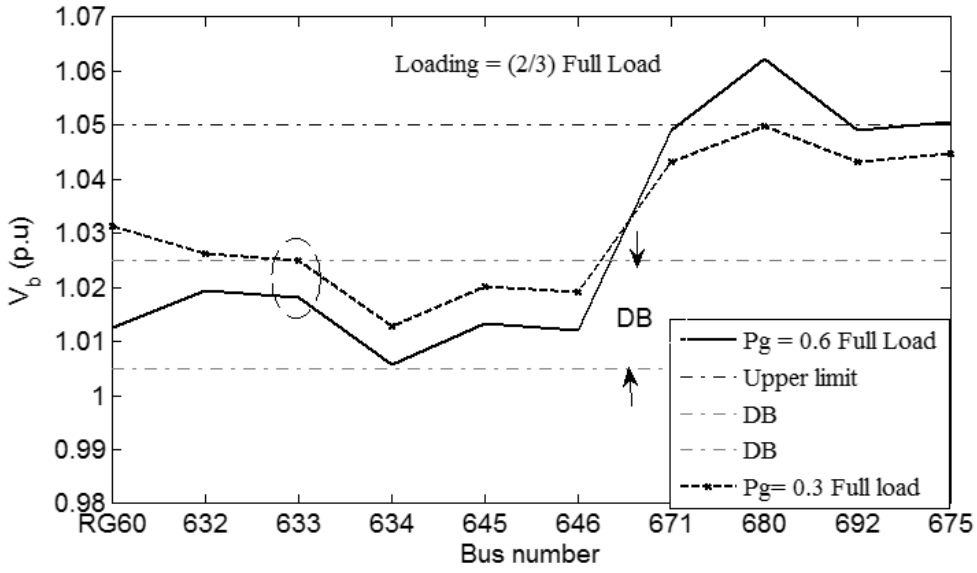

Figure 3.13: The impact of DG on the voltage profile of phase b, the lowest loaded phase, when it is installed after the SVR target point

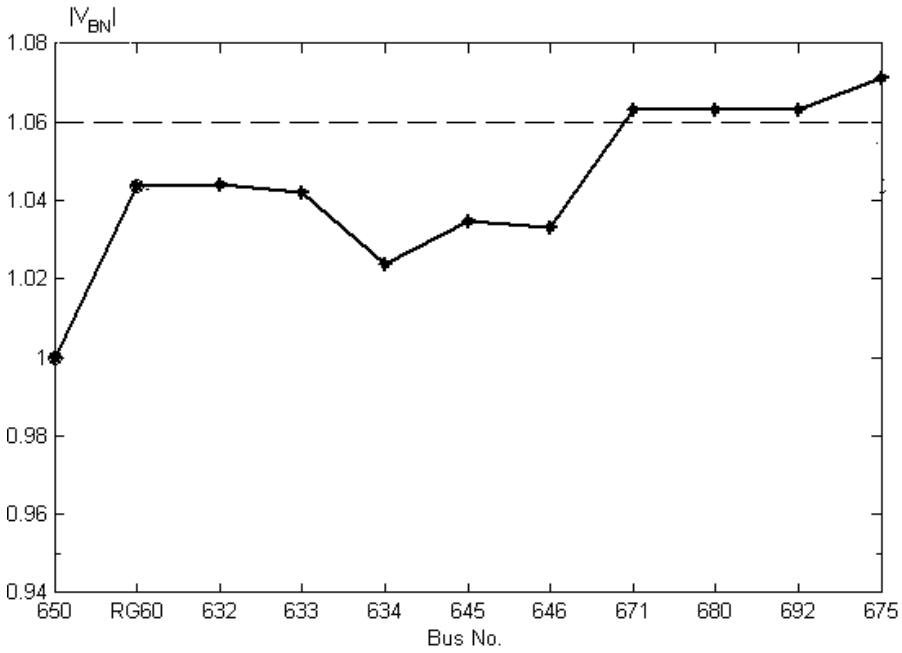

Figure 3.14: Voltage profile at full load at phase (b) when a single phase DG is connected at node 675.

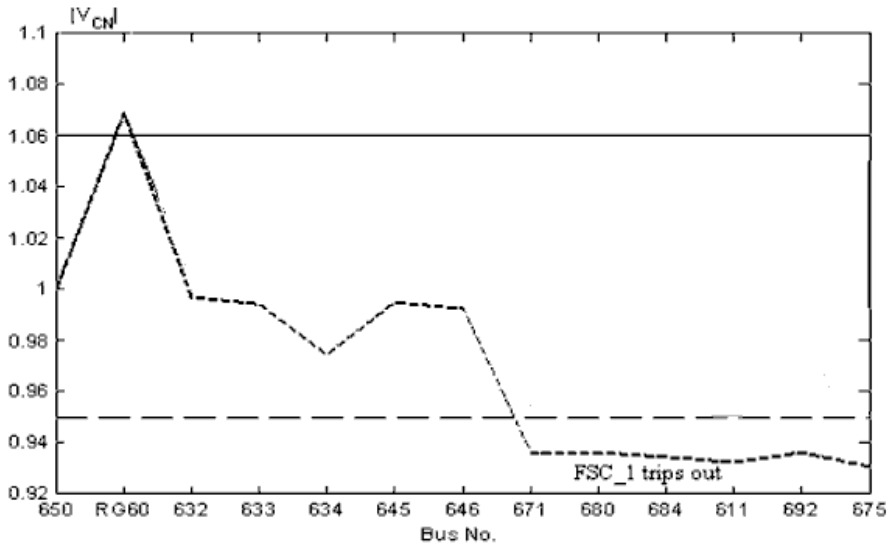

Figure 3.15: Voltage profile at phase (c) when a single phase DG is connected at node 675

3.3.2 Impacts of high penetration of renewable energy sources (studies are carried out on the IEEE 34-bus test feeder)

The IEEE 34-bus test feeder shown in Appendix A, Figure A.3, has been chosen in this section to show the impacts of high renewable energy penetration. The IEEE 34 bus test feeder is similar to the IEEE 13 and 37 bus test feeders; however it contains two line voltage regulators. The line regulators have similar operating characteristics like the substation voltage regulator in the IEEE 13 and 37 bus test feeders. As shown in the figure, ten wind turbines each of them has 50 KW rating have been installed at buses 806,808,816,828,832,890,842,846,860, and 840. The total penetration of the wind turbines is 20% of the substation rating. One day study has been selected to show the impacts of high wind power penetration on the operation of the line regulators and the voltage profile. Figure 3.16 shows a typical load profile of both residential and commercial loads in per unit. The load profile data gives the load power every 30 minutes time interval. It is assumed that all residential and commercial loads at all load nodes are following the profile shown in Figure 3.16 based on their ratings. Figure 3.17 shows the wind speed in m/s and the generated wind power in KW during the studied day. The wind speed data are given every 10 minutes. The specifications of the Polaris 50 KW wind turbines have been chosen to match IEC class II standards which are compatible with the measurements of the wind speed at the selected site [95]. The generated wind power has been calculated based on the 50 KW Polaris wind turbines specifications [95]. Figure 3.18 shows the change of tap operation for the two line regulators at phase (a) during the studied period. The results show that the number of tap operation for phases a, b and c are 56, 47 and 55 for SVR1 and 54, 60 and 64 for SVR 2, respectively. The results show that highly excessive tap operation occurs with high penetration of wind generation. Figure 3.19 shows the variation of the voltage profile at node 890 during the studied period, with and without wind generation. As shown in the figure, the voltage fluctuation increases with the high penetration of wind generation. This voltage fluctuation is not acceptable in many industrial and sensitive loads.

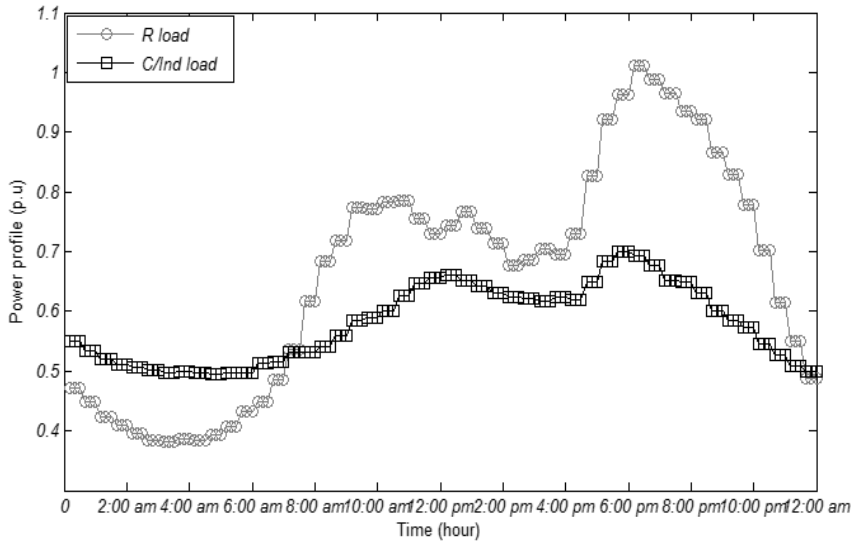

Figure 3.16: Typical residential and commercial/Industrial load profile for the studied day.

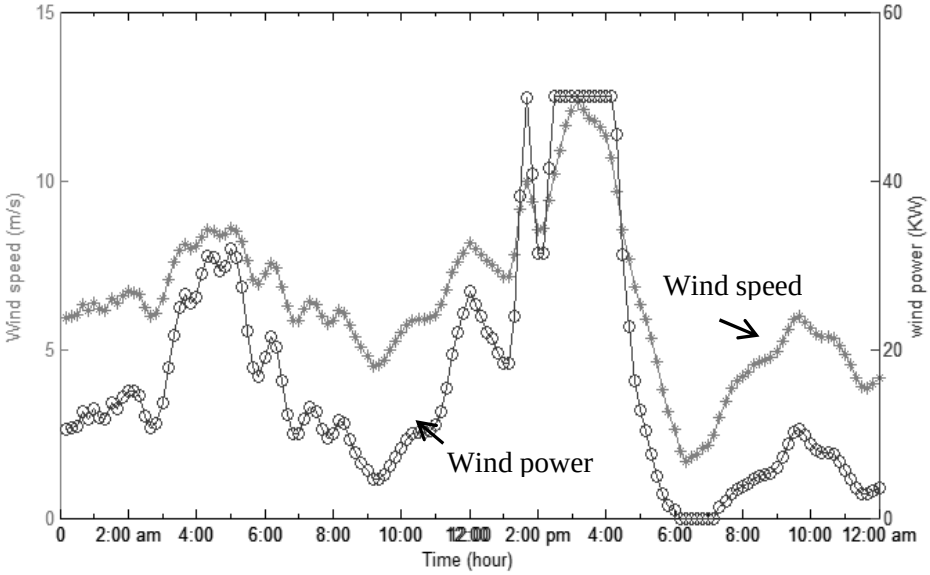

Figure 3.17: The wind speed data and the generated power profile of the 50 KW Polaris wind turbine during the studied day.

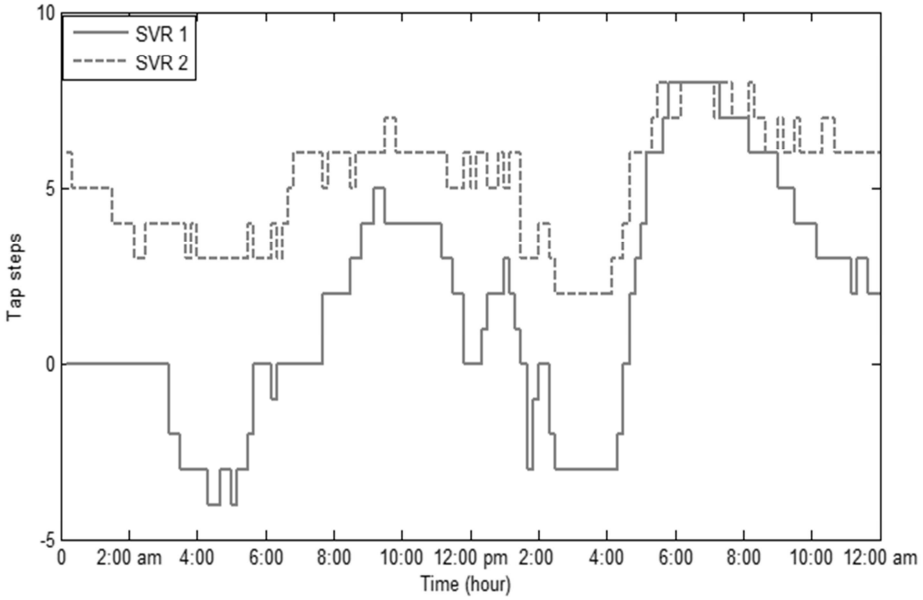

Figure 3.18: The change of tap operation of the two line regulators due to the change of the wind power during the studied day.

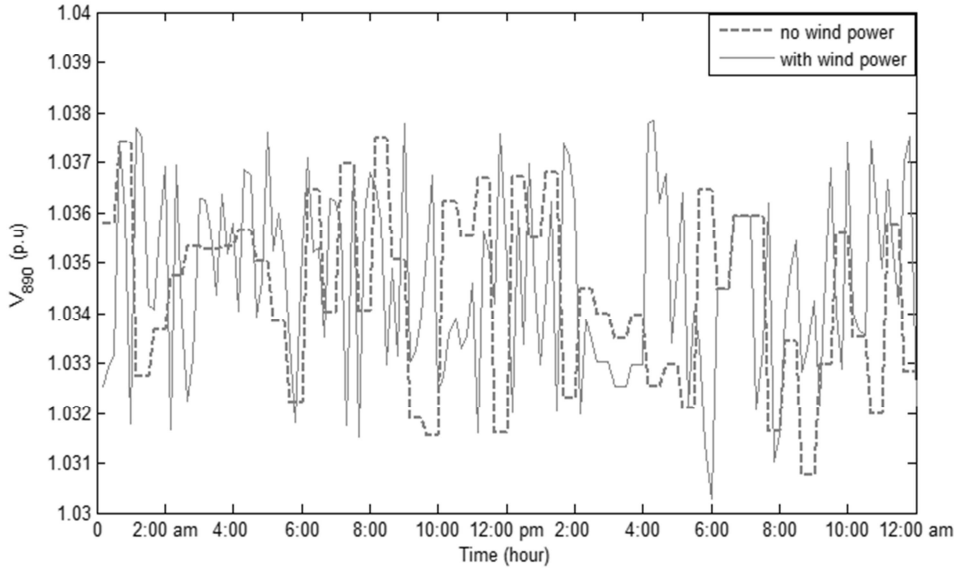

Figure 3.19: The voltage fluctuation of node 890 of the IEEE 34 bus test feeder with and without wind power generation.

3.3.3 Impacts of the DG mode of operation (studies are carried out on the IEEE 37-bus test feeder)

Table A.1 in Appendix A shows the data for eight DG units connected to the IEEE 37-bus feeder. It is assumed that all DG units have the capability to operate in PQ and PV modes except DG # 2 and 8, which operate at 0.9 lag power factors (absorb reactive power) in all operating conditions.

3.3.3.1 When DG units operate in PQ mode

First we considered that controllable DG units operate at maximum generation power and unity power factor. In this case the tap settings for SVR are 4 and 5 for phases *AB* and *CB* respectively. Figure 3.20 shows the voltage profile when all DG units operate in PQ mode and SVR operates at 4 and 5 taps compared with the voltage profile in the base case.

3.3.3.2 When DG units operate in PV mode

When a DG operates in PV mode, its voltage set point is required to be adjusted such that it doesn't conflict with other voltage control devices. To demonstrate this issue, consider that the six controllable DG units shown in Table A.1 are adjusted to regulate their local positive sequence voltage. Figure 3.21 and Figure 3.22 show the voltage profile for phase *CA* and the total real power loss after SVR actions when DG units operate in PV mode with set points equal to 1.0 and 1.025 per unit and when DG units operate with unity power factor. The figures show that the least improvement in voltage profile and total system loss is achieved with improper setting for DG units in PV mode. In contrast, the best improvement occurs when DG units operate in PV mode with proper set points.

3.3.3.3 Individual Impacts of SVR and DG units on the system performance

Figure 3.23 shows the absolute of the line voltage between phases *A* and *B* when both SVR and DG units are connected individually. As shown in the figure, SVR has a significant impact on the voltage profile. DG units cause raise in the voltage in case of unity power factor mode due to the impact of the injected active power. The raise of voltages increases when controllable DG units operate in PV mode due to the impact of the injected reactive power. Figure 3.24 shows the total real power loss at different scenarios. The figure shows that DG units have significant impact on the system power losses compared with the SVR. Moreover, DG units help in achieving greater reduction in the system real power losses during heavy loading conditions. In contrast, DG units may have negative impacts on the real power loss in case of light loading conditions.

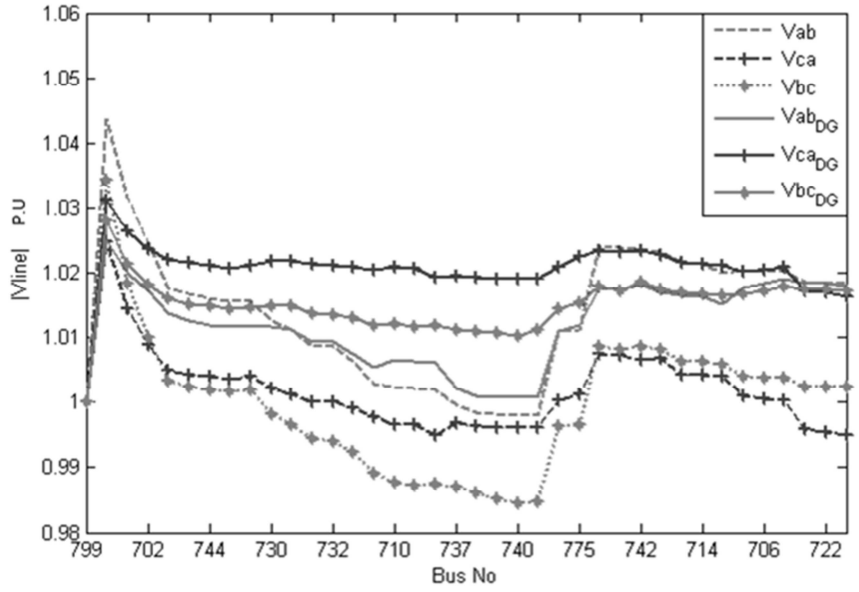

Figure 3.20: Line voltages in per unit with and without DGs when DGs operate in PQ mode

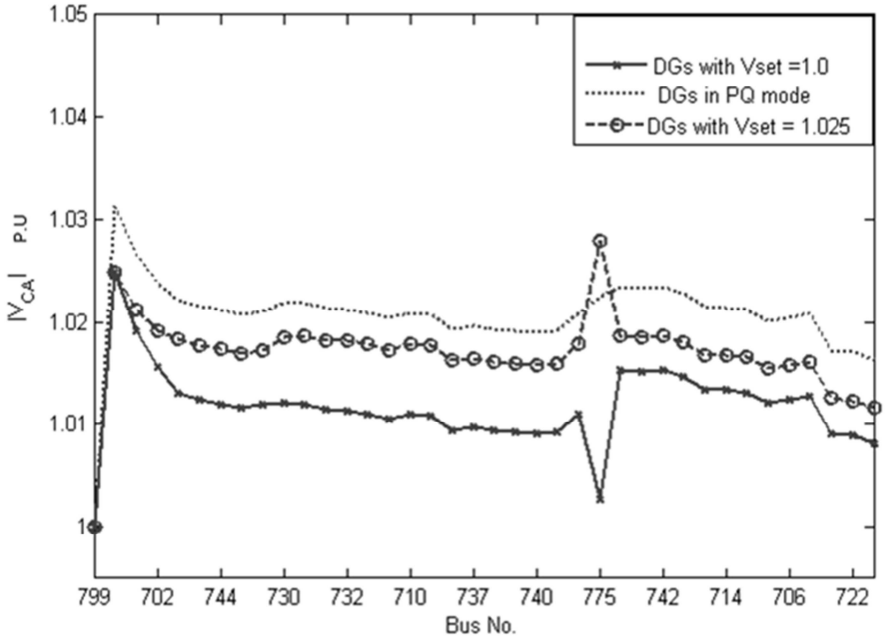

Figure 3.21: Voltage profile in per unit of the feeder after SVR operation and DGs operate at different modes and set points.

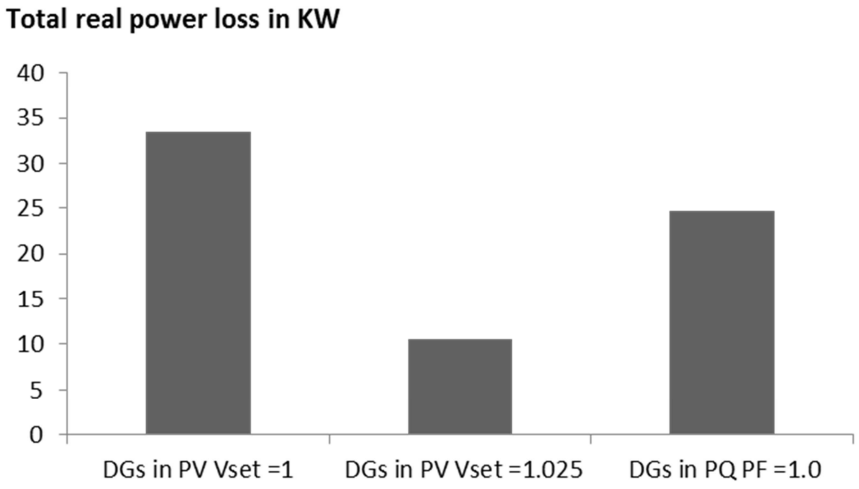

Figure 3.22: Total real power loss after SVR operation and DG units operate at different modes of operation

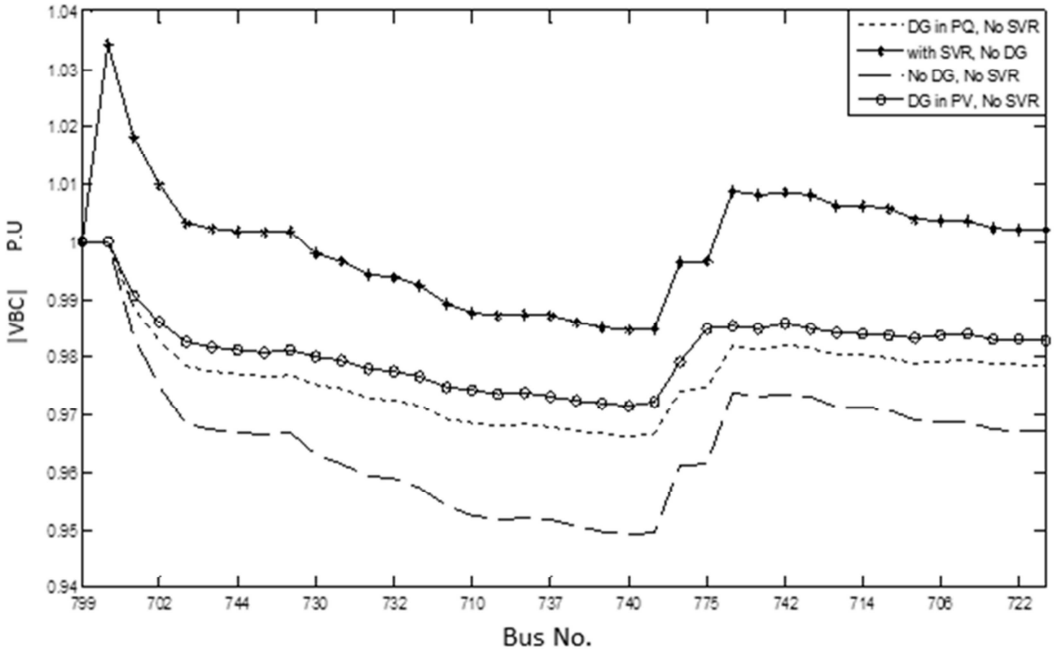

Figure 3.23: The impact of DGs and SVR on the voltage profile when they are connected individually.

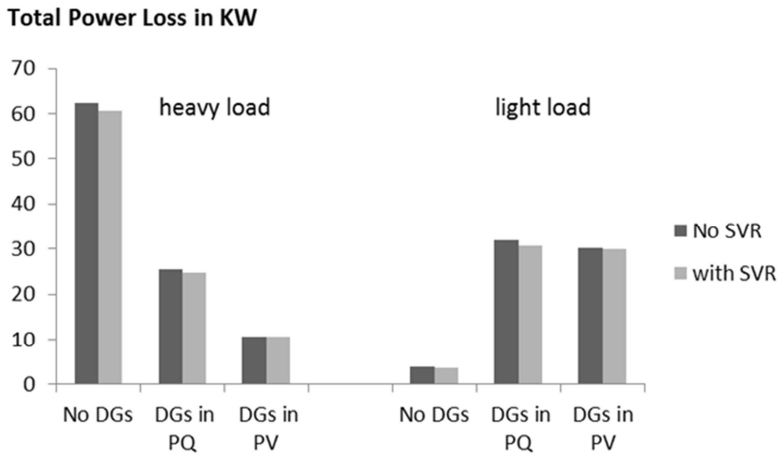

Figure 3.24: Total real power loss at different scenarios.

3.4 Discussion

In this chapter, the idea of using the element incidence matrix has been applied in solving a generalized unbalanced three phase power flow for distribution systems. This method could be easily implemented because it depends mainly on the construction of the element incidence matrices. The results have been compared with IEEE results to test the effectiveness of the proposed algorithm.

Using the developed power flow algorithm, the issues of voltage and reactive power control in distribution systems have been analyzed in order to shed the light on the potential conflicts that are expected with high DG penetration. The results show that with the existence of high DG penetration excessive wear and tear, improper decision for voltage and reactive power control devices are expected. In consequence undervoltages, overvoltages unaccepted voltage fluctuations, voltage unbalance and change in the system losses will be produced. Furthermore, the results show that voltage regulators have a powerful effect on the voltage profile if it is compared with DG units and it cannot be deactivated even with high penetration of DG units even if those units operate in PV mode. In contrast, DG units have a significant impact on the total system power losses, if it is compared with the impact of voltage regulators. Therefore, it is concluded from the studies in this chapter that utility voltage and reactive power control devices can no longer use conventional control techniques. Thus, an evolution for voltage and reactive power control techniques from their passive form to an active control is necessary.

Chapter 4

Voltage and Reactive Power Impacts on Successful Operation of Islanded Microgrids

4.1 Introduction

This chapter presents a probabilistic technique to assess the impacts of voltage and reactive power on the successful operation of islanded microgrids [96]. The assessment takes the stochastic nature of DG units and loads variability, the special operational characteristics for islanded microgrids, the different configurations of microgrids, and the microgrids dynamic stability into consideration. New reliability indices have been proposed to account for the effect of voltage and reactive power constraints. The proposed assessment technique is also used to evaluate the impact of the reactive power sharing control scheme on the probability of microgrid islanding success. To facilitate these studies, the proposed assessment technique employs a microgrid model that reflects the special characteristics of microgrid operation. Simulation studies have been carried out to validate the proposed technique.

4.2 Islanded Microgrid Model

The majority of DG units are interfaced with the utility grid via power electronic inverter systems [29-31, 97, 98]. To accommodate such DG interface in the islanded microgrid systems and overcome the limitations of centralized control schemes, decentralized droop control is usually proposed [29-31, 97, 98]. Droop controlled DG controllers in islanded microgrids are dictated to control the DG unit output voltage magnitude and frequency. Droop control realizes active power sharing by introducing droop characteristics to the frequency of the DG unit output voltage given as:

$$\omega = \omega^* - Kp \times P_G \tag{4.1}$$

where ω is the DG output voltage angular frequency, ω^* is the nominal frequency set point at no generation, Kp is the active power static droop gain, P_G is the three-phase injected active power by the DG unit. From (4.1), it can be seen that the introduced droop characteristics provide a means of feedback between the different droop-based DG units in the islanded microgrid to ensure that they are all producing voltages with the same steady state angular frequency. Similarly, the reactive power sharing among the different DG units in the microgrid is achieved through the control of the DG unit output voltage magnitude as follows:

$$|V| = V^{*} - Kq \times Q_G \tag{4.2}$$

where $|V|$ is the DG output voltage magnitude, V^{*} is the nominal output voltage magnitude set point at no generation, Kq is the reactive power static droop gain, and Q_G is the injected three-phase reactive power by the DG unit. The reactive power control is accomplished in the droop-based DG unit *d-q* frame that rotates with the angular speed ω. The output voltage magnitude is aligned to the d-axis of the DG reference frame and the output voltage q-axis component is set to zero such that the three-phase output voltages for a DG unit connected to bus *n* can be given by the inverse Park transform as follows [97]:

$$\begin{bmatrix} V_n^a \\ V_n^b \\ V_n^c \end{bmatrix} = \begin{bmatrix} v_{od,n} Cos(\omega t) \\ v_{od,n} Cos\left(\omega t - \frac{2\pi}{3}\right) \\ v_{od,n} Cos\left(\omega t + \frac{2\pi}{3}\right) \end{bmatrix} = \begin{bmatrix} |V_n| Cos(\omega t) \\ |V_n| Cos\left(\omega t - \frac{2\pi}{3}\right) \\ |V_n| Cos\left(\omega t + \frac{2\pi}{3}\right) \end{bmatrix} \tag{4.3}$$

where, v_{od} is the *d*-axis component of the DG output voltage. The selection of the static droop gains for the different droop-based DG units in the islanded microgrid can be based on different criteria including; allowable voltage and frequency regulation, DG units ratings, dynamic stability constraints, DG economics, and required sharing between the DG units.

The remainder of this section presents the details of the islanded microgrid modeling adopted in this work to facilitate the proposed microgrid islanding success studies.

4.2.1 Dynamic model:

The power electronic inverter based interfaces used in the majority of DG units forming the islanded microgrid lacks the physical inertia typically available in the synchronous generators rotating masses. This lack of physical inertia introduces a high level of susceptibility to the choice of system parameters, the system loadability and to system disturbances arising in the microgrid (including system transition between the grid-connected and islanded modes of operation) [29, 30]. In the microgrid grid-connected mode, given the relatively small sizes of the DG units, the system dynamics are mainly dictated by the main grid. As such the lack of physical inertia by the DG units does not pose a critical challenge to the microgrid system operation.

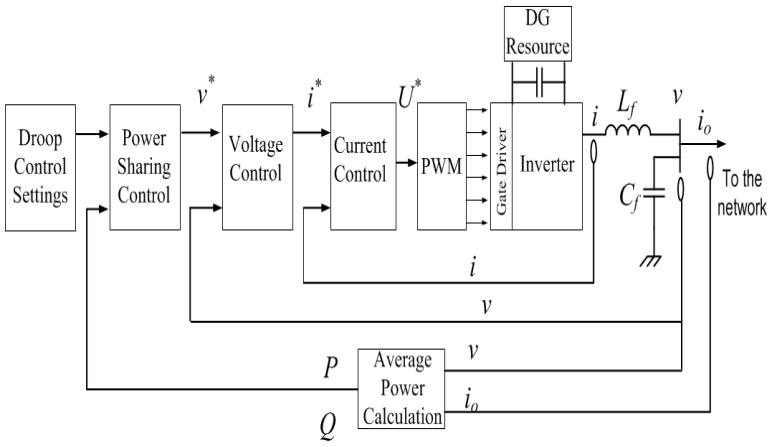

Figure 4.1: Block diagram of the power circuit and control structure of a droop controlled DG unit

On the other hand, in the islanded microgrid mode of operation, the microgrid system is dominated by power electronic inverter interfaced DG units. In this case, the microgrid is critically susceptible to oscillations resulting from system disturbances and improper choice of system parameters [29, 30]. Here, it is worth noting that recent studies have shown that the optimal choice of the islanded microgrid system parameters (e.g. static droop coefficients) can significantly enhance the microgrid stability margin and provide better robustness and disturbance rejection at a specific islanded microgrid loading state [99].

To study the dynamic behavior of the islanded microgrid system, the nonlinear time domain model of the islanded microgrid system is adopted. This model consists of the individual models of the islanded microgrid components as described by their equivalent differential equations interconnect together; namely the DG units, networks and loads.

Figure 4.1 shows a block diagram of the power circuit and control structure of a droop-controlled DG unit. The power circuit consists of a DG resource, an interfacing inverter and an output LC filter to remove the switching harmonics produced by the inverter. The control structure of the droop controlled DG unit consists of three control loops [29-31, 97, 98]. The outermost control loop is used to realize the power sharing between the different DG units in the microgrid. The power sharing control loop achieves the required power sharing functionality through generating the reference magnitude and frequency of the fundamental output voltage at the PCC according to the droop characteristics described by (4.1) and (4.2). The middle control loop is used to control the voltage across the LC filter capacitor by generating the reference signal of the LC filter inductor current. The inner most control loop is the current loop, which is

used to control the LC filter inductor current by generating the inverter reference output voltage i.e. the gating signals.

In [29, 30] it was shown that the dominant dynamics of droop controlled DG units in islanded microgrid systems are mainly dictated by the droop/power controller of the DG unit. Accordingly, it was concluded that the dynamic model of the droop/power controller can be used as a simplified model to represent the droop controlled DG unit in the islanded microgrid dynamic studies. This conclusion has been further investigated and verified in previous microgrid dynamic studies [100]. Accordingly, in this work the droop based DG units are represented by the differential equations modeling the behavior of the power/droop controller.

The differential equations describing the behavior of each droop-based DG unit are written in the respective DG unit *d*-*q* frame that rotates synchronously with the DG unit's output voltage angular speed. The reference frame of one of the islanded microgrid DG units is arbitrary chosen as a common reference frame for the islanded microgrid. For the n^{th} droop-based DG unit, the differential equations describing its behavior can be given as [29-31, 97, 98] :

$$\dot{\delta}_n = \omega_n^* - Kp_n \times P_{G,n} - \omega_{com} \tag{4.4}$$

$$\dot{P}_{G,n} = \frac{3}{2}\omega_c \left[V_n^* \times i_{od,n} - Kq_n \times Q_{G,n} \times i_{od,n}\right] - \omega_c \times P_{G,n} \tag{4.5}$$

$$\dot{Q}_{G,n} = -\frac{3}{2}\omega_c \left[V_n^* \times i_{oq,n} - Kq_n \times Q_{G,n} \times i_{oq,n}\right] - \omega_c \times Q_{G,n} \tag{4.6}$$

where ω_c is the cut-off frequency of the low-pass filter used to obtain the real and reactive powers P_G and Q_G corresponding to the fundamental component from the measured output voltage and currents, i_{od} and i_{oq} are the *d*-axis and *q*-axis components of the DG output currents, respectively, ω_{com} is the rotating frequency of the common reference frame *D*-*Q*, and δ_n represents the angle between the droop-based DG unit reference frame and the common reference frame. From (4.4) it can be seen that $\dot{\delta}_{com} = \delta_{com} = 0$.

To incorporate the individual droop-based DG units' respective models in the complete islanded microgrid dynamic model, the individual droop-based DG unit models are transformed to the common reference frame. The transformation from the n^{th} reference frame d_n-q_n to the common reference frame *D*-*Q* can be given as [29]:

$$\begin{bmatrix} f_D \\ f_Q \end{bmatrix} = \begin{bmatrix} Cos\delta_n & -Sin\delta_n \\ Sin\delta_n & Cos\delta_n \end{bmatrix} \begin{bmatrix} f_{d_n} \\ f_{q_n} \end{bmatrix} \tag{4.7}$$

DG units operating in constant PQ mode are controlled to inject a pre-specified amount of power, i.e. the operation of such units is independent on the microgrid mode of operation (whether islanded or grid connected). Therefore such DG units do not contribute in the control of the islanded microgrid system voltage and frequency. Consequently the dynamic model of such DG units in the islanded microgrid system is similar to the conventional grid-connected voltage source inverter dynamic model [101].

Dynamic studies of conventional power systems usually represent the system network by the nodal admittance matrix equation. The rational is that the time constant of the network elements is usually smaller than that of the synchronous machine-based generation systems. On the other hand, in islanded microgrid systems the time constant of the DG units' power electronic inverter-based interface is comparable to that of the network elements. Accordingly, the network dynamics can affect the overall system stability and dynamic performance. Consequently, in this work the system network is represented by writing the differential equations describing its elements. In the *D-Q* frame, the differential equations describing the line connecting buses *j* and *k* is given as:

$$\dot{i}_{Line,D} = -\frac{R_{Line}}{L_{Line}} \times i_{Line,D} + \omega_{com} \times i_{Line,Q} + \frac{v_{j,D}}{L_{Line}} - \frac{v_{k,D}}{L_{Line}} \tag{4.8}$$

$$\dot{i}_{Line,Q} = -\frac{R_{Line}}{L_{Line}} \times i_{Line,Q} - \omega_{com} \times i_{Line,D} + \frac{v_{j,Q}}{L_{Line}} - \frac{v_{k,Q}}{L_{Line}} \tag{4.9}$$

where R_{Line} and L_{Line} are the line resistance and inductance, respectively.

Loads are represented in the dynamic model by their equivalent admittance [102]. For an RL load connected at bus *n*, the differential equations describing the load behavior can be given in the *D-Q* frame as follows:

$$\dot{i}_{Load,D} = -\frac{R_{Load}}{L_{Load}} \times i_{Load,D} + \omega_{com} \times i_{Load,Q} + \frac{v_{n,D}}{L_{Load}} \tag{4.10}$$

$$\dot{i}_{Load,Q} = -\frac{R_{Load}}{L_{Load}} \times i_{Load,Q} - \omega_{com} \times i_{Load,D} + \frac{v_{n,Q}}{L_{Load}} \tag{4.11}$$

where R_{Load} and L_{Load} are the load resistance and inductance, respectively. Similar equations can be derived for leading PF loads.

To incorporate the network and load models into the overall islanded microgrid model, the voltage at the different system buses is expressed in terms of the system currents. Assuming a sufficiently large virtual resistor R_n between each bus and the ground, the voltage at bus n can be written as

$$v_{n,DQ} = R_n\left(\sum i_{on,DQ} - \sum i_{Load\,n,DQ} + \sum i_{Line\,n,DQ}\right) \tag{4.12}$$

where $\sum i_{on,DQ}$ is the summation of the DG currents injected to bus n, $\sum i_{Load\,n,DQ}$ is the summation of the currents flowing into the different loads connected to bus n, and $\sum i_{Line\,n,DQ}$ is the summation of the currents injected to bus n from the different lines connected to bus n.

The dynamic simulation is then performed by numerically solving the set of differential equations representing the islanded microgrid system. The dynamic model is initialized using a suitable load flow algorithm [89, 97] depending on the initial state under consideration. In this work, the set of differential equations describing the dynamic behaviour of islanded microgrid is solved by a modified *Rosenbrock* formula implemented using the "*ode*" routine given in Matlab. For unbalanced islanded microgrid systems, the dynamic system modeling is performed using the positive sequence component.

4.2.2 Steady-state model:

The steady-state behavior of the islanded microgrid can be simulated by solving the set of power flow equations describing the islanded microgrid. Conventional distribution systems power flow algorithms are not suitable for the islanded microgrid case because; 1) in the conventional power flow formulation, the representation of a DG unit as slack bus means that this DG unit is treated as an infinite bus capable of holding the system frequency and its local bus voltage constant. This representation does not reflect the microgrid configuration where an islanded microgrid system is typically fed from a group of DG units of small and comparable sizes and there is no one generation unit capable of performing the slack bus function. Furthermore, if we consider the DG units owners perspectives, it will be difficult to guarantee the availability of a DG unit that is willing to operate as a slack bus at the time of the microgrid islanding. 2) In conventional power flow formulation, the representation of the DG units as PV/PQ buses, assumes that the required active power generation and/or local voltage at each DG unit are pre-specified. However, this representation does not reflect the reality of the decentralized droop control based microgrid

operation, where both the generated active power and the local voltage at each DG unit are determined locally based on the droop characteristics.

Accordingly, for studying the power flow in an islanded microgrid, there is a need for a new power flow algorithm. This chapter presents a power flow formulation that incorporates the different DG operating modes in a set of nonlinear equations describing the power flow problem in unbalanced islanded microgrid systems. The presented power flow formulation for islanded microgrids takes into accounts that [97];

1- The system frequency acts as a communication medium between the different DG units in the microgrid,

2- The system steady state frequency is not pre-specified and needs to be calculated,

3- There is no slack bus in the system,

4- The generation of active and reactive power from different DG units might be governed by their droop characteristics

The developed algorithm incorporates the different DG operating modes i.e. droop and PQ in a set of nonlinear equations describing the power flow problem in islanded microgrid systems in terms of the different node voltages and power injections. The power mismatch equations for PQ nodes are similar to conventional power flow algorithms [97]. For each PQ node, there are 6 equations describing the relation between the bus voltage magnitudes and angles in three phase systems (i.e. active and reactive power mismatch equations in each phase).

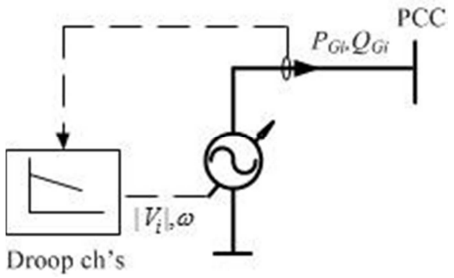

Figure 4.2: Steady-state model of a DG unit operating in droop mode.

Figure 4.2 shows the steady-state, fundamental frequency, power flow model of a DG unit operating in droop mode. As shown in the figure, the DG units operating in the droop mode, comprising the energy resource, the output filter and the power electronic converter, are modeled as an ideal voltage source whose voltage magnitude and frequency are determined using droop equations in (4.1) and (4.2), which are in compliance with the IEEE standard 1547.4 for DG islanded systems [22]. This model is sufficient to calculate steady-state operating point for the electrical variables at the PCC of each DG unit operating in droop mode irrespective of the internal power circuit and control structure of the DG unit used. The internal components of DG units operating in droop mode, including the power electronic interface converter, the output filter, the energy resource and the DG units control structure, do not affect the power flow solution.

The power flow model of droop-based DG units, shown in Figure 4.2, is incorporated in the power flow algorithm proposed in [97]; where for each node *i* connected with a DG unit operating in droop-mode, the power flow equations are given as follow:

$$0 = P_{Li}^{a,b,c}(\omega, |V_i^{a,b,c}|) - P_{Gi}^{a,b,c} + P_i^{a,b,c}(Y_{ij}(\omega), \left|V_i^{a,b,c}\right|, \left|V_j^{a,b,c}\right|, \delta_i^{a,b,c}, \delta_j^{a,b,c}) \tag{4.13}$$

$$0 = Q_{Li}^{a,b,c}(\omega, |V_i^{a,b,c}|) - Q_{Gi}^{a,b,c} + Q_i^{a,b,c}(Y_{ij}(\omega), \left|V_i^{a,b,c}\right|, \left|V_j^{a,b,c}\right|, \delta_i^{a,b,c}, \delta_j^{a,b,c}) \tag{4.14}$$

$$0 = \left|V_i^a\right| - \left|V_i^b\right| \tag{4.15}$$

$$0 = \left|V_i^a\right| - \left|V_i^c\right| \tag{4.16}$$

$$0 = \delta_i^a - \delta_i^b - (2\pi/3) \tag{4.17}$$

$$0 = \delta_i^a - \delta_i^c + (2\pi/3) \tag{4.18}$$

$$0 = P_{Gi}^a + P_{Gi}^b + P_{Gi}^c - P_{Gi}(\omega) \tag{4.19}$$

$$0 = Q_{Gi}^a + Q_{Gi}^b + Q_{Gi}^c - Q_{Gi}(|V_i^{a,b,c}|) \tag{4.20}$$

where $P_{Li}^{a,b,c}$ and $Q_{Li}^{a,b,c}$ are the active and reactive load power at each of the three phases at bus *i*, respectively; $P_i^{a,b,c}$ and $Q_i^{a,b,c}$ denote the calculated real and reactive power injected to the microgrid at each of the three phases at bus *i*, respectively; $P_{Gi}^{a,b,c}$ and $Q_{Gi}^{a,b,c}$ denote the generated real and reactive power at each of the three phases at bus *i*, respectively; P_{Gi} and Q_{Gi} denote the total generated real and reactive power of the three phases at bus *i*, respectively; $|V_i|^{a,b,c}$ is the voltage magnitude at each of the three phases at bus *i*, $\delta_i^{a,b,c}$ is the voltage angle at each of the three phases at bus *i* and *j* represents the set of nodes connected to bus *i*; $Y_{ij}(\omega)$ is the branch admittance element between node *i* and other node *j* [97] . As shown in (4.13)-(4.20), the corresponding vector x_{Di} of unknown power flow variables for droop-bus *i* is given as:

$$x_{Di} = [\delta_i^{a,b,c} \; |V_i^{a,b,c}| \; P_{Gi}^{a,b,c} \; Q_{Gi}^{a,b,c}]^T \tag{4.21}$$

Accordingly, the system of equations describing the power flow in an islanded microgrid of n_{pq} PQ nodes and n_{droop} droop nodes is made of n_{system} equations comprising n_{system} unknowns (including the system steady-state frequency) and n_{system} can be given as:

$$n_{system} = 6 \times n_{pq} + 12 \times n_{droop} \tag{4.22}$$

An arbitrary bus is taken as the system reference by setting its angle to zero i.e. $\delta_{arbitrary}^a = 0$. Typically the DG units are equipped with a current limiter to limit the production of the DG unit to its rated active and reactive capacities $P_{G,\max}$ and $Q_{G,\max}$. To take the DG current limits in consideration in the power flow formulation, the calculated DG active and reactive power generations are compared with their

specified limits. If the calculated power violates its limits, the DG switches from droop-mode to PQ mode and the specified power is kept at the limit value.

A Newton-Trust region method has been used in this work to solve the power flow problem in islanded microgrids [103]. Trust region methods are simple and powerful tools for solving systems of nonlinear equations and large scale optimization problems. Initially they were developed to solve unconstrained optimization problems (i.e. set of nonlinear equations). These methods behave like the Newton-Raphson algorithms featuring a quadratic convergence. Furthermore, they have the advantages of guaranteeing a solution whenever it exists [103] .

4.3 The proposed probabilistic analytical assessment approach:

In this section, a probabilistic analytical approach is presented to calculate the probability of microgrid islanding success and consequently the newly formulated supply adequacy and reliability indices that account for the role of voltage and reactive power constraints. The proposed approach is divided into three steps. In the first step, the probability of creating an island will be determined; this depends on the system configuration, the failure rate, and the repair time of the system components. In the second step, depending on the stochastic behavior of the loads and the wind generation as well as the failure rate of the DG units that are connected to the island, the combined generation load model describing all the possible microgrid states and their respective probabilities are developed. Based on the microgrid states probabilities calculated in the second step, the probability of microgrid islanding success and the newly formulated reliability indices are calculated in the third step. Detailed elaboration of the techniques utilized to carry out each step is hereunder.

4.3.1 Step 1: probability of island creation

In order to measure the probability of island creation, the unavailability U_{up} of the higher level system; upstream of the IID, should be calculated. The unavailability of the upstream system depends on a set $\left\{N_{com}^{up}\right\}$ which contains all the components in the series path between the area EPS and the island under study including the main substation itself. This means that a failure of any component *com* in this path requires waiting the repair time r_{com} of this component in order to successfully restore the power.

$$U_{up} = \sum_{com \in \left\{N_{com}^{up}\right\}} \lambda_{com} r_{com} \tag{4.23}$$

where λ_{com} is the failure rate of component *com*. Hence the probability of fault occurrence in the upstream network ρ_{up} can be calculated as follows:

$$\rho_{up} = \frac{U_{up}}{8760} \tag{4.24}$$

If a fault occurs inside the microgrid due to a failure of one of the microgrid lines, it is assumed that the island will not be created. Accordingly, the probability of island to be uncreated due to a line fault inside the microgrid $\rho_{uncreated}$ is calculated as follows:

$$\rho_{uncreated} = \frac{\sum_{com \in \left\{N_{com}^{in}\right\}} \lambda_{com} r_{com}}{8760} \tag{4.25}$$

where $\left\{N_{com}^{in}\right\}$ is the set containing all the lines inside the microgrid. The probability of islanding creation ρ_{island} is calculated based on (4.24) and (4.25) as:

$$\rho_{island} = \left(1 - \rho_{uncreated}\right) \times \rho_{up} \tag{4.26}$$

4.3.2 Step 2: combined generation load model

An island can be created if and only if there is enough generation to match the island total load and losses. Given the stochastic nature of both the generation and load in the microgrid, a combined generation load model is analytically developed to describe all the possible microgrid states and their respective probabilities. This analytical approach has been previously validated by comparison with MCS in [35, 36]. Assuming that the probabilities of the generation states $\rho_{gen.,state}\left\{s_{gen}\right\}$ are independent on the probabilities of the load states $\rho_{load,state}\left\{s_{load}\right\}$, the probabilities of microgrid states $\rho_{\mu g,State}\left\{s_{\mu g}\right\}$ describing different possible combination of generation and load states can be obtained by convolving their respective probabilities as follows

$$\rho_{\mu g,State}\left\{s_{\mu g}\right\} = \rho_{gen.,state}\left\{s_{gen}\right\} * \rho_{load,state}\left\{s_{load}\right\} \tag{4.27}$$

where $\{s_{gen}\}$ is the set of all possible generation states, $\{s_{load}\}$ is the set of all possible load states, and $\{s_{\mu g}\}$ is the set of all possible microgrid states. Based on this concept, the generation load model for the microgrid can be obtained by listing all possible combinations of generation output power states and load states. Similarly, the different generation states are composed by convolving generation states probabilities based on the state model of each type of DG units. For two DG units with different state models, the combined generation states model can be obtained as follows:

$$\rho_{gen.,state}\{s_{gen}\} = \rho_{DG_1,state}\{s_{DG_1}\} * \rho_{DG_2,state}\{s_{DG_2}\} \tag{4.28}$$

where $\{s_{DG_1}\}$ and $\{s_{DG_2}\}$ are the set of all possible generation states for DG_1 and DG_2 respectively.

Generally, generation states model for non-dispatchable DG units are calculated by dividing the continuous probability density function into several states. For instance, the wind generation states are calculated by dividing the continuous wind annual probability density function (PDF) into several wind speed states with a step of 1 m/sec. In order to consider the probability of wind turbines failure, the wind turbine forced outage rate (FOR_{wind}) is used with wind speed states to calculate the wind output power state $\rho_{wind,State}$. As such the probability of a wind state *s* can be calculated as follows:

$$\rho_{wind,State(s)} = \left(\int_{v_{s,\min}}^{v_{s,\max}} f(v).dv \right) \times \left(1 - FOR_{wind}\right) \tag{4.29}$$

where $f(v)$ is the distribution probability of wind speed, $v_{s,\,min}$ and $v_{s,\,max}$ are the wind speed limits of state *s*.

On the other hand, dispatchable generation units are usually represented by the two states model. The probability that the dispatchable generation unit is out of service is equal to its forced outage rate ($FOR_{disp.}$). On the other hand, the probability that a dispatchable generator can generate its rated power can be calculated by using $FOR_{disp.}$ as follows:

$$\rho_{disp,state} = 1 - FOR_{disp} \tag{4.30}$$

4.3.3 Step 3: calculation of islanding failure / success probability

Unlike the previous studies which only considered active power adequacy, in this work shortage in reactive power, dynamic stability and voltage constraints at the different load points are considered along

with the active power as necessary conditions for islanded microgrid success. Based on the generation-load model described in step 2, the necessary but insufficient condition for microgrid islanding success is checked for each microgrid state using

$$\begin{cases} S_{G\max}(s) \geq S_L(s) + S_{Loss}(s) \\ \& \\ Q_{G\max}(s) \geq Q_L(s) + Q_{Loss}(s) \end{cases} \tag{4.31}$$

where, $S_{Gmax}(s)$ is the apparent power capacity of the DG units, $S_L(s)$ is the load apparent power, $Q_{Gmax}(s)$ is the reactive power capacity of the DG units, $Q_L(s)$ is the load reactive power and $Q_{Loss}(s)$ is the reactive power loss and spare capacity. $S_{Loss}(s)$ is the apparent power loss and security margin. Security margin is considered to enable the microgrid to respond to unexpected and sudden increase in the local power demand [104]. Different options can be used to define the security margin for the islanded microgrid. One of these options is to define the security margin to represent a certain amount of reserve power. Accordingly in this work, the power reserve was arbitrarily defined as 5% of the total demand in the microgrid [104]. The power loss in the island is considered to be 5% of the microgrid demand. Thus, the probability of microgrid islanding failure due to insufficient generation $\rho_{fail}^{mismatch}$ and the consequent expected active power not supplied $TW_{fail}^{mismatch}$ can be calculated as follow:

$$\rho_{fail}^{mismatch} = \sum_{s=1}^{n_{state}} \rho_{\mu g\_state}(s); \quad \forall \begin{cases} S_{G\max}(s) < S_L(s) + S_{Loss}(s) \\ or \\ Q_{G\max}(s) < Q_L(s) + Q_{Loss}(s) \end{cases} \tag{4.32}$$

$$TW_{fail}^{mismatch} = \sum_{s=1}^{n_{state}} TW_{\mu g\_state}(s) \times \rho_{\mu g\_state}(s); \forall \begin{cases} S_{G\max}(s) < S_L(s) + S_{Loss}(s) \\ or \\ Q_{G\max}(s) < Q_L(s) + Q_{Loss}(s) \end{cases} \tag{4.33}$$

where n_{state} is the total number of microgrid states and $TW_{\mu g\_state}(s)$ is the total active power demand of the islanded microgrid for state s and it is given as follow:

$$TW_{\mu g\_state}(s) = \sum_{i=1}^{n_{bus}} W_{\mu g\_state}(s,i) \tag{4.34}$$

where, $W_{\mu g\_state}(s,i)$ is the active power demand of load point i at state s. Conventionally, supply adequacy including the loss of load probability LOLP, the loss of load expectation LOLE, the loss of energy expectation LOEE can be calculated as follow:

$$LOLP = \rho_{island} \times \rho_{fail}^{mismatch} \tag{4.35}$$

$$LOLE(hr/year) = LOLP \times 8760 \tag{4.36}$$

$$LOEE(MWh/year) = \left(\rho_{island} \times 8760\right) \times TW_{fail}^{mismatch} \tag{4.37}$$

The supply adequacy indices shown in (4.35)-(4.37) designate the ability of the DG units in the islanded microgrid to meet the load demand during all possible microgrid states in terms of having sufficient generation capacity. Note that the supply adequacy indices are calculated only when the microgrid is created. Therefore, the loss of load probability $\rho_{uncretad}$ and the loss of load duration ($\rho_{uncretad}$ *8760) when the microgrid is uncreated are not considered in the supply adequacy indices and it is considered only in the customers reliability indices. In the conventional microgrid reliability studies all load points in the entire microgrid are treated as one customer and, therefore, the average interruption duration index SAIDI can be calculated as follow

$$SAIDI = LOLE + \rho_{uncreated} \times 8760 \tag{4.38}$$

Equations (4.35)-(4.38) do not consider the probability of microgrid instability and unsatisfactory operation arising from voltage violations at different load points. To consider the microgrid instability, dynamic simulations are carried out using the dynamic model described in section 4.2.1. The microgrid stability at each state *s* is assessed using two sequential stages. The first stage investigates the dynamic behaviour of the islanded microgrid during and subsequent to the transition from grid-connected to islanded mode. The second stage investigates the dynamic behaviour of the islanded microgrid operation during and subsequent to small changes in the demand. Only if active and reactive power sharing stabilization is achieved in both stages without overshooting beyond any of the system operational boundaries (i.e. generated power, current and frequency), the microgrid is considered to be successful. The initial operating conditions for the dynamic simulations for the first stage at each state are extracted by running the generic power flow algorithm presented in *chapter 3* [89] for the microgrid during the grid connected mode. Such initial conditions consider that all available droop-based DG units are operated in

PQ mode with zero output power. Thus the probability of microgrid success $\rho_{success}$ considering both mismatch and dynamic stability can be obtained as follows:

$$\rho_{success} = 1 - \rho_{fail} \tag{4.39}$$

where, ρ_{fail} is the total probability of microgrid failure due to insufficient generation and dynamic instability. Accordingly, the adequacy and reliability indices given in (4.35)-(4.38) can be reformulated considering both insufficient generation and dynamic instability. In this case the corresponding expected active power not supplied due to insufficient generation or dynamic instability TW_{fail} is given by

$$TW_{fail} = \sum_{s=1}^{n_{state}} TW_{\mu g\_state}(s) \times \rho_{\mu g\_state}(s);\ \forall s \notin \left\{S^{success}\right\} \tag{4.40}$$

where, $\left\{S^{success}\right\}$ is the set of all successful islanded microgrid states.

The ANSI voltage standard [11] shows that sustained voltage levels falling outside range B will result in unsatisfactory operation of utilization equipment and overvoltages/undervoltages protective devices shall operate to protect such equipment. Accordingly, even if the microgrid is successful at a given state, still some load points might not be served due to violating the voltage constraints. Therefore, calculating the probability of voltage violation at any load point within the microgrid during the islanded microgrid operation should be considered.

For each state *s* at which the microgrid is successful, the islanded microgrid power flow algorithm in section 4.2.2 is computed. After convergence of the power flow algorithm, the voltage magnitude in each load point *i* at state *s*, *V(s,i),*is compared with the specified limits V_{high} and V_{low} described in [11].

$$V_{high} \geq V(s,i) \geq V_{low} \tag{4.41}$$

Thus, the probability that a voltage violation exists at any load point ρ_{VV} within the microgrid during the islanded operation can be given as:

$$\rho_{VV} = \sum_{s=1}^{n_{state}} \rho_{\mu g\_state}(s);\ \forall s \in \left\{S^{success}\right\} \& \left(\exists \left\{V(s,i) > V_{high}\ or\ V(s,i) < V_{low}\right\}\right) \tag{4.42}$$

The status of the operation of the individual load points in particular can be determined based on the designed undervoltages/overvoltages protection schemes. However, even if the load points do not have

their own protection devices, due to their unsatisfactory operation in case of voltage violation [11], they should be accounted as interrupted loads. Accordingly in this work, it is assumed that the voltage violation at some load points will result in an interruption of these load points. The new adequacy indices are reformulated to include the effect of partial loss of loads due to voltage violation in the islanded microgrid as follow:

$$TLOLP = \rho_{island} \times \left(\rho_{fail} + \rho_{VV} \right) \tag{4.43}$$

$$TLOLE\left(hr / year\right) = TLOLP \times 8760 \tag{4.44}$$

$$TLOEE(MWh / year) = \left(\rho_{island} \times 8760 \right) \times \left(TW_{fail} + TW_{partial} \right) \tag{4.45}$$

where TLOLP is the total loss of load probability, TLOLE is the total loss of load expectation and TLOEE is the total loss of energy expectation considering the voltage violation; $TW_{partial}$ is the expected partial power not served due to voltage violation and it represents the summation of the loss of energy expectation at all load points entire the microgrid as shown in (4.46).

$$TW_{partial} = \sum_{i=1}^{n_{bus}} W_{VV}(i) \tag{4.46}$$

where W_{VV} represents the expected active power not served at load point i due to voltage violation and it can be given as follow:

$$W_{VV}(i) = \sum_{s=1}^{n_{state}} W_{\mu g\_state}(s,i) \times \rho_{\mu g\_state}(s);\ \forall\ s \in \left\{ S^{success} \right\} \& \left(\exists \left\{ V(s,i) > V_{high}\ or\ V(s,i) < V_{low} \right\} \right) \tag{4.47}$$

The probability that load point i is not served during the islanding operation due to voltage violation can be given as follow:

$$\rho_{unserved}(i) = \sum_{s=1}^{n_{state}} \rho_{\mu g\_state}(s);\quad \forall s \in \left\{ S^{success} \right\} \& \left\{ V_{high} < V(s,i)\ or\ V_{low} > V(s,i) \right\} \tag{4.48}$$

While the probability that load point i is served during the microgrid islanding is given as follow:

$$\rho_{served}(i) = 1 - (\rho_{fail} + \rho_{unserved}(i)) \tag{4.49}$$

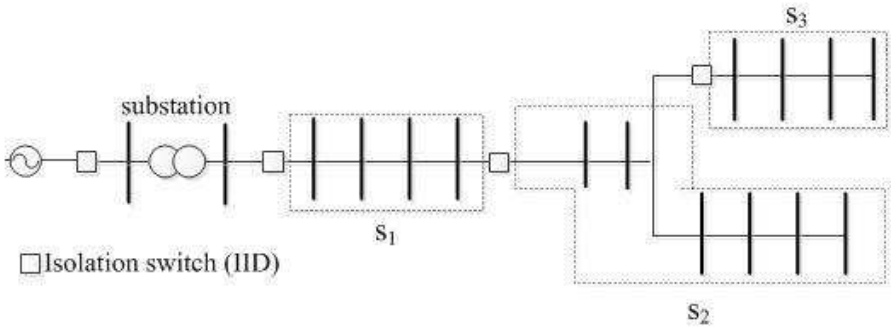

Figure 4.3: Simple radial distribution network

Thus, it is possible to define the interruption duration at each load point *i* considering one created microgrid using:

$$U_{mg}(i) = U_{no,mg}(i) - \rho_{island} \times \rho_{served}(i) \times 8760 \tag{4.50}$$

where $U_{no,mg}$ is the interruption duration with no microgrids formation. It is worth noting that a load point can belong to different possible microgrid configuration depending on the fault and isolation switches locations. Figure 4.3 shows a typical radial distribution system. As shown in the figure, the distribution system is modeled in terms of segments. Each segment is a group of components with only one isolation switch at its upstream. Based on this structure, one islanded microgrid will be created to include all downstream segment(s) if and only if a fault occurs at their upstream segment. For instance, a microgrid will be created containing s_2 and s_3 if and only if a fault occurs at s_1. Depending on the locations of the isolation switches and faults, for a load point *i* falling in more than one possible microgrid, the outage duration can be calculated using:

$$U(i) = U_{no,mg}(i) - \sum_{m=1}^{MG} \rho_{island} \times \rho_{served}(i) \times 8760 \tag{4.51}$$

where, *MG* is the number of possible microgrids containing load point *i*. Consequently, using the interruption duration of each load point that considers all possible microgrid formation, it is possible to give the *SAIDI* as follow:

$$SAIDI = \frac{\sum_{i=1}^{n_{bus}} U(i) * N(i)}{\sum_{i=1}^{n_{bus}} N(i)} \quad (4.52)$$

where, *N(i)* is the number of customers connected at load point *i*. The above calculations in (4.31)-(4.52) give the Local Distribution Company (LDC) and the microgrid customers a good indication not only on the impact of the sufficiency of active power generation but also on the impact of reactive power, dynamic stability and voltage constraints on the adequacy and reliability evaluation of the islanded microgrid operation. Figure 4.4 shows a flowchart that summarizes the proposed probabilistic approach.

4.4 Case Studies

Traditionally, the reliability and supply adequacy studies do not consider whether the system under study is balanced or unbalanced. However, given that the proposed approach requires a detailed islanded microgrid simulation model, the nature of the system under study (i.e. balanced or unbalanced) has to be considered. In this section, balanced and unbalanced radial distribution test systems have been used to test the effectiveness of the proposed algorithm. The proposed algorithm was implemented in MATLAB environment. Different case studies have been carried out to evaluate the microgrid success and reliability indices under different conditions that affect the system operation. Different scenarios have been considered in each case study to show the impact of different assessment criteria on the islanded microgrid probability of success, supply adequacy and reliability indices. In the first scenario, the islanding is assumed to be not allowed. In the second scenario the assessment criterion is based on the active power only. In the third scenario, the assessment criterion is based on the active and reactive power generation-load mismatch. In the fourth scenario, the assessment criterion is based on the active power, reactive power as well as the stability consideration. The fifth scenario is similar to the fourth scenario; however it is assumed that voltage violation at any load point will result in an interruption of this load point only.

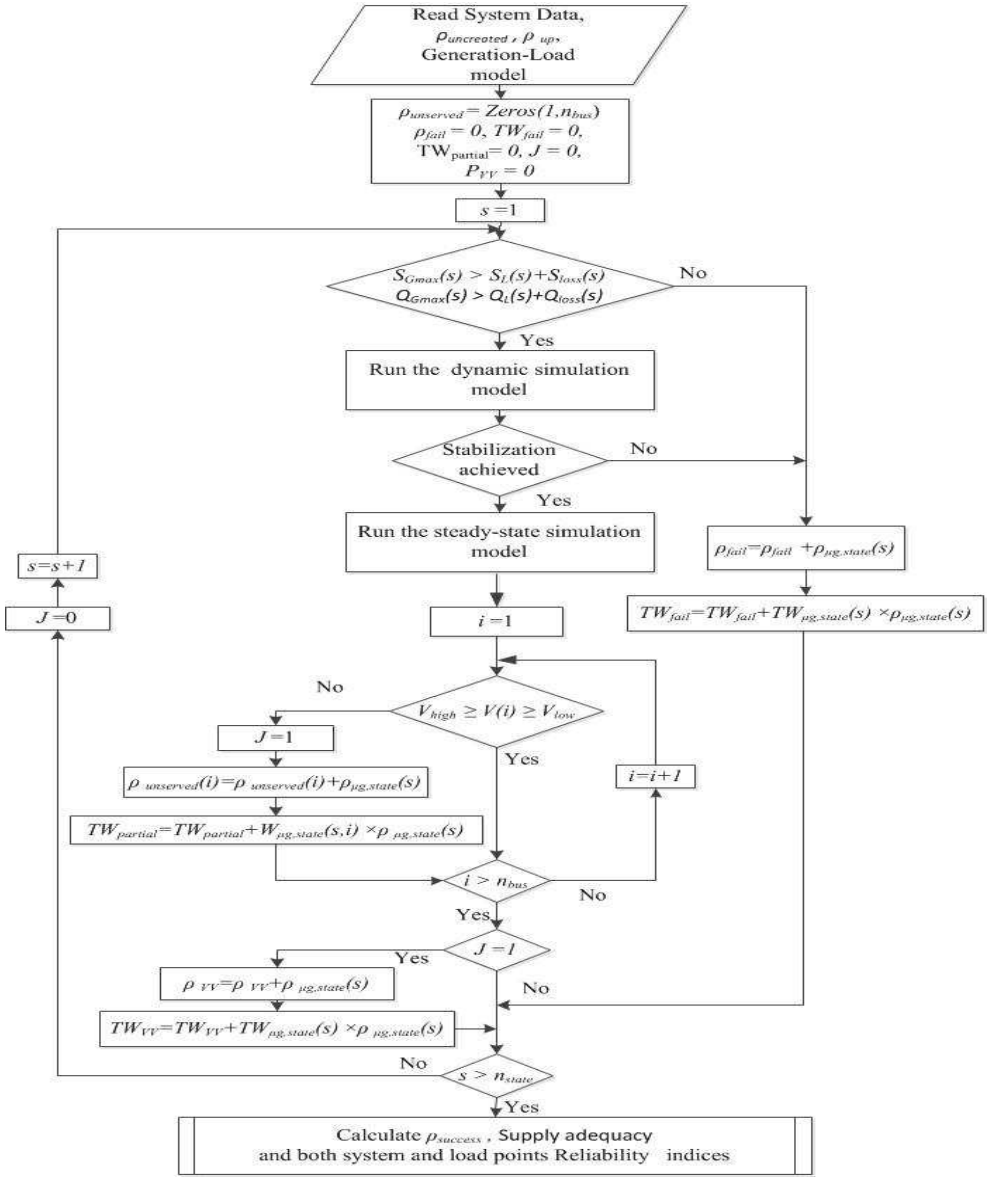

Figure 4.4: A flowchart of the proposed probabilistic analytical approach

It is worth noting that in this work, the choice of the droop controlled DG units static droop coefficients was governed by two important results from the literature. First, in [99] it was shown that the proper choice of system droop coefficients can enhance the system relative stability margins at a particular system state. Second, in [30] it was shown that the system relative stability decreases as the system loading increase. As such, in this work the static droop coefficients were chosen according to reference

[99] to ensure system stability at the system state with the highest system load, the availability of all droop-based dispatchable units and the minimum wind penetration to meet the load demand.

The proper choice of system parameters adopted in this work aims to minimize the impacts that systems dynamics can have on the islanded microgrid success and as such highlight the main purpose of the study in terms of the voltage and reactive power impacts on the islanded microgrid successful operation. Nonetheless, the dynamic analysis described in section 4.2.1 is still adopted to check the system stability in the transition to the island and in the moment subsequent to the islanding.

4.4.1 Balanced Microgrids

The 69-bus test system [105] shown in Figure A.4, has been used to demonstrate the impacts of voltage and reactive power constraints on the probability of microgrid islanding success. The load and line data of the test system are given in Table A.2. Four dispatchable DG units are connected to the system, two at bus #35, one at bus #46 and one at bus #50. One wind based DG unit is located at bus #52. The detailed parameters, ratings and mode of operation of these DG units during the islanded microgrid are shown in Table A.3. The probability of a line fault occurring in the 69-bus system $P_{uncreated}$ is calculated based on the system reliability data; where the failure rate and repair time for each line are 0.04 (f/km-yr) and 5 hrs, respectively [106]. Further, the probability of a fault occurring in the upstream network of the 69-bus system has been calculated based on the upstream network reliability data i.e. substation. Typical reliability data of the different substation configurations can be found in [107]. In this work, the ring bus configuration has been selected to represent the substation reliability data. As shown in Figure A.4, the 69-bus system contains six IIDs capable of forming six possible microgrids, depending on the fault location. Table A.4 gives the values of ρ_{up} and $\rho_{uncreated}$ for the different possible microgrid formations in the 69-bus system and the corresponding IIDs. Such values have been calculated using the reliability data and the equations given in section 4.3.1.

In order to extract the combined generation load model, the set of states and their corresponding probabilities of loads and generations are required. In this work, the system peak load was assumed to follow the hourly load shape of the IEEE-RTS [108]. Based on this assumption the load is divided into ten states using the clustering techniques developed in [109] which verifies that choosing ten equivalent load states rendered a reasonable trade-off between accuracy and fast numerical evaluation. Table A.5 shows the set of load levels as a percentage of the peak load, its corresponding power in MVA for the 69-bus test system and its corresponding probabilities. The wind speed profile for the year under study has been estimated from the previous three years historical data [35]. Table A.6 shows the wind speed levels,

their respective number of hours, generated powers in KW and probabilities for each wind turbine. The set of load states shown in Table A.5 is combined with the set of wind power states shown in Table A.6 for each wind turbine and the two states of each dispatchable DG units to extract the generation-load model.

4.4.1.1 Case study #1: Base case

Table 4.1 and Table 4.2 show the islanded microgrid probability of success and supply adequacy indices for microgrid #1 (i.e. created due to a fault upstream of IID# A) and the SAIDI of the test system considering all possible created microgrids at the different scenarios, respectively. As shown in the tables, the reactive power constraints in the third scenario have significant effect on the assessment of the microgrid success compared with the conventional assessment in the second scenario. The results also show that the fourth and fifth scenarios have the same probability of success for the microgrid; however, the results in the fourth scenario do not show the partial loss of microgrid loads due to voltage violation at some load points. As shown in the fifth scenario, voltage constraints have considerable effect on the supply adequacy and system reliability indices and, hence, on the successful integration of microgrids in ADNs. The results in Table 4.2 show that the improvement in SAIDI in the fifth scenario is less than those obtained in the second scenario, due to considering the voltage and reactive power constraints.

4.4.1.2 Case study #2: Impacts of DG locations

This case study shows the impact of voltage and reactive power constraints on the islanded microgrid success when the location of the DG units in case study #1 is changed. The four dispatchable DG units of case study # 1 are now allocated at bus # 8, bus # 22, bus # 35 and bus #46. The wind based DG unit has the same location of case study #1. Table 4.3 and Table 4.4 show the supply adequacy indices and the SAIDI in this case study, respectively. It is worth noting that there are no changes in the first to third scenarios due to the change of the DG locations. Comparing the results obtained in case study #1 and case study #2, it can be seen that the location of the DG units can play a significant role in determining the probability of microgrid islanding success, the supply adequacy indices and SAIDI index when voltage and reactive power constraints as well as dynamic stability are taken in consideration. These results suggest that if the DG units allocation do not consider the islanded microgrid scenario (as in the current practices), then the voltage and reactive power constraints will be of significant importance in the evaluation of the probability of microgrid islanding success.

Table 4.1: Supply adequacy indices for microgrid #1 (case study #1)

Scenario #	$\rho_{success}$	*TLOLP*	*TLOLE (min.)*	*TLOEE (MWh)*
1	0	12.929E-05	67.95	3.7095
2	0.9094	1.171E-05	6.16	0.4096
3	0.8253	2.258E-05	11.87	0.7737
4	0.8149	2.393E-05	12.58	0.8242
5	0.8149	11.81E-05	62.05	2.6186

Table 4.2: SAIDI for case study #1

Scenario #	*1*	*2*	*3*	*4*	*5*
SAIDI	18.98	17.63	17.73	17.74	18.12

Table 4.3: Supply adequacy indices for microgrid #1 (case study #2)

Scenario #	$\rho_{success}$	*TLOLP*	*TLOLE (min.)*	*TLOEE (MWh)*
4	0.8253	2.258E-05	11.87	0.7737
5	0.8253	9.463E-05	49.74	1.7052

Table 4.4: SAIDI for case study #2

Scenario #	*1*	*2*	*3*	*4*	*5*
SAIDI	18.98	13.68	13.97	13.97	14.48

4.4.1.3 Case study # 3: Reactive Power Sharing

This case study shows the impact of unequal reactive power sharing on the islanded microgrid success. In the previous case studies, the conventional droop equations expressed by (4.1) and (4.2) have been used in compliance with the IEEE standard 1547.4 for DG islanded systems [22]. This conventional droop technique is capable of providing nearly exact active power sharing between the DG units in the islanded microgrid. On the other hand, the reactive power sharing between the DG units is not exact and depends on the system parameters i.e. mismatches in the power line impedances [32]. To study the effect that unequal reactive power sharing can have on the successful operation of islanded microgrids, this case study considers a possible algorithm to achieve equal reactive power sharing [110]. The work in [110] shows a possible algorithm to achieve equal reactive power sharing among the droop-based DG units forming the islanded microgrid through the use of a low bandwidth non-critical communication.

Table 4.5: Supply adequacy indices for microgrid #1 (case study #3)

Scenario #	$P_{success}$	*TLOLP*	*TLOLE (min.)*	*TLOEE (MWh)*
4	0.8206	2.276E-05	7.164	0.7776
5	0.8206	5.365E-05	28.2	1.6457

Table 4.6: SAIDI for case study #3

Scenario #	*1*	*2*	*3*	*4*	*5*
SAIDI	18.98	17.63	17.73	17.74	17.84

Each DG unit in the islanded microgrid provides a microgrid central controller (MGCC) with information about the reactive power delivered to the microgrid. Depending on the DG units' ratings and the total reactive power demand, the MGCC then determines the amount of reactive power that each DG unit should supply. Using the calculated reactive power references, the MGCC then regulates the value of the nominal output voltage magnitude set point V^* of the different DG units by using a Proportional-Integrator (PI) controller to implement the equal reactive power sharing. This reactive power sharing algorithm was incorporated in the islanded microgrid steady state and dynamic model described in section 4.2 Using PI controllers with proportional gain and integral gains of 2E-3and 0.04 respectively, case study #3 was performed.

Table 4.5 and Table 4.6 show the probability of microgrid success and supply adequacy indices and the SAIDI in this case study, respectively. Similar to case study # 2, there are no changes in the first to third scenarios due to implementing the equal reactive power sharing algorithm. As shown in the tables, the probability of microgrid success, supply adequacy indices and SAIDI have been improved compared with the results in case study # 1. However, still the voltage constraints have considerable effect and it should be considered in the assessment of the microgrid success.

Table 4.7 shows the probability of each load point to be served during the microgrid operation taken the voltage constraints into account for the three case studies under consideration. The table also gives the outage duration of the different load points considering all possible microgrids in the network. This table is presented to give more insight on the impact of voltage and reactive power constraints on the outage duration at the different load points. As shown in the table, the voltage and reactive power constraints have considerable impacts on the assessment of load points' reliability.

Table 4.7: The reliability evaluation for each load point

Bus #	No Microgrid	Case Study #1		Case Study #2		Case Study #3	
	U (hrs)	P_{served}	U (hrs)	P_{served}	U (hrs)	P_{served}	U (hrs)
5	16.83	0.6217	16.13	0.8254	14.77	0.7795	15.95
6	16.83	0.5559	16.20	0.8254	14.77	0.7698	15.96
7	16.83	0.5142	16.25	0.8228	14.77	0.7643	15.97
8	16.83	0.5133	16.25	0.8228	14.78	0.7599	15.97
9	16.83	0.4958	16.27	0.8228	14.78	0.7599	15.97
10	16.83	0.4504	16.32	0.8215	14.77	0.7419	15.99
11	16.83	0.4365	16.34	0.8228	14.77	0.7369	16.00
12	32.53	0.4305	32.04	0.8214	18.54	0.7359	31.70
13	32.53	0.3984	32.08	0.8214	18.54	0.6922	31.75
14	32.53	0.3783	32.10	0.8203	18.54	0.6458	31.80
16	32.53	0.3720	32.11	0.8194	18.54	0.6407	31.81
17	32.53	0.3672	32.12	0.8188	18.54	0.6385	31.81
18	32.53	0.3672	32.12	0.8188	18.54	0.6385	31.81
20	32.53	0.3549	32.13	0.8188	18.54	0.6360	31.81
21	32.53	0.3549	32.13	0.8188	18.55	0.6360	31.81
22	32.53	0.3549	32.13	0.8188	18.55	0.6360	31.81
24	32.53	0.3549	32.13	0.8188	18.55	0.6360	31.81
26	32.53	0.3523	32.13	0.8188	18.55	0.6360	31.81
27	32.53	0.3523	32.13	0.8188	18.55	0.6360	31.81
28	3.61	0.6222	2.91	0.8254	2.68	0.7795	2.73
29	3.61	0.6342	2.89	0.8254	2.68	0.7795	2.73
33	12.44	0.7598	9.34	0.8254	9.27	0.8239	9.27
34	12.44	0.8149	9.28	0.8254	9.27	0.8239	9.27
35	12.44	0.8149	9.28	0.8254	9.27	0.8239	9.27
36	3.61	0.6222	2.91	0.8254	2.68	0.7795	2.73
37	3.61	0.6342	2.89	0.8254	2.68	0.7795	2.73
39	3.61	0.6342	2.89	0.8254	2.68	0.7795	2.73
40	3.61	0.6342	2.89	0.8254	2.68	0.7795	2.73
41	6.21	0.6742	3.21	0.8254	3.04	0.8054	3.06
43	6.21	0.7167	3.16	0.8254	3.04	0.8239	3.04
45	6.21	0.7171	3.16	0.8254	3.04	0.8239	3.04
46	6.21	0.7171	3.16	0.8254	3.04	0.8239	3.04
48	16.83	0.6217	16.13	0.8254	14.77	0.7795	15.95
49	16.83	0.6336	16.11	0.8254	14.77	0.7795	15.95
50	16.83	0.6350	16.11	0.8254	14.77	0.7795	15.95
51	16.83	0.5133	16.25	0.8228	14.77	0.7599	15.97
52	16.83	0.5190	16.24	0.8228	14.77	0.7599	15.97
53	16.83	0.4679	16.30	0.8227	14.78	0.7419	15.99
54	16.83	0.4365	16.34	0.8214	14.79	0.7369	16.00
55	16.83	0.4134	16.36	0.8153	14.81	0.7156	16.02
59	16.83	0.1532	16.66	0.7194	15.29	0.5850	16.17
61	21.90	0.1003	21.79	0.6754	20.56	0.5850	21.24
62	21.90	0.1003	21.79	0.6754	20.58	0.5850	21.24
64	21.90	0.0869	21.80	0.7524	20.60	0.5850	21.24
65	21.90	0.0869	21.80	0.7607	20.65	0.5850	21.24
66	16.83	0.4365	16.34	0.8215	14.77	0.7369	16.00
67	16.83	0.4365	16.34	0.8215	14.77	0.7369	16.00
68	32.53	0.4223	32.05	0.8214	30.47	0.7291	31.71
69	32.53	0.4223	32.05	0.8214	30.47	0.7291	31.71

Table 4.8: Supply adequacy indices and SAIDI of the unbalanced test system

Scenario #	$\rho_{success}$	*TLOLP*	*TLOLE (min.)*	*TLOEE (MWh)*	*SAIDI (min.)*
1	0	12.929E-05	67.95	2.709	134.9
2	0.8593	1.819E-05	9.56	0.4241	76.5
3	0.7598	3.105E-05	16.32	0.7376	83.3
4	0.7595	3.109E-05	16.34	0.7381	83.2
5	0.7595	5.835E-05	30.67	0.9471	87.5

4.4.2 Unbalanced networks

The 25-bus unbalanced distribution test system, shown in Figure A.5, has been used to test the proposed approach applicability for unbalanced distribution systems [111]. The line and bus data of the 25 bus test system are given in Table A.7, Table A.8 and Table A.9. The failure rate and repair time for each line are 0.065 (f/km- yr) and 5 hrs respectively. The substation reliability data is assumed to be the same as the 69-bus test system. Two dispatchable DG units are located at buses #19 and #22. Three wind DG units are located at buses #5, #8 and #22 respectively. Table A.7 shows the detailed parameters, ratings and mode of operation of each DG unit during the islanded microgrid. Wind and load states have been extracted with similar states to the balanced case studies. The system contains one isolation switch at the substation, thus there is only one islanded microgrid that will be created when a fault occurs upstream the substation. Table 4.8 shows the probability of success and supply adequacy indices for the five scenarios under study in the created islanded microgrid. The table shows also the SAIDI due to considering the created islanded microgrid. The results show that voltage and reactive power constraints have considerable effect on the unbalanced microgrid success.

4.5 Discussions:

In this chapter, the impacts of voltage and reactive power constraints on the successful operation of islanded microgrids have been studied. An islanded droop-based microgrid simulation model that takes the special operational characteristic of islanded microgrids has been adopted to validate the impacts of voltage and reactive power constraints. A probabilistic analytical approach has been developed to execute the proposed study taking into consideration the uncertainty in both loads and wind generation. Supply adequacy indices have been modified to consider the voltage and reactive power constraints. The simulation studies show that voltage and reactive power constraints have significant impacts on the probability of microgrid islanding success. It is concluded in this work that the impacts of voltage and reactive power on the microgrid islanding success is highly dependent on the DG locations, ratings , types

and control schemes that are currently unplanned for the islanded microgrid operation. Therefore, the issue of voltage and reactive power constraints must be considered in the design, planning and operation of islanded microgrids.

Chapter 5

Capacitor Planning in Active Distribution Networks Considering Islanded Microgrids

5.1 Introduction

One of the most important issues in SG is to achieve a proper implementation of ADNs considering islanded microgrids. The first stage of such proper implementation is to assess the possibility of successful operation using the current control schemes. Chapter 3 and chapter 4, show that reactive power and voltage regulation aspects will play a significant role on the assessment of the successful operation of ADNs and islanded microgrids. Such assessment should be followed by new planning approaches, the second stage of the proper implementation, that take into account the characteristics of DG units and the special philosophy of operation for islanded microgrids. Appropriate planning of ADNs considering islanded microgrids will facilitate the SG objectives.

VAR or shunt capacitor planning is one of the most important planning practices that are generally applied in distribution networks to improve the voltage profile, reduce the total system losses and increase the system capacity. Conventionally, the objective of capacitor planning problem is to determine the optimal size and location of installed capacitors for various loading conditions. In this process, the utility aims to maximize the total saving by energy loss reduction through proper installation of shunt capacitors.

In this chapter, the problem of capacitor planning is revised to accommodate more objectives under the SG paradigm. A probabilistic formulation for the problem of shunt capacitor planning in distribution networks is presented. The proposed formulation takes into consideration the implementation of islanded microgrids as well as the stochastic nature of generation and loads into account. Genetic Algorithm (GA), a population based searching algorithm, is utilized to solve the formulated planning problem.

5.2 Required Information Pre-formulating the Capacitor Planning Problem:

Pre-formulating the problem of capacitor planning in ADNs, it is required to do the following procedures:

1- Divide the distribution system under study into a set of possible created islands $\{N_{is}\}$ based on the locations of IIDs and DG units.

2- Develop the set of generation-load states $\left\{N_{st}^{gr}\right\}$ for the whole ADN under study (grid-connected configuration considering all possible microgrids).

3- Develop the set of generation-load states for each possible microgrid inside the ADN under study.

4- Calculate the probability of creation for each islanded microgrid using (4.23)-(4.26).

5- Construct the set of unsuccessful states $\left\{N_{fail}^{Q/VV}\right\}$ due to shortage in reactive power and/or voltage violation for each created microgrid in islanded condition. $\left\{N_{fail}^{Q/VV}\right\}$ can be obtained from the probabilistic evaluation study described in Chapter 4.

Figure 5.1 shows a flowchart that summarizes the steps of forming $\left\{N_{fail}^{Q/VV}\right\}$ and the probability of failures for each load point due to active power mismatch, shortage of reactive power and voltage violation. The overall probability of each load point to be not served during an island is given in (5.1); where $\left\{N_{lp}^{is}\right\}$ is the set of load points within a created island.

$$\rho_{fail}(lp, is) = \rho_{fail}^{P} + \rho_{fail}^{Q} + \rho_{fail}^{VV}(lp); \quad \forall lp \in \left\{N_{lp}^{is}\right\} \& is \in \{N_{is}\} \tag{5.1}$$

Currently, most of the events that might initiate the transition to islanded conditions in microgrids are unscheduled events (inadvertent events that typically occur due to the outage of area EPS or equipment failure). Appropriate planning of islands for such events will improve the microgrids customers' reliability significantly. As the anticipated time spans of islands due to inadvertent events are adequately short, the cost of energy loss in islanded condition can be neglected compared with the cost of energy loss in grid-connected condition. Consequently, it is better to evaluate the benefits of capacitor planning considering the improvement of microgrid customers' reliability when island is initiated. Thus part of the capacitor planning problem should reflect the economic benefits due to the reduction of customers' cost of interruption in islanded condition that is accompanied with the shortage in reactive power and/or voltage violation during the islanded condition. Details of the problem formulation of capacitor placement considering islanded microgrids are presented in the next section.

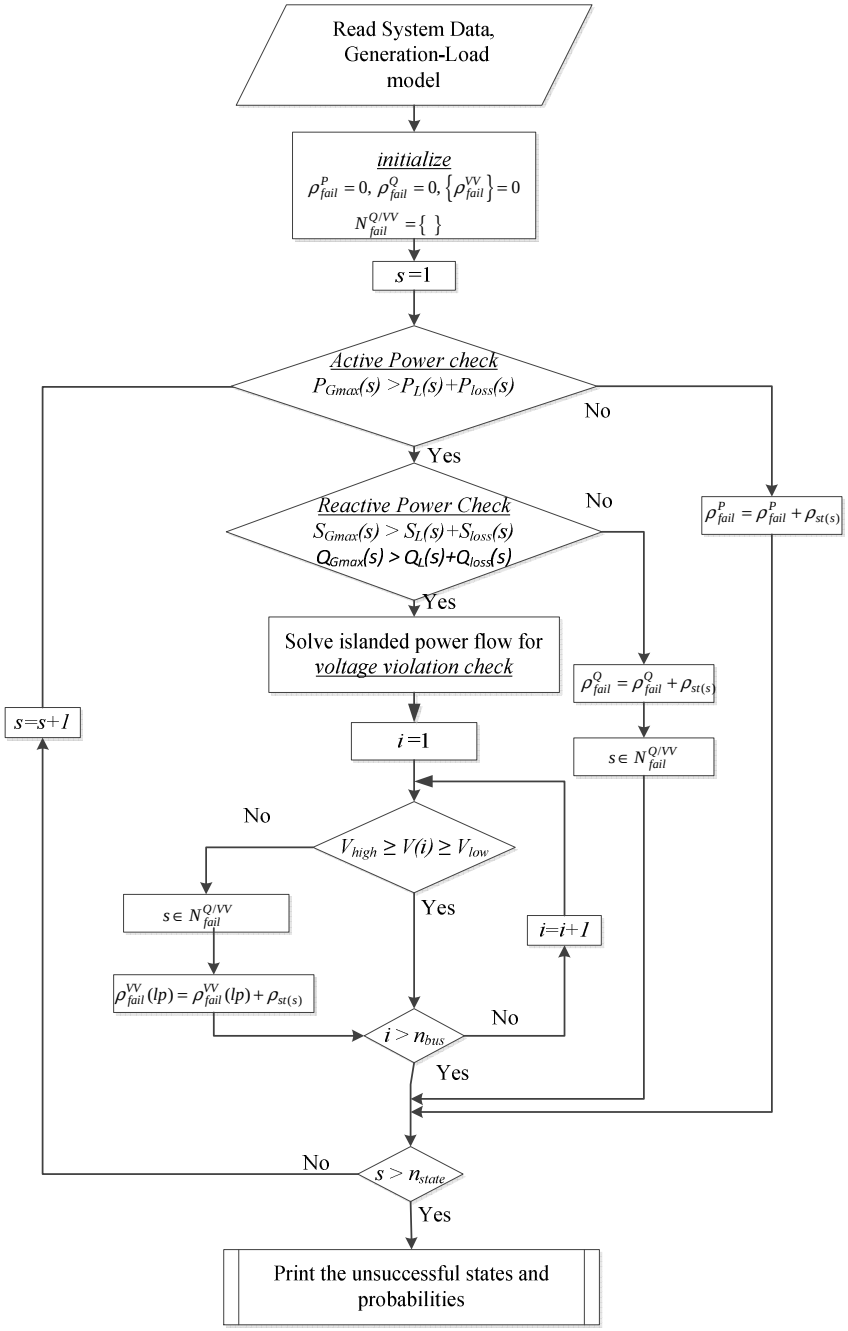

Figure 5.1: The required procedures to construct $\left\{N^{Q/VV}_{fail}\right\}$ and the corresponding probabilities

5.3 The Problem Formulation:

Consider $\{N_c\}$,and $\{N_{bus}\}$ are the set of candidate locations of capacitors and the set of buses for each possible configuration (grid-connected or islands), respectively. The objective function of capacitor planning in ADNs considering microgrids in islanded condition can be defined as follows:

$$\min_{\left(\left\{u_k^0\right\},\left\{u_{k(s)}^{gr}\right\},\left\{u_{k(s)}^{is}\right\}\right)} \quad \sum_{k\in\{N_C\}} C_k(u_k^0) + \quad CE_{loss} \quad + \sum_{is\in\{N_{is}\}} C_{\text{int}}(is) \tag{5.2}$$

where

$$C_k\left(u_k^0\right) = K_c \frac{u_k^0}{u_o} + K_c^{ins}\left(u_k^0\right);\ \forall k \in N_c \tag{5.3}$$

$$CE_{loss} = K_e \sum_{s\in\left\{N_{st}^{gr}\right\}} \rho_{st(s)}^{gr} \times 8760 \times P_{loss}\left(\left\{z_{(s)}^{gr}\right\},\left\{u_{k(s)}^{gr}\right\}\right) \tag{5.4}$$

$$C_{\text{int}}(is) = \sum_{lp\in\left\{N_{lp}^{is}\right\}} \rho_{fail}(lp,is) \times P_{lp} \times \sum_{com\in\left\{N_{com}^{up}\right\}} C_{(lp,com)}\lambda_{(lp,com)} \tag{5.5}$$

subject to capacitor units in each candidate location *k* satisfy the following equality and inequality constraints:

$$u_k^0 = l_k \times u_o; \quad \forall k \in \{N_c\} \tag{5.6}$$

$$0 \le u_{k(s)}^{gr} \le u_k^0; \quad \forall\left(k\in\{N_c\}, s\in\left\{N_{st}^{gr}\right\}\right) \tag{5.7}$$

$$0 \le u_{k(s)}^{is} \le u_k^0; \quad \forall\left(k\in\{N_c\}, is\in N_{is}, s\in\left\{N_{fail(is)}^{Q/VV}\right\}\right) \tag{5.8}$$

and subject to the ADN in normal parallel satisfy the power mismatch equations G_i and voltage constraints as follows:

$$G_i\left(\left\{z_{(s)}^{gr}\right\},\left\{u_{k(s)}^{gr}\right\}\right) = 0;\ \forall\left(i\in\left\{N_{bus}^{gr}\right\}, s\in\left\{N_{st}^{gr}\right\}\right) \tag{5.9}$$

$$V_i^{\min} \le |V_{i(s)}^{gr}| \le V_i^{\max}; \quad \forall\left(i\in\left\{N_{bus}^{gr}\right\}, s\in\left\{N_{st}^{gr}\right\}\right) \tag{5.10}$$

where,

u_o	The standard size of one capacitor bank
$\{u_k^0\}$	The sizing vector whose components are multiplies of the standard size of one capacitor bank
$\{u_{k(s)}^{gr}\}$	The control setting vectors at each state *s* in normal parallel
$\{u_{k(s)}^{is}\}$	The control setting vectors at each state *s* in islanded condition
C_k	The cost of capacitor placement at location *k* with sizing u_k^0
K_c	the cost of one bank of capacitor
K_c^{ins}	The cost associated with the capacitor installation at location *k*.
CE_{loss}	The total cost of energy loss in normal parallel condition
K_e,	The energy cost in ($/KWh)
P_{loss}	The total system power losses in normal parallel condition
G_i	The set of power mismatch equations for each bus *i*
$\{z_{(s)}^{gr}\}$	The set of state variables of the power flow equations (voltages and angles) for each state *s* in normal parallel condition
$\lvert V_{i(s)}^{gr} \rvert$	The voltage magnitude for each bus *i* at each state *s* during the normal parallel mode
C_{int}(is)	The total cost of interruption for a set of load points within a created island $\{N_{lp}^{is}\}$ due to outage of the upstream network and the probability of each load point to be not served during the island
P_{lp}	The average consumed power
$\lambda_{(lp,com)}$	The failure rate of the load point *lp* within the island due to a component *com* failure in the upstream network

$C_{(lp,com)}$ The sector customer damage function SCDF for load point *lp* within the island

Equation (5.4) represents the total cost of energy losses during the normal parallel operation mode considering the probabilistic model of loads and DG units. As shown in (5.5), the cost of interruption for each load point within the created island is formulated to be a function of the probability of this load point to be not served during the island $\rho_{fail}(lp,is)$. Based on the evaluation of the probability of each load point to be not served in islanded condition described in section 5.2, $\rho_{fail}(lp,is)$ is incorporated in the problem of capacitor planning as follows:

$$\rho_{fail}(lp,is) = \rho^{P}_{fail}(lp,is) + \sum_{s \in N^{Q/VV}_{fail(is)}} B^{is}_{(lp,s)}\left(u^{is}_{k(s)}\right) \times \rho^{is}_{st(s)} \tag{5.11}$$

where *B* is a binary variable indicates the impacts of capacitor placement on the unsuccessful states of islands due to voltage and/or reactive power constraints. For each load point *lp* and state *s*, *B* equals zero when both the island power mismatch equations and voltage constraints given as:

$$G_i\left(\left\{z^{is}_{(s)}\right\},\left\{u^{is}_{k(s)}\right\}\right) = 0;\ \forall\left(i \in \left\{N^{is}_{bus}\right\}, s \in \left\{N^{Q/VV}_{fail(is)}\right\}\right) \tag{5.12}$$

$$V_i^{\min} \le |V^{is}_{i(s)}| \le V_i^{\max};\quad \forall\left(i \in \left\{N^{is}_{bus}\right\}, s \in \left\{N^{Q/VV}_{fail(is)}\right\}\right) \tag{5.13}$$

are satisfied (the load point is served due to capacitor placement) and it equals one otherwise; where $\left\{z^{is}_{(s)}\right\}$ is the set of state variables of the power flow equations (voltages and angles) for each state *s* in islanded conditions.

Note that the power mismatch equations G_i depend on the type of each node and the mode of operations. The generic power flow algorithm described in section 3.2 is implemented in case of normal parallel operation mode to solve the mismatch equation in (5.9) and the power flow algorithm described in section 4.2.2 is implemented to solve the mismatch equations in (5.12) for islanded microgrids.

5.4 The Proposed Optimization Technique:

The above formulation of the capacitor placement is a combinatorial optimization problem with non-differentiable objective function. The meta-heuristic optimization techniques family proved its effectiveness in solving such complicated practical problems. In this work GA, which has been widely used in the previous works to solve the conventional problem of capacitor planning [42-44], is utilized.

GA is a powerful general-purpose technique for solving combinatorial optimization problems. GA is a search heuristic that mimics the process of natural evolution. The evolution usually starts from a population of randomly generated individuals and happens in generations. In each generation, the fitness of every individual in the population is evaluated, multiple individuals are stochastically selected from the current population (based on their fitness), and modified (recombined and possibly randomly mutated) to form a new population. The new population is then used in the next iteration of the algorithm. Commonly, the algorithm terminates when either a maximum number of generations has been produced, or a satisfactory fitness level has been reached for the population. Generally, the population consists of chromosomes, and each chromosome consists of a number of genes. In capacitor planning problem, each chromosome in the population consists of a number of genes equals double the number of the candidate locations ($n_{genes}=2\times n_c$); where for each candidate location, there are two genes. One gene carries binary values, which indicate the decision of installing capacitor units. The other gene carries integer values, which indicate the number of capacitor units to be installed at each candidate location. Details of the mechanism of population updates and convergence criterion can be found in [43].

Solving the capacitor planning problem yields the sizing vector $\left\{u_k^0\right\}$, which determines the locations to install capacitors and the corresponding sizes of capacitors to be installed. Also, the solution yields the control setting vectors in normal parallel and islanded conditions $\left\{u_{k(s)}^{gr}\right\}$ and $\left\{u_{k(s)}^{is}\right\}$, which determine the types of capacitors to be installed and the corresponding control setting for each state s at each configuration. Figure 5.2 shows a flowchart of the proposed solution for the problem of capacitor planning in ADNs considering microgrids in islanded conditions. Details of the procedures shown in Figure 5.2 are explained hereunder:

1- Input system parameters and the external initial population (the candidate size and locations in a set of chromosomes).

2- Perform the following for every external chromosome *ch* in each population at each state *s* in normal parallel mode:

   a. Set internal initial population, upper limits and lower limits based on the size and locations in the current external chromosome *ch*. The internal population represents the control settings vector.

   b. Run the generic power flow algorithm of normal parallel mode for each control setting vector.

c. Calculate the internal fitness function (system losses) at each candidate control setting vector

d. Check convergence:

i. If convergence is not achieved, update the control setting vector and go to 2.b.

ii. Else, calculate $CE_{loss}(s)$ for the current state using the optimal control settings obtained from 2.a-2.d.

e. Add a penalty factor to the fitness function, if the constraints in (5.9)-(5.10) are not satisfied. If a penalty factor is applied, skip the following steps and go to step 2.

3- Perform the following for every external chromosome *ch* in each population at each state *s* in each island configuration:(internal nonlinear problem)

a. Set internal initial population, upper limits and lower limits based on the size and locations in the current external chromosome *ch*. The internal population represents the control settings vector.

b. Run the generic islanded microgrid power flow algorithm mode for each control setting vector.

c. Check for the constraints in (5.12)-(5.13). If they are not achieved, update the control setting vector and go to 3.b

d. Once a control setting vector satisfy the constraints in (5.12)-(5.13), remove the current state from $\left\{N_{fail}^{Q/VV}\right\}$ and its corresponding probability of failure.

e. Update the total cost of interruption using (5.5)

4- Calculate the fitness function in (5.2)

5- Check the convergence

a. If all chromosomes are the same or the maximum number of iterations is achieved then print the solution and stop.

b. Else, update the populations and go to 2.

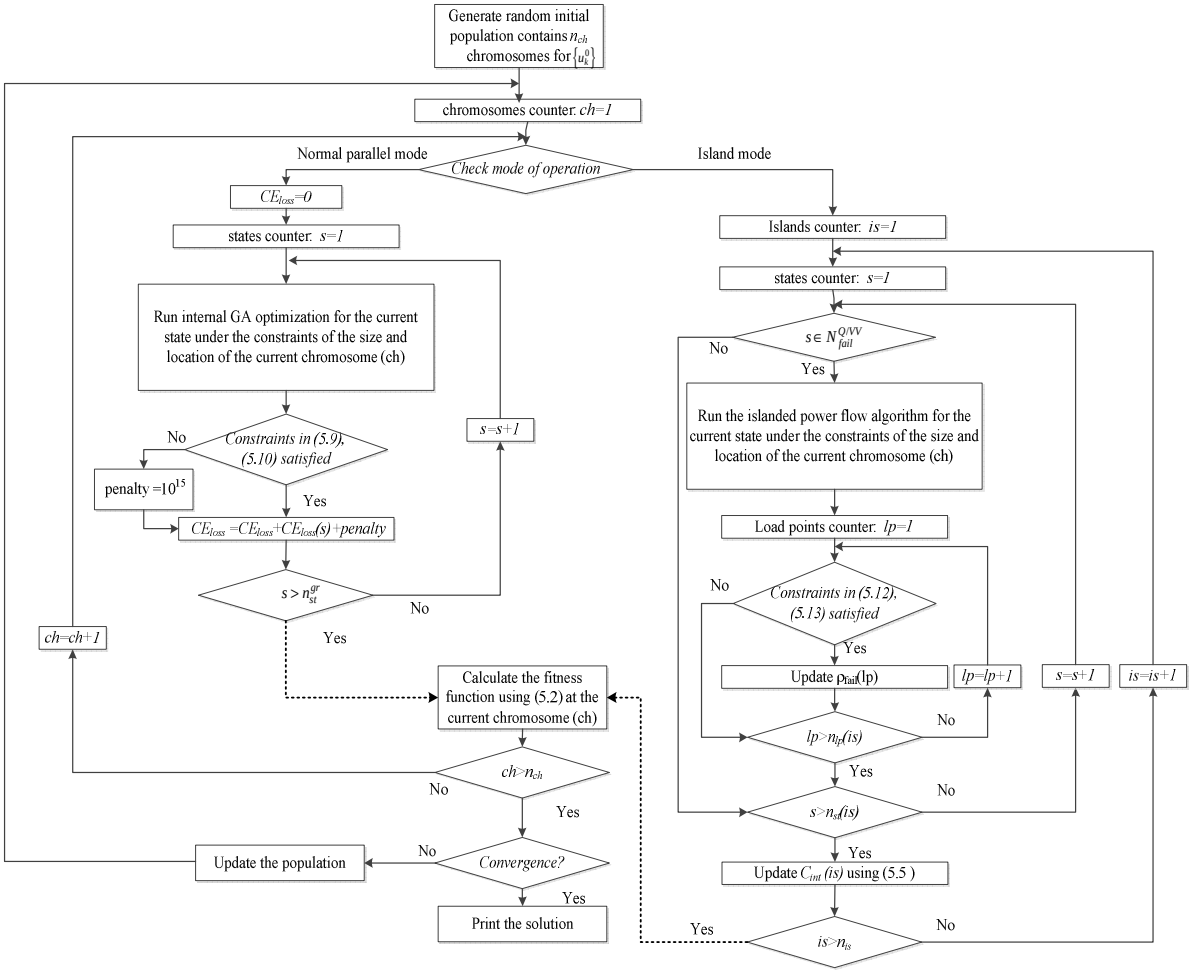

Figure 5.2: A flowchart of the proposed capacitor planning approach in ADNs considering islanded microgrids

5.5 Case Studies

In this section, the 69-bus test system shown in Figure A.4 has been used to test the effectiveness of the proposed capacitor planning approach. The proposed algorithm was implemented in MATLAB environment. Six participating and three non-participating DG units are connected to the system. The detailed types, parameters, ratings and mode of operation of these DG units during the islanded condition are shown in Table A.11. Data used in this work for SCDF of each load type is taken from the recent reliability worth assessment in [112]. As shown in Figure A.4, the 69-bus system contains six IIDs; based on the DG locations, five of them are capable of forming microgrids. Table A.4 gives the calculated values of ρ_{up} and $\rho_{uncreated}$ for the different possible microgrids formations in islanded conditions and their

corresponding IIDs. The set of load states shown in Table A.5 is combined with the set of wind power states shown in Table A.6 for each wind turbine and the two states of each participating DG unit to extract the generation-load model for each possible configuration.

Different case studies have been carried out to evaluate the importance of the proposed capacitor planning approach.

5.5.1 Base case: before capacitor placement

Different scenarios have been considered in the base case study to show the role of voltage and reactive power constraints on the assessment of the island success pre-capacitors installation. It is assumed in the first scenario that the assessment criterion is based on the active power only. In the second scenario, the assessment criterion is based on both active and reactive power generation-load mismatch. In addition to active and reactive power mismatch, the third scenario takes into consideration the voltage constraints. Table 5.1 shows the probability of island failure, the total outage durations in minutes, expected energy not supply (EENS) in MWh and cost of interruption in K$ for microgrid #1. As shown in the table, the reactive power constraints in the second scenario affect the assessment of the island success. The third scenario shows that voltage constraints have considerable effect on the island failure and, hence, on the successful integration of microgrids in ADNs.

Table 5.2 shows the cost of interruption for all microgrids during islanded condition due to active power mismatch, shortage in reactive power and voltage violation.

Table 5.3 shows the probability of island failure, the outage duration and the EENS in all possible microgrids due to the shortage in reactive power as well as the voltage violation. As shown in the tables, microgrid # 4 has successful operation in all operating conditions and no further planning is required. The rest of microgrids need proper planning for active power mismatch, reactive power mismatch and voltage constraints. It is worth noting that active power mismatch needs a supply adequacy planning for DG units and/or applying a load shedding mechanism during the island operation; however this issue is out of the scope in this work.

The total cost of energy losses in normal parallel operation mode without capacitor placement has been calculated using an optimal power flow that determines the tap settings of the substation LTC at each state. The total cost of energy losses for the base case without capacitor placement has been found to be 172.306 *K$*.

Table 5.1: Evaluating the islanding failure of microgrid #1 using different criterion

Scenario #	ρ_{fail}	*Outage (min.)*	*EENS (MWh)*	C_{int} *(K$)*
2	0.1188	8.07	0.9879	1.495
3	0.137	9.31	1.154	1.7244
4	0.7126	48.42	5.081	8.970

Table 5.2: C_{int} in *K$* for all possible microgrids due to different aspects

microgrid #	P_{match}	$Q_{shortage}$	$V_{violation}$	*Total*
1	1.495	0.229	7.245	8.97
2	129.196	43.371	5.349	177.916
3	0	0	0	0
4	373.624	43.656	7.001	424.28
5	39.389	2.19	5.13	46.71

Table 5.3: Reliability evaluation due to reactive power and voltage constraints for all possible microgrids without capacitor placement

microgrid #	$\rho_{fail}^{Q/VV}$	$Outage^{Q/VV}$ *(min)*	$EENS^{Q/VV}$ *(MWh)*
1	0.5938	40.35	4.093
2	0.2483	36.92	3.074
3	0	0	0
4	0.1184	93.85	2.824
5	0.02145	16.98	0.3561

5.5.2 With capacitor placement

Ten candidate buses for capacitor placement have been chosen based on the sensitivity studies that have been done in [42] for the 69-bus test system. It is assumed that a maximum of four 200-KVAr capacitor banks could be allocated at each candidate bus. Table 5.4 gives the list of candidate buses, cost of energy loss and the cost of investment for capacitor placement [47]. Two case studies have been carried out in this section. In the first case study, the capacitor planning has been done without considering the microgrid in islanded conditions. In the second case study, microgrids in islanded conditions have been taken into account. Table 5.5 shows the optimum capacitor placement and the total cost of investment for the two case studies. Table 5.6 presents the total saving of energy losses in normal parallel mode and the total saving in cost of interruption for each possible created microgrid in islanded condition for the two case studies.

Table 5.4: Required data for capacitor placement

Candidate Locations	K_c *($/KVAr)*	K_c^{ins} *($)*	K_e *($/KWh)*
12,13,18,19,22,60,62,63,65,66	4	1000	0.06

Table 5.5: Optimum capacitor placement

location	**Rating in KVAr**	
	Case#1	***Case #2***
22	0	200
60	600	600
62	600	600
63	600	600
65	600	600
66	0	600
Total cost (K$)	13.60	18.80

Table 5.6: Total saving in K$ for all possible configurations

Configuration	**Case# 1**	**Case# 2**
Normal parallel	84.907	90.385
microgrid# 1	4.227	7.313
microgrid # 2	43.039	48.72
microgrid # 3	0	0
microgrid # 4	50.66	50.66
microgrid # 5	0	7.32
Total saving (K$)	182.833	204.398

The results in case #1 show that capacitor placement without considering the microgrids in islanded condition reduces the probability of unsuccessful operation of islands; however still the failure of island operation due to voltage and reactive power constraints is significant. As shown in the results of case #2, the cost of interruption due to the shortage in reactive power and voltage regulation issues has been mitigated when microgrids has been considered in the capacitor planning problem. Consequently, the probability of island failure, the outage duration and the EENS shown in Table 5.1 are completely eliminated when a proper capacitor planning is applied. Therefore, capacitor planning in ADNs considering microgrids in islanded conditions will bring more saving and it will help in the successful integration for the concept of microgrids.

5.6 Discussion:

In this chapter, a new formulation for the problem of capacitor planning in distribution networks has been proposed. The proposed formulation takes into account the operation of microgrids in islanded condition. The probabilistic analytical approach described in Chapter 4 has been used to determine the unsuccessful states of each created island due to shortage in reactive power and voltage regulation aspects. Also, the generic power flow algorithms that have been developed for grid-connected and islanded microgrids in Chapter 3 and Chapter 4 respectively are integrated into the problem formulation. The impacts of voltage and reactive power constraints in the successful operation of islanded conditions have been modeled in the objective function of the capacitor planning problem in the form of cost of interruption. GA has been used to solve the proposed problem formulation. The simulation results show that proper capacitor planning considering microgrids will facilitate a successful implementation for the concept of microgrids in ADNs. It is worth noting that the framework of the planning approach presented in this chapter is generic and it can be easily adopted for other planning studies in ADNs considering microgrids in islanded conditions.

Chapter 6

A Two Ways Communication-Based Distributed Voltage Control for Active Distribution Feeders

6.1 Introduction

The interactions described in Chapter 3 and Chapter 4 beside other interactions between DG units and utility devices make the trend of the research aims to tackle these challenges by converting the distribution system control structure from its passive appendage into active control. Such trend is in line with the SG paradigm that will provide new digital technologies such as monitoring, automatic control and communication facilities to improve the overall performance of the network. Active control schemes monitors the system by making measurements or state estimation and based on these chooses control actions that are implemented on the system (via communication links). An important aspect of active control is to find a suitable control structure that will take advantage of the inherent scalability and robustness benefits of DG units.

Peer-to-peer, multi-agent or distributed control scheme is considered as a promising control structure in SG. Distributed control structures are expected to be able to deal or at least relieve the interactions between DG units and utility devices and facilitate seamless integration of high DG penetration in distribution networks. SG technologies have been applied in this chapter to construct a distributed control that has the capability to provide proper coordinated voltage control in active distribution feeders. The functions of each controller have been defined according to the concept of intelligent agents and the characteristics of the individual DG unit as well as utility regulators. Unlike previous works, in this chapter a detailed well-defined framework for the distributed control scheme that includes the following features has been presented:

1- The number of control agents and their organization paradigm.
2- The detailed internal structure and operation mechanism to be implemented in each controller
3- The proper coordination and communication protocols among controllers in a distributed control model
4- The proper simulation models to verify the dynamic and slow oscillation effectiveness of the distributed control structure

6.2 The Framework of the Proposed Distributed Control Structure

The distributed control structure consists of components called control agents. These control agents try, through communication and negotiation with other control agents, to: (1) determine the current as well as the predicted states of the system and (2) make decisions (set their local actuators or communicate with other agents) in such a way that their own objectives are met as closely as possible and any constraints are satisfied.

6.2.1 The number of control agents and their organization paradigm

A first important distinguishing feature in multiagent control structures is the number of control agents and their organization paradigm [65]. Figure 6.1 shows the proposed distributed control structure for proper voltage and reactive power control in ADNs [113]. As shown in the figure, each device, i.e. LTC, SVR, SC, FSC and DG, has its own intelligent controller which has the capability to optimize its operation via local measurements and two ways communication acts.

6.2.2 Interior structure and operation mechanism of each control agent:

There is not yet a universal consensus on the definition of an agent. According to Wooldridge, an agent is merely “a software or hardware entity that is situated in an environment and is able to autonomously react to changes in that environment.”[62]. Basically, under this definition some exiting systems could be classified as agents. For instance, a shunt capacitor could be considered as an agent if it locally takes a decision to switch ON or OFF based on the measurement of its local voltage. Therefore, renaming existing systems or new systems using existing technologies as agents, offers nothing new and in consequence, there will be no concrete engineering benefit. Therefore, there is a need to know how agents and multiagent systems can be distinguished from the current systems.

In order to distinguish between the existing systems and agents, Wooldridge extends the concept of an agent by extending the definition of autonomy to flexible autonomy, i.e. intelligent agent [114]. In this case, intelligent agent has three additional properties; they are reactivity, pro-activeness, and social ability. Intelligent agents are required to be both proactive and reactive. The agent’s pro-activeness implies the use of objectives. A reactive agent is one that will change its behavior in response to changes in the environment. An important aspect in decision making is balancing proactive and reactive aspects.

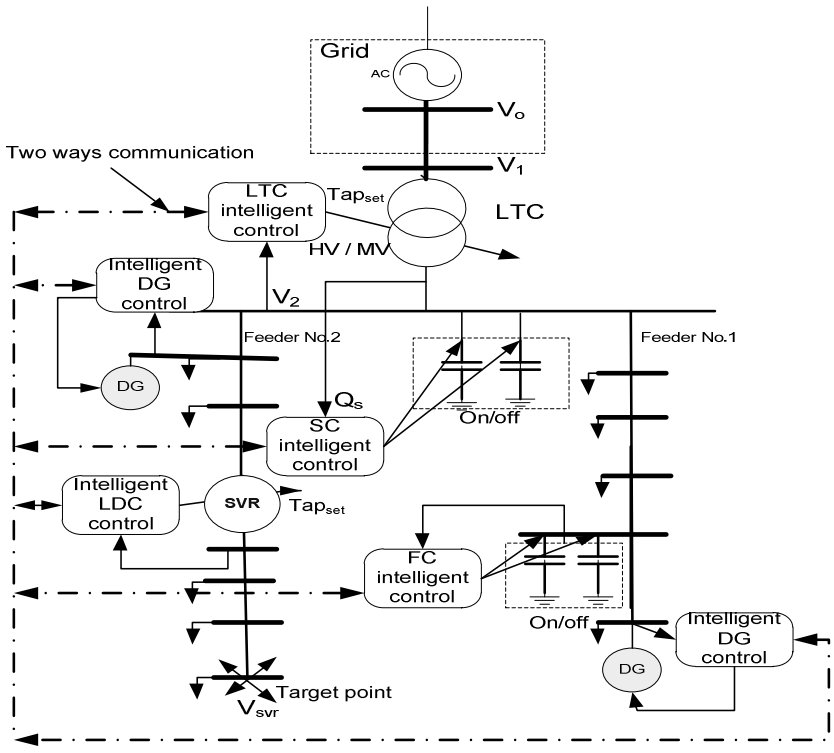

Figure 6.1: The proposed distributed control structure for voltage regulation in ADNs.

The key to reconcile these features, thus making agents suitably reactive, is identifying significant changes in the situation; these are events. The third property of agents is that they are social that is, agents interact with other agents. There are many forms in which this interaction can take place, ranging from exchanging messages according to pre-defined protocols to forming teams that work towards a common goal.

Based on the distinguish properties of intelligent agents, a number of different approaches have been emerged as candidates for intelligent agent's architecture. One of the architectures that is suitable for power system applications and is proposed in this work, views the system as a rational agent having certain mental attitudes of Beliefs, Desires and Intentions (BDI model) [114]. Figure 6.2 shows a typical architecture of a control agent based on the BDI theory. As shown in the figure, a BDI intelligent agent could be composed of six elements: a communicator, a bidirectional interface, beliefs, desires a decision maker and a control algorithm module. The communicator connects the agent to the information channel, which enables the agent to communicate and negotiate with other agents for the coordinated execution of proper tasks.

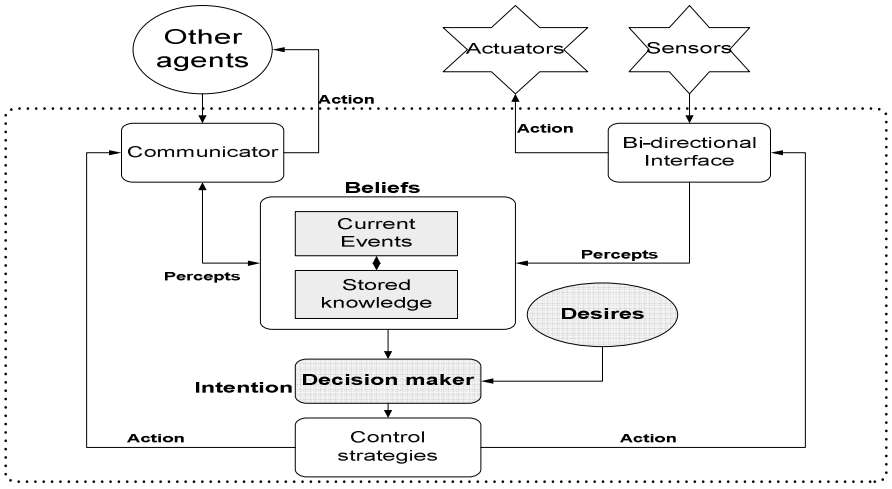

Figure 6.2: The BDI control agent's interior structure.

The bidirectional interface receives the data from the sensor system which is used to perceive the information of the surroundings. Also, it sends the actions to the actuators upon receiving commands sent by the decision maker. Both the communicator and the bidirectional interface are percepts, which enable the agent to determine the current events of the environment such as normal or contingency operation.

One consequence of being unable to sense the entire environment at once is that an agent needs to maintain a cache for information that it has received. These are the agent's beliefs. A belief is some aspect of the agent's knowledge or information about the environment, itself or other agents. As shown in Figure 6.2, beliefs could be divided into two parts; they are current events and stored knowledge (data base).

Desires, also known as (objectives, aims or goals), are the set of tasks that the agent is willing to achieve. The decision maker is the core of each control agent. The important role of the decision maker is to evaluate the beliefs and desires. Based on this evaluation, it decides which control task(s) should be achieved in the current state of affairs (intention). The control algorithm module (set of plans or control strategies) provides the control algorithms for executing the control task. The choice of the proper control strategy is mainly based on the beliefs and tasks. Sometimes, there is just one control strategy that is suitable to achieve all control tasks. The control algorithm may be based on mathematical approach such as solving an optimization problem or it depends on some heuristic rules. The control algorithm may need coordination with other agents or it can be done locally.

6.2.3 Coordination among control agents via communication acts

An obvious problem in multiagent systems is how to get agents to communicate with one another. There are many forms that this communication can take, ranging from exchanging messages according to pre-defined protocols to forming teams that work towards a common goal [115]. In the early 1990s, the DARPA Knowledge Sharing Effort (KSE) began to develop the Knowledge Query and Manipulation Language (KQML) and the associated Knowledge Interchange Format (KIF) as a common framework via which multiple expert systems could exchange knowledge. KQML is essentially an outer language for messages; it defines a simple format for messages, and 41 performatives [116].

In 1995, the Foundation for Intelligent Physical Agent (FIPA) began its work on developing standards for agent systems. The centerpiece of this initiative was the development of an ACL [114]. This ACL is superficially similar to KQML: it defines an outer language for messages. It defines 20 performatives such as Inform, agree and propose for defining the intended beliefs of messages. FIPA was officially accepted by the IEEE as its eleventh standards committee on 8 June 2005. The FIPA ACL has been given a formal semantics, in terms of a Semantic Language (SL). SL is a quantified multimodal logic, which contains modal operators for referring to the beliefs, desires as well as a simple dynamic logic style apparatus for representing agent's actions [114]. The semantics of the FIPA ACL map each ACL message to a formula of SL, which defines a constraint that the sender of the message must satisfy if it is to be considered as conforming to the FIPA ACL standard. The semantics also map each message to an SL-formula that defines the rational effect of the action.

Table 6.1 categorizes the 20 performatives provided by the FIPA communication language. Based on the FIPA standard, these 20 performatives could be classified into three speech acts. They are informing, requesting and composite speech acts.

6.2.3.1 Informing messages:

Probably the simplest form of communication that can take place between two agents involves the exchange of information. Such information exchange will usually result in belief changes. Attempt to communicate information are known as representative speech acts [114]. The paradigm example of representative acts involves agents uttering simple declarative sentences. Inform messages are required to help agent(s) well define the events or states. Assume an agent has some sensors which tell agent that the system is in state (s) and some actuators which decided to take an action (a) based on the state (s).

Table 6.1: Performatives provided by the FIPA communication language [114].

Performative	*Passing Information*	*Requesting Information*	*Negotiation*	*Performing Actions*	*Error Handling*
accept-proposal			√		
agree				√	
cancel		√		√	
cfp			√		
confirm	√				
disconfirm	√				
failure					√
inform	√				
inform-if	√				
inform-ref	√				
not-understood					√
propose			√		
query-if		√			
query-ref		√			
refuse				√	
reject-proposal			√		
request				√	
request-when				√	
request-whenever				√	
subscribe		√			

These actions can lead to a new state of the system. If these sensors do not operate perfectly, the action will be incorrect and will not achieve the objective of the control agent.

6.2.3.2 Requesting:

Inform speech acts are attempts by the speaker agent to get the hearer to believe some state of affairs. In contrast, request speech acts (directive) are attempts by the speaker to modify the intentions of the hearer. There are two different types of requests [114].

1- Requests to bring about some state of affairs. An example of such a request would be when one agent said “voltage regulation is required”. Such requests is called “request-that.”

2- Request to perform some particular action. An example of such a request would be when one agent said”Set the taps at 10.” This request is called “request to.”

6.2.3.3 Composite speech acts:

Agents can engage in many and varied types of social interaction. Cooperative problem solving is a much more sophisticated and structured form of social interaction compared with informing and requesting acts. Cooperative problem solving occurs when a group of control agents choose to work together to achieve a common goal. One of the generalized models that attempts to account for the mental state of control

agents as they are engaged in the cooperative problem solving process, is presented in [114] . The model consists of four stages:

1- *Recognition*: where, the cooperative problem solving process begins when some agent recognizes the potential for cooperative action. This recognition may come about because an agent has a goal that it doesn't have the ability to achieve on its own, or else because the agent prefers a cooperative solution. This agent could be called the *initiator* agent.
2- *Team Formation*: during this stage, the *initiator* agent at the first stage solicits assistance or subscription. If this stage is successful, then it will end with a group of agents having some kind of nominal commitment to collective action, these are *participant* agents.
3- *Plan Formation*: during this stage, both the *initiator* and *participant* agents attempt to negotiate a joint plan that they believe will achieve the desired goal (their *intention*).
4- *Team action*: during this stage, the newly agreed plan of joint action is executed by the agents, which maintain a close relationship throughout.

6.2.3.3.1 FIPA Contract-Net-Protocol

FIPA contact net protocol (CNP) is one of the interaction protocols that match the above model. CNP is one of the well-defined approaches. It specifies the interaction between agents for fully automated negotiation through the use of contracts [117]. At any time, any control agent can be an *initiator*, a *participant* or both. CNP creates a means for contracting as well as subcontracting tasks, in this sense *initiator* and *participants* are contractors.

As shown in Figure 6.3, CNP is composed of a sequence of four main steps. *First:* the initiator solicits proposals from other agents by sending a Call for Proposal (CFP) message that specifies the action to be performed and, if needed, conditions upon its execution. *Second:* the responders can then reply by sending a *Propose* message including the preconditions that they set out for the action. Alternatively, responders may send a *Refuse* message to refuse the proposal or, eventually, a *Not-understood* to communicate communication problems. *Third:* the initiator can then evaluate all the received proposals and make its choice of which agent proposals will be accepted and which will be rejected. *Fourth:* once the responders whose proposal has been accepted (i.e. those that have received an *Accept-proposal* message) have completed their task, they can, finally, respond with an *Inform* of the result of the action (eventually just that the action has been done) or with a *Failure* if anything went wrong.

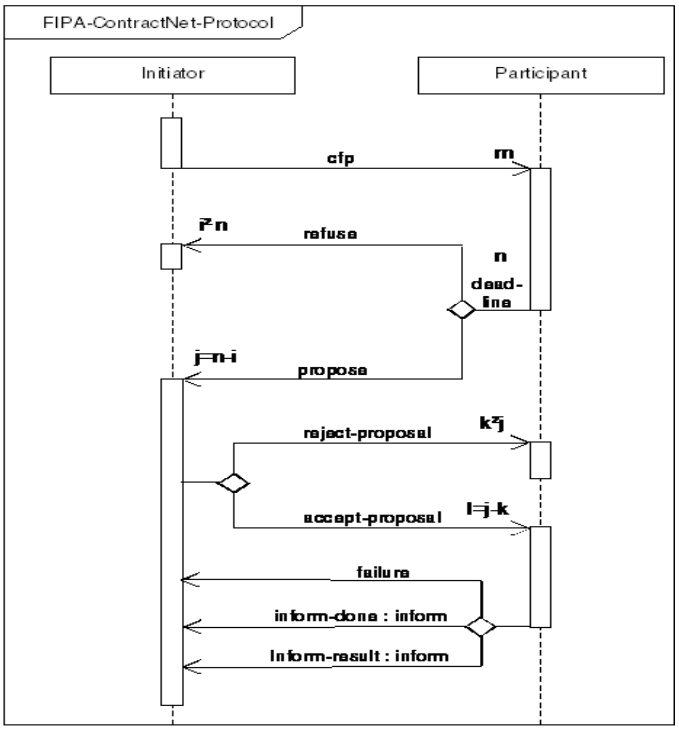

Figure 6.3: FIPA contract net protocol [118]

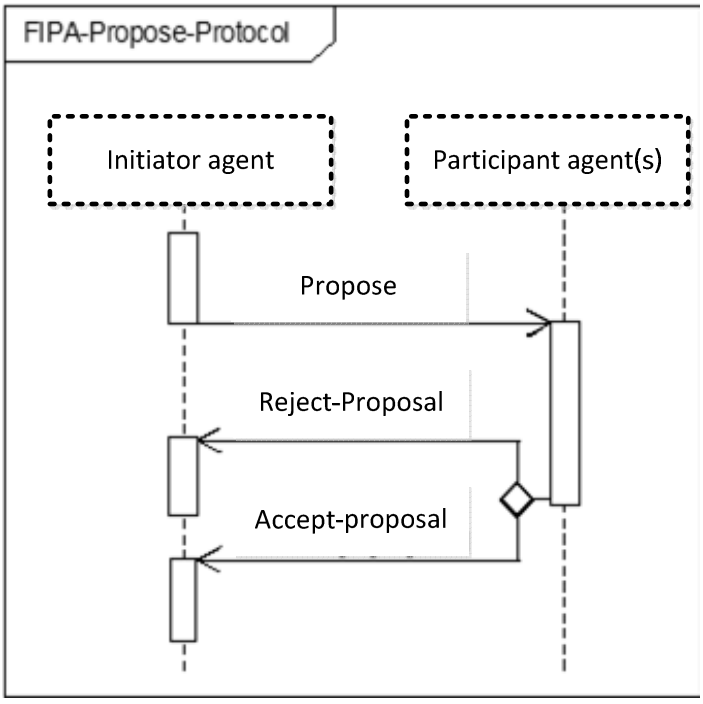

Figure 6.4: FIPA propose protocol [118]

6.2.3.3.2 FIPA- Propose

As shown in Figure 6.4, this interaction protocol allows the *Initiator* to send a *propose* message to the *Participant* indicating that it will perform some action if the *Participant* agrees. The *Participant* responds by either accepting or rejecting the proposal, communicating this with the *accept-proposal* or *reject-proposal* communicative act, accordingly. Completion of this interaction protocol with an *accept-proposal* act would typically be followed by the performance by the *Initiator* of the proposed action and then the return of a status response.

6.3 Communication Aspects of the Proposed Control Scheme

In this section, some of the important aspects that are related to the practical implementation of the proposed two ways communication control are highlighted.

6.3.1 Practical implementation issues of two ways communication:

Communication is a fundamental element of the SG; the appropriate design for physical, data and network communications layers are a topic of intense debate. The SG could exploit multiple types of communications technologies, ranging from fiber optics to wireless to wire-line. Power line communication (PLC) might be a good candidate in our scenario: it is the only technology that has a deployment cost comparable to wireless, since the lines are already there [119].

6.3.2 Messaging and control agents' reliability

If the physical communication medium (wired or wireless) is not reliable, messages that are sent by a control agent may never arrive, arrive too late, arrive multiple times, or arrive out of order. Also when the messages arrive, the service may crash and lose some messages. Actually in wired or wireless communications, many techniques can be used to prevent these issues and increase the messaging reliability. For example, in many of communication systems a Cyclic Redundancy Check (CRC) code is designed to detect accidental changes to the transmitted data, and is commonly used in wireless and wired networks [120]. Furthermore, for more advanced communication networks, block or convolutional codes (also called error-correction codes) are used extensively in wireless networks. These codes permit reliable communication of an information sequence over a channel that adds noise, introduces bit errors, or otherwise distorts the transmitted signal [121]. By using these types of coding, the probability that the destination will wrongly detect the signal is so minimal and it can be assumed that the signal will be detected correctly at the destination.

6.3.3 Synchronization issue:

In most distributed communication systems, relatively short packets of data are transmitted asynchronously. Therefore, packet acquisition, or burst synchronization, has to be performed for each individual packet. A reliable synchronization method is mandatory to avoid undue signaling overhead and excessive packet loss. In [122] a fast burst synchronization for PLC systems operating below 500 kHz and transmitting data rates of up to about 500 kbps, as is typical in various PLC network applications, was proposed. The authors in [123] showed that a very little additional guard space between transmissions is required to achieve proper synchronization.

6.3.4 The value of exchanging messages:

One of the important features in building a distributed control structure is minimizing the exchanging messages. Reducing the exchanging messages could be achieved by estimating the value of *inform* messages. When an agent receives an *inform* message from another agent or from a sensor, the value of the received inform message depends on its impact that this message has on the action of the control agent, or how large is the change in the control agent's action. In general, the value of an *inform* message could be calculated using (6.1) [124], where E_1 is the expected *utility* or reward when the agent takes the action without the *inform* message and E_2 is the expected utility when the agent takes the action considering the *inform* message.

$$Value\,of\ \inf = E_2 - E_1 \tag{6.1}$$

For example, consider an *inform* message sent from a DG agent to the LTC/SVR agent at a certain time which contains its location, generated power and voltage. This message is valuable when it leads the LTC/SVR agent to figure out that its local estimation will not achieve its objective. On the other hand, the values of this *inform* message is zero if it will not affect the action of the LTC/SVR agent. Therefore, the values of any inform message should be calculated before it is sent to the LTC/SVR agent. The value of informing messages could be calculated directly in the sending agent through offline simulations. Another way of calculating the value of informing messages is learning through online interaction.

6.4 The Detailed Operation Mechanism and Coordination Protocols between the Control Agents

Figure 6.5 shows the objectives of voltage regulators, shunt capacitors and DG control agents that they should consider. As shown in the figure, all control agents have a common objective; minimizing the voltage deviation along the feeder. Further, each control agent has its own objective and constraints regarding the preferences and capability of the device. For instance, regulation devices aim to minimize the number of operations per day (so as not to cause unnecessary wear and increase their lifetime). This section describes the operation mechanism of each control agent and their coordination via two ways communication based on the framework of the proposed distributed control structure that has been illustrated in the previous section.

6.4.1 LTC/SVR control agent operation mechanism

Figure 6.6 shows the proposed internal architecture of the LTC/SVR controller. The architecture is based on the intelligent BDI agent model shown in Figure 6.2 and the LDC control. The details of the proposed architecture are described hereunder:

1- LTC/SVR control agent estimates the voltage at its target point using its local measurements and LDC calculations (2.2)-(2.3).

2- To avoid improper estimation of the voltage at the target point, each DG control agent that is connected between LTC/SVR and its target point sends an *inform* message which contains its location and its generated power.

3- The *percepts* from steps 1-2 help the LTC/SVR control agent *beliefs* module to properly estimate the voltage at the target point. Let P_g, Q_g and V_g be the real power, reactive power and bus voltage for a DG that is installed at a distance d from the substation. The modified expression of the relay voltage should be as shown in (6.2); where L is the total length of the feeder and CTP is the current transformer ratio. It is worth noting that the second term in (6.2), due to the installed DG, is calculated using the *inform* message(s).

$$V_{relay} = V_{relay\_LDC} - \left(\frac{P_g - jQ_g}{(CTP)V_g^*} \right) \left(\frac{L-d}{L} \right) (R_{set} + jX_{set}) \tag{6.2}$$

4- Other control agents (DG units and shunt capacitors) send a *propose* message to LTC/SVR control agent when they are connected after the LTC/SVR target point. They observe

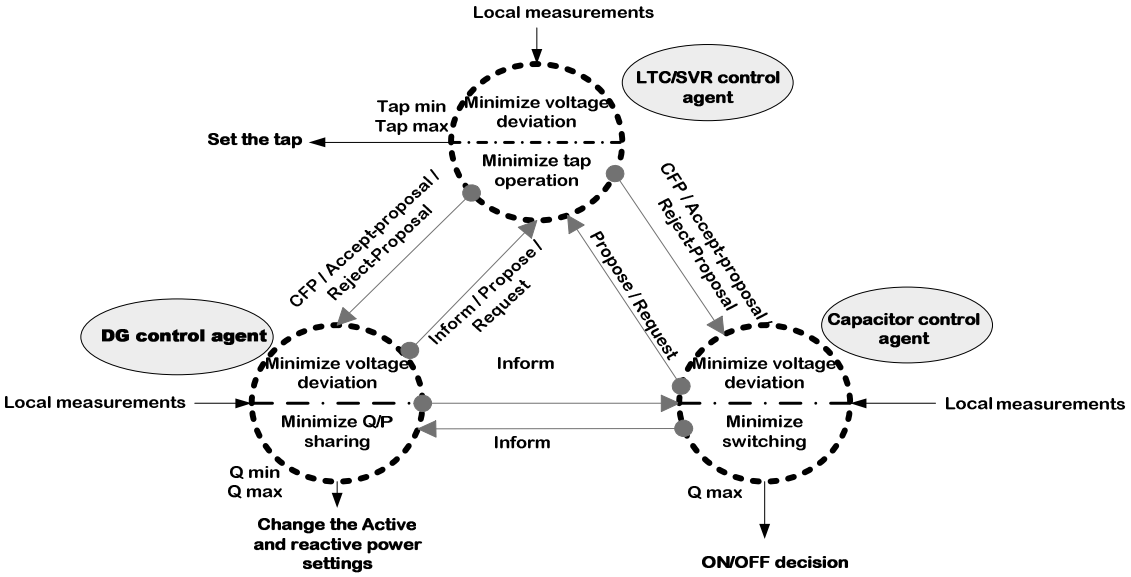

Figure 6.5: Coordination via two ways communication among control agents for proper voltage regulation

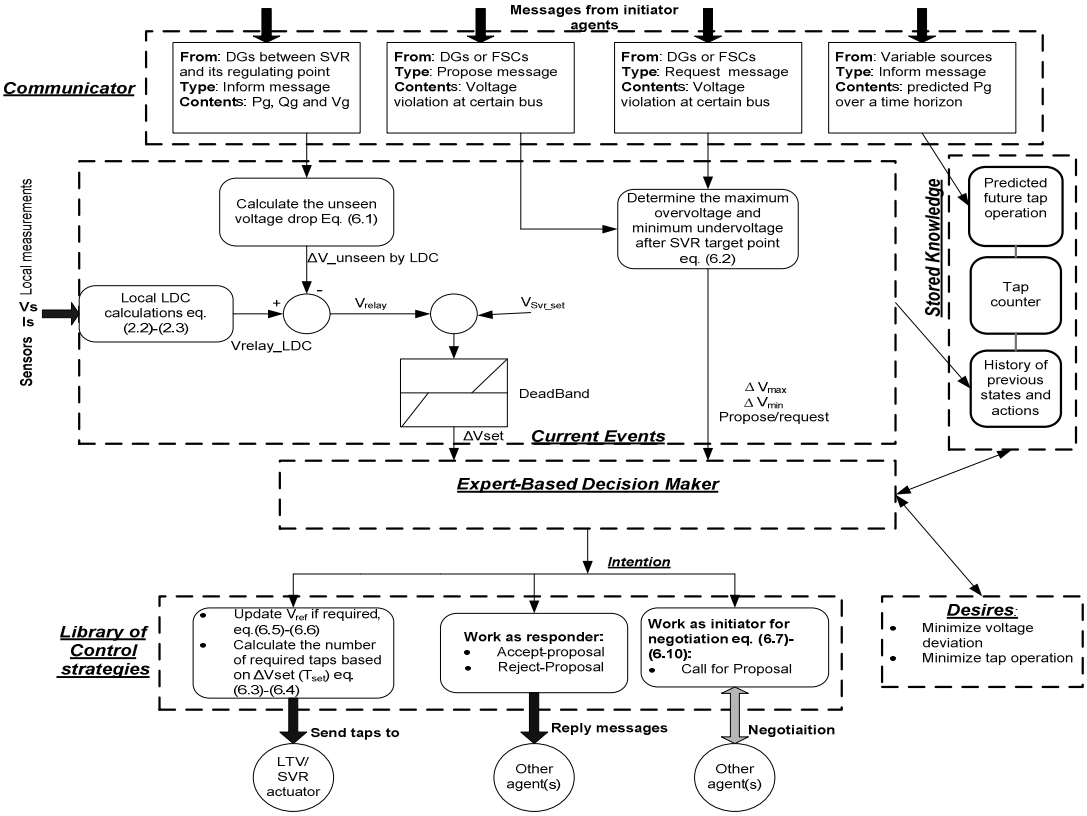

Figure 6.6: The internal architecture of the proposed LTC/SVR control agent

overvoltages or undervoltages in their local or adjacent nodes, and they have the capability to regulate the voltage.

5- In the case where these control agents don't have the capability to regulate the voltage, they send a *request* message to the LTC/SVR control agent.

6- Based on the *percepts* of steps 4-5, the *beliefs* module of the LTC/SVR control agent determines the maximum overvoltage or the minimum undervoltage using:

$$\Delta V_{\max} = \max\left(V_m - V_{\max}\right),\ \Delta V_{\min} = \min\left(V_{\min} - V_m\right) \tag{6.3}$$

where V_{max} and V_{min} are the maximum and minimum voltages that allowed in the system and V_m is the voltage at certain bus.

7- If DG units are variable power sources, the LTC/SVR control agent receives *inform* messages from their control agents at each time horizon, for example every 3 hours (depending on the forecasting accuracy), containing the predicted generated power over this horizon. These *inform* messages help the LTC/SVR control agent *beliefs* module to predict excessive operation of the LTC/SVR due to intermittent sources over the specified time horizon. This prediction could be determined by carrying out offline simulations if the forecasted load and generation are available. This task could be done using a SCADA system, if it exists. *In this chapter, we assume that the predicated tap operation is given.*

8- The LTC/SVR agent *beliefs* module sends four inputs to its decision maker. These inputs are ΔV_{set} (voltage deviation of the target point with respect to its reference), *propose* (includes $\Delta V_{max}/\Delta V_{min}$*), request (*includes $\Delta V_{max}/\Delta V_{min}$*),* and *Average ET* (predicted excessive tap operation). The four variables have been coded as shown in Table 6.2. In this work, the inputs have been coded as crisp values. However, ΔV_{set}*, Average ET,* and the contents of the *propose/request* messages could be represented as fuzzy sets by defining fuzzy membership functions [125].

9- The decision maker of the LTC/SVR control agent has four outputs. These outputs are T_{set} (set the tap), V_{set}^{u} (update the reference voltage of the target point), *reply* (send reply to a message), CFP (decision of negotiation by call for proposal). The four outputs have been coded as shown in Table 6.3.

Table 6.2: Codes of the input variables of the LTC/SVR decision maker

Code	ΔV_{set}	*propose*	*request*	*Average ET*
0	Within DB	No message	No message	Taps<10/day
1	Over DB	Overvoltages	Overvoltages	10<Taps<15
2	Under DB	Undervoltages	Undervoltages	Taps >15

Table 6.3: Codes of the output variables of the decision maker

Code	T_{set}	V_{set}^{u}	*reply*	*CFP*
0	no change	no change	no reply	no
1	down	down	accept	start
2	up	up	reject	cancel

Table 6.4: Input-output mapping in the LTC/SVR decision maker

Inputs				Outputs			
ΔV_{set}	*propose*	*request*	*ET*	T_{set}	V_{set}^{u}	*reply*	*CFP*
1	0	0	0	1	0	0	0
1	1	0	0	1	0	2	0
1	0	1	0	1	0	1	0
0	1	0	0	0	0	1	0
0	0	1	0	0	1	1	0
0	0	1	1	0	0	1	1
2	0	0	1	2	0	0	0

10- The decision maker of the LTC/SVR agent performs a mapping between the inputs and the outputs to achieve the objectives of the LTC/SVR agent (minimizing the voltage deviation or the tap operation). An expert-based decision making has been used in this work to map the inputs and outputs of the decision maker. The rules have been extracted based on the simulations presented in Chapter 3. Table 6.4 shows the inputs-outputs mapping of the LTC/SVR decision maker.

11- Note that at each specific time, the decision maker of the LTC/SVR agent selects one of the objectives; 1) perform voltage regulation by itself (by setting the tap directly or update the reference of the target point) or 2) start negotiation with other agents by sending a call for proposal.

12- The control strategies module of the LTC/SVR receives the decision from the decision maker and executes this decision. When the LTC/SVR agent decides to perform voltage regulation, one of these actions will be executed at each time *i*:

$$Tap^{i} = Tap^{i-1} - round\left(\frac{V_{relay}^{i} - V_{svr\_set}^{i}}{0.75}\right) \qquad if\ T_{set}^{i} = 1 \tag{6.4}$$

$$Tap^{i} = Tap^{i-1} + round\left(\frac{V^{i}_{svr\_set} - V^{i}_{relay}}{0.75}\right) \qquad if\ T^{i}_{set} = 2 \tag{6.5}$$

$$V^{i}_{svr\_set} = V^{i-1}_{svr\_set} - \Delta V_{\max} \qquad if\ V^{u,i}_{set} = 1 \tag{6.6}$$

$$V^{i}_{svr\_set} = V^{i-1}_{svr\_set} + \Delta V_{\min} \qquad if\ V^{u,i}_{set} = 2 \tag{6.7}$$

13- If the LTC/SVR agent fails to perform voltage regulation or decides to reduce the tap operation, it works as an initiator and starts negotiation for voltage regulation using *CNP*. Other control agents, which propose participation, will be evaluated by the LTC/SVR agent based on certain criteria. In this work the sensitivity analysis is used for the evaluation. Sensitivity analysis can be described by the sensitivity matrix *S* [69].

$$\Delta V_L = S\Delta U \tag{6.8}$$

where, ΔVL is the state variable vector containing all voltages at load nodes; ΔU is the control variable vector containing voltage control, reactive power injection or real power change of participant agent(s); S is the sensitivity matrix of voltages at the load bus with respect to the control variable at the control agent node. The sensitivity matrix is mainly based on the system bus impedance matrix and the operating point. The sensitivity of bus voltages due to the changes of active and reactive power injection can be represented by linear equations as follows:

$$\begin{bmatrix} \Delta P \\ \Delta Q / V^{o} \end{bmatrix} = \begin{bmatrix} J_{p\theta} & J_{pV} \\ J_{q\theta} & J_{qV} \end{bmatrix} \begin{bmatrix} \Delta\theta \\ \Delta V \end{bmatrix} \tag{6.9}$$

The effect of active and reactive power generation change on bus voltages can be considered separately from (6.9) by (6.10) and (6.11); where A and B are the sensitivity matrices for the change of injected real and reactive power respectively. These equations express the ability of the DG/FSC to contribute to voltage regulation by varying its active and reactive power generation [126].

$$[\Delta P] = \left[J_{pV} - J_{p\theta} J^{-1}_{q\theta} J_{qV}\right][\Delta V] = [A][\Delta V] \tag{6.10}$$

$$\left[\Delta Q / V^{o}\right] = \left[J_{qV} - J_{q\theta} J_{p\theta}^{-1} J_{pV}\right][\Delta V] = [B][\Delta V] \tag{6.11}$$

6.4.2 DG/FSC control agent operation mechanism

The detailed interior structure of DG/FSC control agents based on the BDI model is presented hereunder:

1- DG/FSC control agent measures its local voltage, line real power and reactive power.

2- The *percepts* from step 1 help the DG/FSC control agent *beliefs* module properly estimate the voltage at adjacent nodes using [51]:

$$V_{d+1}^2 = V_d^2 - 2\left(r_d P_d + x_d Q_d\right) + \left(r_d^2 + x_d^2\right)\left(\frac{P_d^2 + Q_d^2}{V_d^2}\right) \tag{6.12}$$

where P_d, Q_d and V_d are the bus voltage, the line real power and the reactive power for a DG that is installed at a distance d; r_d and x_d are the equivalent resistance and reactance between the DG and its adjacent.

3- The *beliefs* module determines the current state of the voltage at the DG/FSC location and other adjacent node(s), V_{state}.

4- The *beliefs* module for a DG control agent determines the amount of available reactive power at each time step *i* where:

$$Q_{g\_av}^{i} = Q_g^{total} - Q_g^{i} \tag{6.13}$$

$$Q_g^{total} = \sqrt{S_{rat}^2 - \left(P_g^i\right)^2}\ \text{, and} \quad Q_g^{\min} \le Q_g^{total} \le Q_g^{\max} \tag{6.14}$$

While the *beliefs* module of a FSC control agent determines the amount of available reactive power at each time step *i* using:

$$Q_{FSC\_av}^{i} = Q_{FSC}^{unit}\left(n_{banks}^{total} - n_{banks}^{on}\right) \tag{6.15}$$

where, Q_{FSC}^{unit} is the amount of reactive power for each capacitor bank, n_{banks}^{total} is the total number of capacitor banks and n_{banks}^{on} is the number of capacitor banks that are already in service.

5- The *beliefs* module for DG/FSC control agent could receive *Inform* messages from neighbor agents to get knowledge of voltages state at other nodes. *This is not considered in this chapter*.

6- The *beliefs* module for DG/FSC control agent could receive *CFP*, *reply to proposal* or *reply to request* from the LTC/SVR control agent.

7- The *beliefs* module for DG/FSC control agent sends five inputs to its decision maker. These inputs are V_{state} (state of the voltage at local and adjacent nodes), $Q_{g\_av}/Q_{FSC\_av,}$ *CFP, RP* (reply to proposal) and *RR* (reply to request). The five variables have been coded as shown in Table 6.5.

8- The decision maker of the DG control agent has five outputs. These outputs are Q_{g_set} (set the generated reactive power), V_{g_set} (DG operates in PV mode with reference voltage), P_{g_set} (real power curtailment), *propose* message to the LTC/SVR agent (in case the DG has the capability to regulate the voltage) and *request* message to the LTC/SVR agent (in case the DG doesn't have the capability to regulate the voltage). While, the FSC control agent has three outputs; they are B_{bank_set} (set the status of each capacitor bank), *propose* message to the LTC/SVR agent and *request* message to the LTC/SVR agent). The outputs of DG/FSC control agents have been coded as shown in Table 6.6.

9- The decision maker of the DG/FSC agent does a mapping between the inputs and the outputs to achieve the objectives of the DG/FSC control agent. Table 6.7 shows the inputs-outputs rules that have been extracted using the expert-knowledge and simulation for DG control agent. Similar rules have been also extracted for the FSC control agent.

10- Note that in case of DG control agent, only the status of one output can be changed in each input-output action and some of the outputs such as Q_{g_set} and V_{g_set} cannot be activated at the same time.

11- The control strategies module of the DG/FSC control agent receives the decision from the decision maker and executes this decision. Figure 6.7 and Figure 6.8 show the details of the control strategies module of DG and FSC control agents, respectively. As shown in Figure 6.7, based on the outputs of the decision maker a proper action is taken by the control strategies to set the reference values of the real and reactive power of the DG. Note that MPPT is the maximum power point tracking, PI is the proportional integrator controller and S_{dd} is the local sensitivity of DG voltage with respect to its real power. Figure 6.8 shows that the amount of required reactive power $Q_{required}$ for the FSC control agent is calculated based on the local sensitivity or via the CNP. Once $Q_{required}$ is calculated, the number of capacitor banks that will change their status is determined using the following:

$$n_{banks}^{ON \leftrightarrow OFF} = ceil\left(\frac{Q_{required}}{Q_{FSC}^{unit}}\right) \tag{6.16}$$

Table 6.5: Codes of the input variables of the DG/FSC decision maker

Code	V_{state}	Q_{g_av}/Q_{FSC_av}	*CFP*	*RP*	*RR*
0	Normal	N/A	N/A	N/A	N/A
1	Over	Low	Over	Accept	Accept
2	Under	High	Under	Reject	Reject

Table 6.6: Codes of the output variables of the DG/FSC decision maker

Code	Q_{g_set}	V_{g_set}	P_{g_set}	B_{bank_set}	*Propose*	*Request*
0	Hold	Not active	MPPT	Hold	N/A	N/A
1	Lag	V_{max}	Curtailment	Switch/local	Over	Over
2	Lead	V_{min}	Curtailment	Switch/CNP	Under	Under

Table 6.7: Input-output mapping of the DG decision maker

Inputs					Outputs				
V_{state}	Q_{g_av}	*CFP*	*RP*	*RR*	Q_{g_set}	V_{g_set}	P_{g_set}	*propose*	*request*
1	0	0	0	0	0	0	0	0	1
1	0	0	0	2	0	0	1	0	0
1	2	0	0	0	0	0	0	1	0
1	2	0	1	0	0	1	0	0	0
1	2	0	2	0	0	0	0	0	0
0	1	1	0	0	0	0	0	1	0
0	1	0	1	0	1	0	0	0	0

where Q_{FSC}^{unit} is the reactive power of each capacitor bank. It is worth noting that the number of capacitor banks will change their status from ON to OFF if $Q_{required}$ is calculated due to overvoltages and their status will be changed from OFF to ON if $Q_{required}$ is calculated due to undervoltages.

6.5 Simulation Studies

To verify the effectiveness of the proposed distributed control scheme, two types of simulations have been carried out. Details of the simulation studies are explained hereunder:

6.5.1 One shot simulation (analytical studies):

This type of simulation aims to show the importance of some specific features of the proposed distributed control without implementing the whole control structure. The simulations have been carried out in MATLAB by running a generic distribution system power flow program at a certain operating point (no continuous operation) [89]. The IEEE 13 bus unbalanced test feeder shown in Figure A.1 has been used to show the important features of the distributed control.

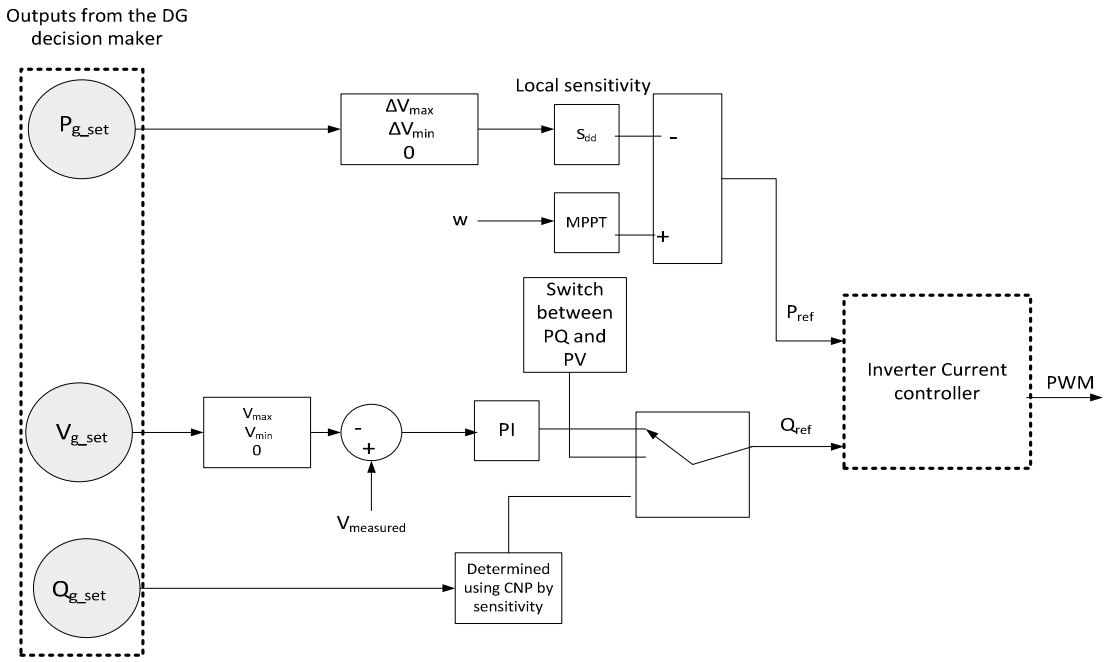

Figure 6.7: The control strategies module of an inverter-based DG control agent

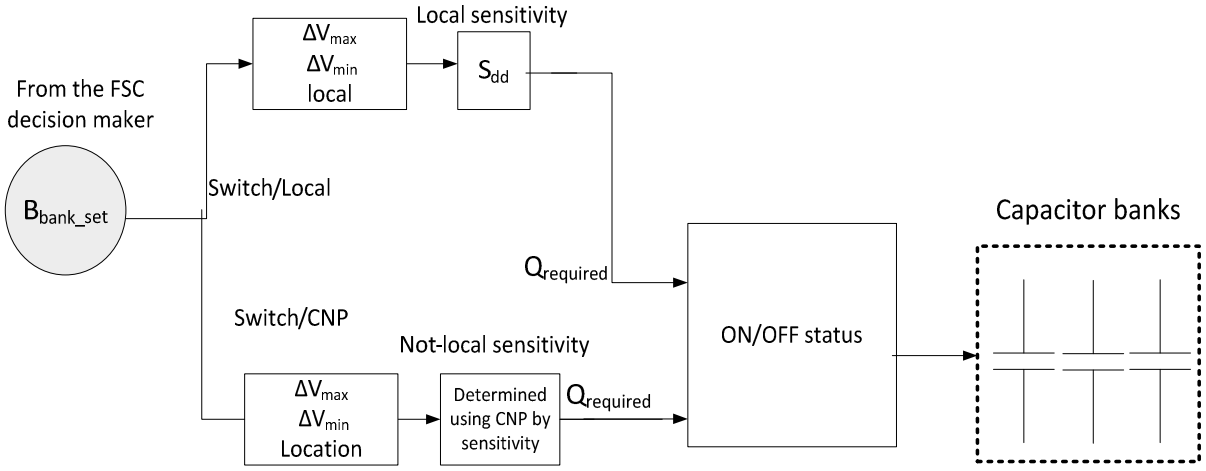

Figure 6.8: The control strategies module of the FSC control agent

6.5.1.1 The importance of sending *Inform* messages from DG to SVR control agent:

Figure 6.9 shows the SVR tap operation for phase c when a DG is installed close to the SVR without and with sending *informing* messages. Without *inform* messages the SVR calculates the number of required taps based on the LDC measurements. In this case, the number of required taps decreases with the increase of the generated power and causes the improper voltage regulation shown previously in Figure 3.6. In contrast, the *inform* messages trigger a correction for the LDC calculation and thus correct the number of taps which are required for proper voltage regulation as shown in Figure 6.10.

6.5.1.2 The importance of having knowledge of a predicted excessive tap operation in a future short time horizon:

Figure 6.11 shows the tap change over a 3-hour horizon with and without having knowledge of a predicted excessive tap operation. The figure shows that the SVR agent could avoid excessive tap operation when it has knowledge of the predicted tap operation. When excessive tap operation is predicted, SVR agent could decide to start negotiation with intermittent sources agents by CNP to reduce the predicted excessive operation. In this scenario, three DG units at nodes 634,671 and 680 have been switched from unity power factor to 0.9 power factor lead.

6.5.2 Simulation model with a multi-agent platform (continuous time simulation)

In this section a simulation model has been proposed to do full implementation and continuous time simulation of the proposed distributed control. Figure 6.12 shows the proposed continuous time simulation model. As shown in the figure, this simulation model consists of three main components; they are the Simulink model, TCP/IP communication middleware (interface between Simulink and Java) and a multiagent system platform (JADE). The model is presented in detail due to the lack of information allowing researchers to find a proper interface between Simulink and a multiagent platform. Simulink™ has been used to model the distribution system. The main purpose of using Simulink is to represent the dynamic change of loads and DG power. The JADE platform is a famous Java™ framework for developing FIPA-compliant agent applications. It provides the required communication infrastructure and platform services [127]. Using JADE, it is easy to implement the proposed distributed control structure. In this work, the modules of each control agent have been implemented in JADE and the sensors and the actuators of the devices have been implemented in Simulink™. The communication middleware allows the multi-agent platform to send/receive data to/from the actuators/sensors in Simulink™.

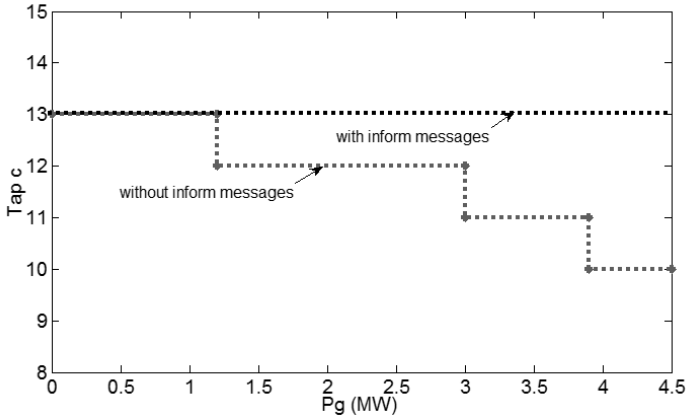

Figure 6.9: SVR tap operation without and with receiving *inform* messages

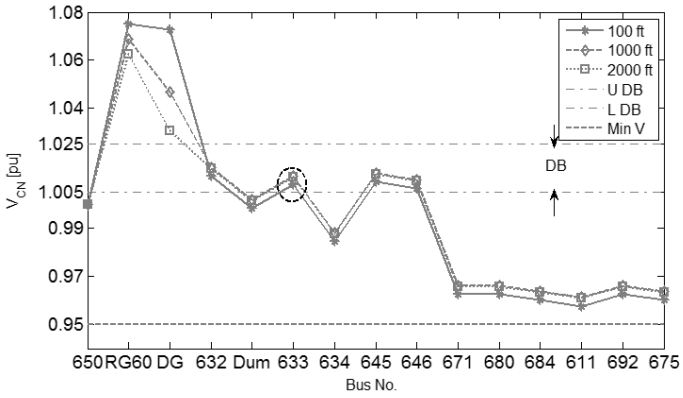

Figure 6.10: Voltage profile of phase c with inform messages

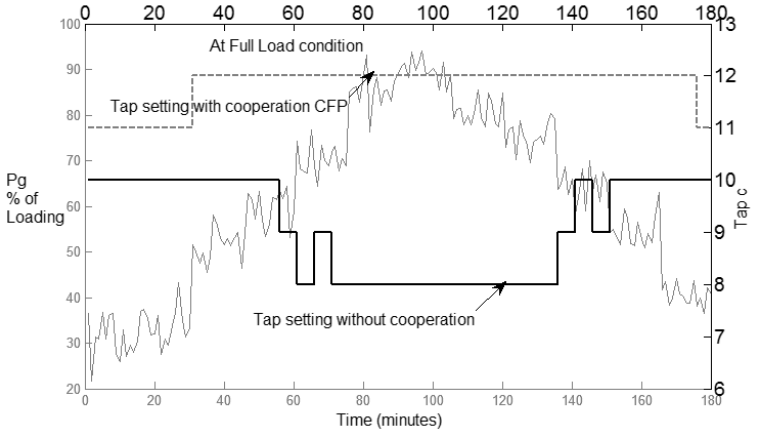

Figure 6.11: Variation of the SVR taps with the variation of the generated power from intermittent sources with and without cooperation.

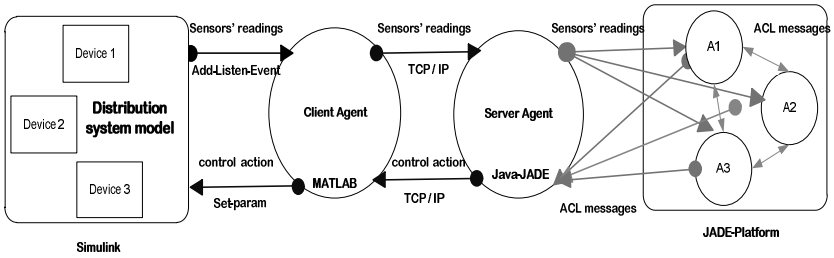

Figure 6.12: The proposed continuous time simulation model

In this work, a client/server socket communication has been proposed as a communication middleware between JADE and Simulink [128]. In this Simulation model, the Client is the implementation in Simulink and the Server is the multi-agent system in JADE. To open a client socket in Simulink, a Simulink function call "*Add-Listen-Event*", has been used. This function is used to send the readings of the sensors at each time step to the MATLAB workspace. The advantage of using this function is that it makes synchronization easy by halting the Simulink model time step until it the sensors have executed. This function is used to call a client *m* file call client agent, which in turn sends a connection request to a server JADE file call server agent. After the server agent accepts the connection request, the client agent starts to send the readings of the sensors to the server agent through TCP/IP communication. Then the server Java file distributes these readings to the multi-agent system through agent communication language (ACL) and waits to receive the control actions from the multi-agent system. The server agent sends the multi-agent system control actions to the client agent through TCP/IP. Finally, the client agent sends the control action for each actuator in the Simulink model using a MATLAB function call "*set-param*".

To verify the effectiveness of the proposed distributed control, the 16-bus balanced radial distribution test system shown in Figure A.6 has been selected [129]. The balanced test system has been used instead of the 13 bus unbalanced feeder to simplify the implementation in Simulink^{TM}. The 69/13.8 kV transformer has been modified to include an LDC-based LTC with 32 taps. The system consists of three main feeders. The 13.8 KV distribution substation is equipped with a three phase 1.5 MVAr shunt capacitor bank. Table A.12 gives the bus and line data of the 16-bus test system. Table A.13 shows the types, ratings and locations of the installed DG units. As shown in the table, four DG units (two are dispatchable and two are non-dispatchable) are connected in different locations of the studied system.

6.5.2.1 Base case without the proposed multi-agent structure

Figure 6.13 shows the load and generation profiles over 24 hours. Figure 6.14 shows the voltage profile at load buses when the DG units operate at unity power factor and the LTC operates with the traditional control technique. The figure shows that during the first 6 hours the load voltage at bus 15 and 16 violates its upper limits.

6.5.2.2 With the proposed control structure

Figure 6.15 shows the exchanging messages among the control agents during the day. As shown in Figure 6.15 once a voltage violation occurred at bus 16 at 00:00, S_G agent initiated the *FIPA-propose* protocol. It sent a *propose* message to the LTC agent. The contents of the *propose* message are voltage regulation at local bus (bus 16) by adjusting the voltage to 1.05 p.u. Then the LTC agent sent an *accept-proposal* message to the S_G agent. Figure 6.16 shows the voltage profile at bus 16 when the S_G agent executed its action. At 3:00 AM, a voltage violation occurred again due to the increase of the wind power. In this case, the S_G agent couldn't regulate the voltage because it reached its limits of reactive power absorption. As shown in Figure 6.15, the S_G agent sent an *FIPA-Request* message to the LTC agent. Then, the LTC sent an agree message to the S_G agent. However, to avoid excessive tap operation of the LTC, the LTC agent initiated an *FIPA-Contract-Net protocol* with other control agents. PV and SC control agents sent a *Refuse* messages to the LTC agent. Both the DFIG and MT agents sent a *propose* message to the LTC including their sensitivity to the voltage at bus 16 and their available reactive power capacity. The LTC agent accepted the proposal of the DFIG due to its higher sensitivity. Figure 6.16 shows the voltage profile at bus 16 when the DFIG agent executed its action. Figure 6.17 shows the absorbed reactive power from the S_G and DFIG when they participated in the voltage regulation. The rest of the messages are *Inform* messages to the LTC agent. Figure 6.18 shows the LTC and SC operation during this day. As shown in the figure, the LTC preferred the cooperation during light loads to prevent its excessive operation. Alternatively, the LTC preferred to regulate the voltage by itself during the rest of the day.

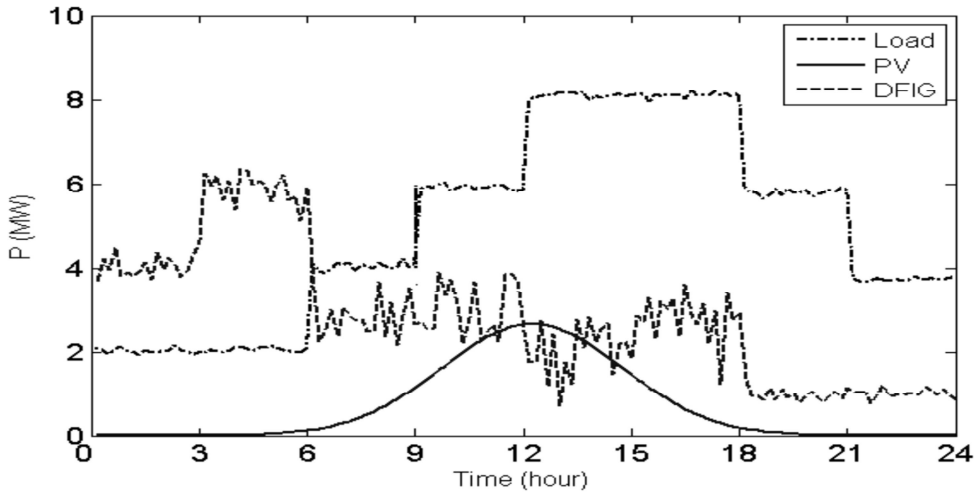

Figure 6.13: Load and generation real power profile over 24 hours.

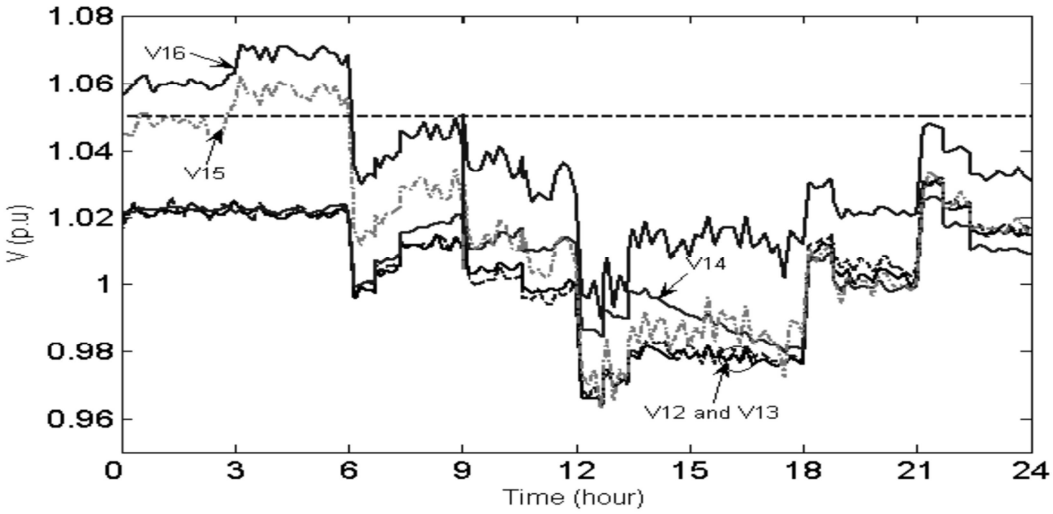

Figure 6.14: Voltage profile at load buses without the proposed control structure

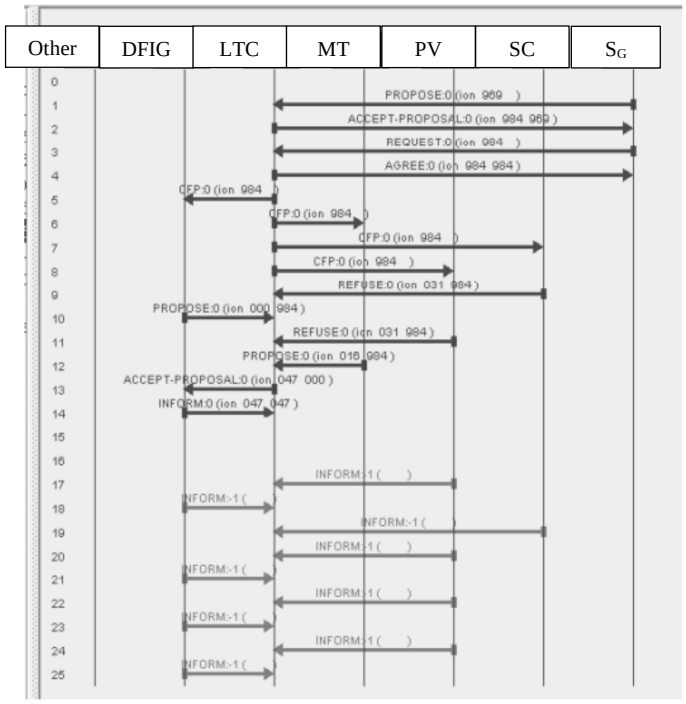

Figure 6.15: Exchanging messages between control agents.

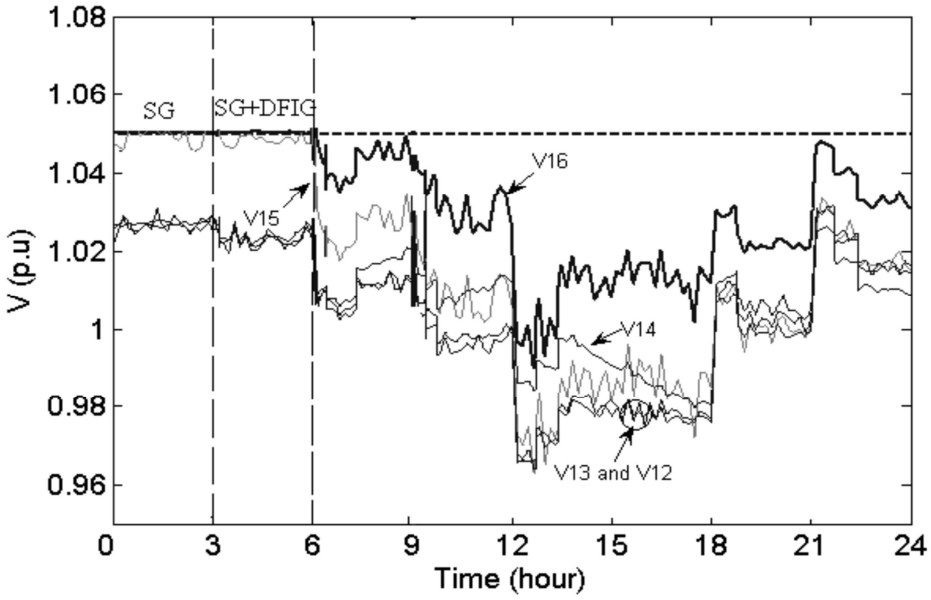

Figure 6.16: Voltage profile at load buses with the proposed control structure

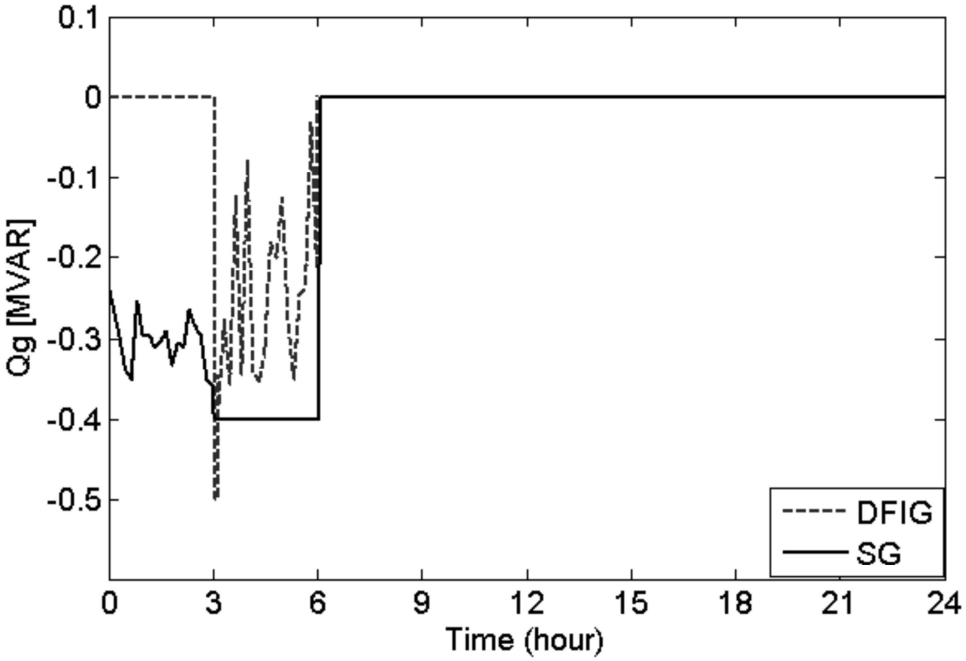

Figure 6.17: The absorbed reactive power in the S_G and DFIG.

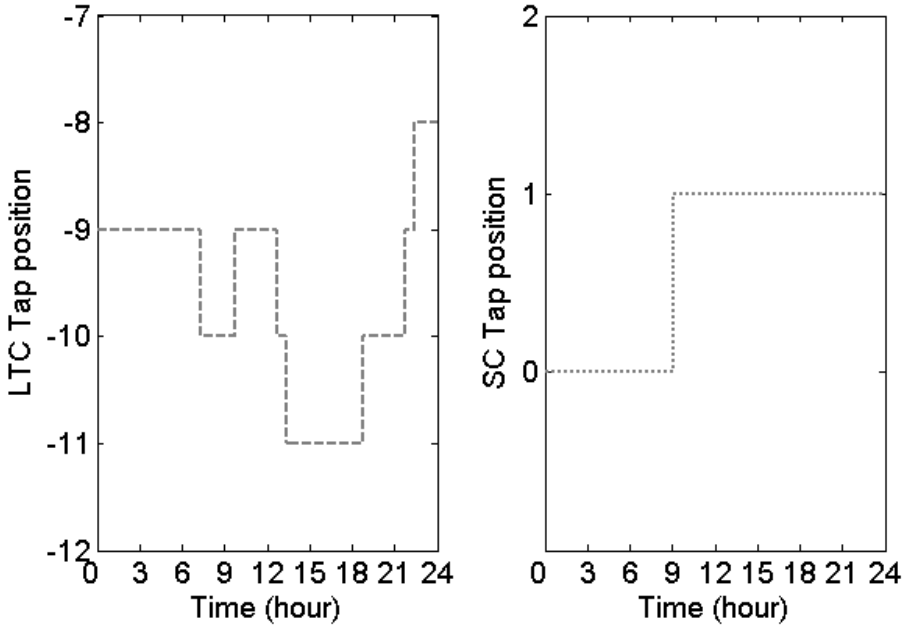

Figure 6.18: LTC and SC operation during the day

6.6 Discussion

In this chapter, a distributed control structure has been proposed for voltage regulation in active distribution feeders, under SG paradigm. The proposed control structure consists of three main types of controllers: LTC/SVR, DG and shunt capacitor controllers. The operation mechanism of each controller has been built based on the concept of BDI intelligent agents. An expert-based decision maker has been implemented in each controller to achieve its objectives and meet its constraints. Coordination via communication protocols has been proposed to avoid interference between the autonomous operations of different controllers. To verify the effectiveness, robustness and autonomous operation of the proposed control structure, a continuous time simulation model has been proposed. The results show that proper coordination via two ways communication is a promising solution to avoid conflicts between devices. This control structure and its implementation could facilitate the applications of SG technologies for autonomous voltage regulation in future distribution systems.

Chapter 7

A Cooperative Voltage and Reactive Power Control for Multiple Feeders in Active Distribution Networks

7.1 Introduction

Conventionally, LDC feature is an integral part of the substation LTC. However, LDC control has several drawbacks when it is integrated with a LTC that is connected on multiple feeders with unbalanced load diversity. These drawbacks are related to the difficulty of determining proper LDC settings (equivalent circuit parameters and the load reference voltage) and the hysterical tap changing mechanisms of the LTC [130]. In the previous chapter a distributed control scheme for voltage regulation in distribution feeders has been developed. A modified communication-based LDC control for LTC/SVR has been presented. However, the work presented in the previous chapter is designed for LTC/SVR that typically uses LDC control. Thus the previous chapter did not consider the case of multiple feeders having a substation LTC and unbalanced load diversity that is expected to face serious challenges with LDC control and DG integration.

In addition, an infeasible solution may occur for multiple feeders in ADNs due to the unbalanced load diversity and high DG penetration. The infeasible solution occurs when the difference between the overall maximum and minimum voltages exceeds the specified regulation band (V_{max}, V_{min}) as shown in (7.1). The infeasible solution will confuse the operation of LTC and may result in improper settings and excessive tap operation i.e. hunting.

$$V_{\max}^{sys} - V_{\min}^{Sys} > V_{\max} - V_{\min} \tag{7.1}$$

Furthermore, appropriate decisions in control agents cannot be taken without proper knowledge of the current state of the network. In the previous chapter, since almost no information is available beyond the local measurements of the control agents, proper decisions might be unreachable. Therefore, development of a state estimator for such control structure is a challenging task. The biggest challenge is due to the absence of enough information [131, 132]. In ADNs with multiple feeders having unbalanced load diversity and high penetration of intermittent power sources, the problem of state estimation will be more challenging. Hence new real time measurements and communication links must be provided for proper state estimation.

Finally, it was observed that taking a decision for voltage regulation without considering the feeder losses, might result in excessive system losses. Therefore, there is a need for modifying the previous work to take into account the total system losses.

Accordingly, in this chapter a cooperative control scheme is proposed to: 1) provide a proper state estimation algorithm for the voltage profile, 2) mitigate the interference between LTC and DG operation and guarantee a proper voltage regulation in all operating conditions, 3) relieve the stress on tap operation of LTC and FSC, 4) avoid unnecessary DG active power curtailment, and 5) take the total system losses into consideration. The proposed control scheme will be applied in case of multiple feeders having a substation LTC, unbalanced load diversity and high DG penetration. The proposed cooperative control formulates the problem of voltage and reactive power control based on a multiagent control scheme, where each device is considered as a control agent. Based on the framework presented in the previous chapter, the multiagent control scheme consists of the interior structure of control agents and the exchanging messages between them. A BDI model has been used for the interior structure of each control agent. The FIPA performatives have been used as communication acts between the control agents.

The remainder of the chapter is organized as follows: in Section 7.2 a distributed voltage profile estimation algorithm has been developed. Sections 7.3 and 7.4 present the detailed interior structure of the proposed LTC and DG control agents respectively. In section 7.5, a flowchart describing the detailed distributed control scheme between LTC and DG control agents is presented. Simulation results with different case studies have been carried out in Section 7.6 to demonstrate the effectiveness of the proposed approach. Section 7.7 presents the discussion of the chapter.

7.2 Distributed Voltage Profile Estimation:

In this section, a distributed cooperation protocol for voltage profile estimation is developed. The cooperation protocol aims to provide the LTC control agent with the current state of the minimum and maximum voltages in each feeder, which is considered as an adequate knowledge for appropriate LTC decision making. Figure 7.1 shows the structure of a distribution feeder under the concept of distributed state estimation. As shown in the figure, it is assumed that the voltage and branch power meters are placed at the locations of LTC, DG units, FSC or any other locations, based on optimal placement study of meters. Based on the meter placements, each distribution feeder is divided into segments. Each state estimator (SE) control agent estimates the voltage profile within its downstream

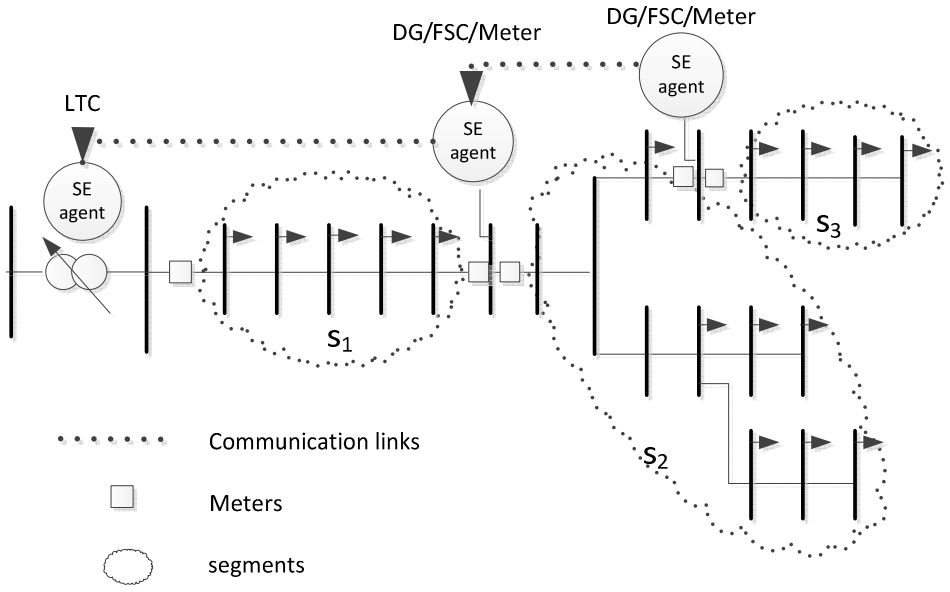

Figure 7.1: Active distribution feeder with distributed state estimation.

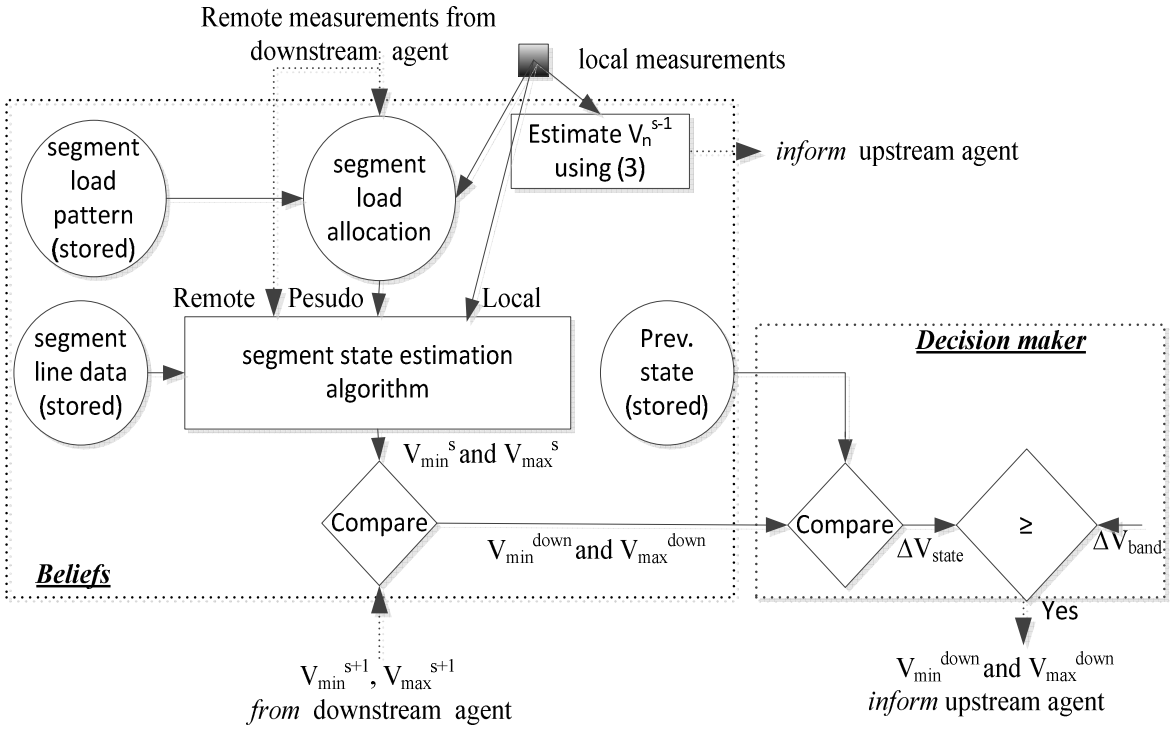

Figure 7.2: The interior structure of segment control agents for voltage profile estimation.

segment. Figure 7.2 shows the structure of each SE control agent for voltage estimation. The detailed interior structure for voltage estimation of a control agent at segment *s* can be summarized as follows [133]:

7.2.1 Beliefs module:

1- It receives its real-time local measurements of branch power for the upstream node of its downstream segment and the downstream node of its upstream segment (P_o^s,Q_o^s, P_n^{s-1}, Q_n^{s-1}) and the voltage magnitude V_o^s for the downstream segment which represents V_{n+1}^{s-1} for the upstream segment.

2- From the real-time local measurements of branch power and voltage magnitude, it estimates the voltage magnitude at the first node of its downstream segment (V_1^s) and the last node of the upstream segment (V_n^{s-1}) using (6.12) .

3- It sends *inform* message contains P_n^{s-1}, Q_n^{s-1} *and* V_n^{s-1} to the upstream control agent and it receives *inform* message contains the real-time measurements for the last branch and node of its downstream segment from the downstream control agent (P_n^s, Q_n^s *and* V_n^s) if any.

4- It allocates the load demand within the downstream segment to provide pseudo measurements to guarantee the observability of the segment. A real-time load modeling technique that incorporates the customer class curves and provides the uncertainty in the estimates is used in the state estimation algorithm [134]. For a segment *s* at time *t*, the real-time load estimates of load point *i*, $P_{Li}(t)$ can be obtained as follows:

$$P_{Li}^s(t) = \left(P_o^s - P_n^s - P_{loss}^s\right)\left[\frac{\sum_{j=1}^{C} LMF_j(t)\times ADC_{i,j}}{\sum_{i=1}^{n}\sum_{j=1}^{C} LMF_j(t)\times ADC_{i,j}}\right] \qquad (7.2)$$

where, P_{loss}^s is the real power loss for segment *s*, *C* is the number of load classes, $ADC_{i,j}$ is the average daily customer demand at load point *i* belonging to class *j* at time *t* and LMF_j is the class-specific load model factor belonging to class *j* at time *t*. The power factor of each load point at time *t* is obtained by historical information.

5- Let *z* denotes the vector containing the measurements and w_i and $h_i(x)$ represent the weight and the measurement function associated with measurement z_i, respectively. The solution of the state estimation problem is obtained by minimizing the performance index *J* given as [131, 132]:

$$\min\ J = \sum_{k=1}^{M} w_k \left(Z_k - h_k(x)\right)^2 \tag{7.3}$$

where *M* is the number of real-time and pseudo measurements of the segment. Different methods have been proposed in the literature to solve (7.3). A branch-based state estimation algorithm has been used in this work [135]. The algorithm depends on calculating the node voltages (state variables) using backward/forward sweep power flow combined with the adjustment of the pseudo measurements (modify the allocated load demands) to satisfy the real-time measurements constraints.

6- Once the voltage profile in the segment is estimated, the *beliefs* module determines the minimum and the maximum voltages in the segment ($V_{\min}^{s}$, $V_{\max}^{s}$).

7- It receives the minimum and maximum voltage from the downstream control agent ($V_{\min}^{s+1}$, $V_{\max}^{s+1}$) if any.

8- It compares the values in steps 6 and 7 using (7.4) and it sends the overall downstream minimum and maximum voltages to the decision maker.

$$V_{\min}^{down} = \min_{down}\left(V_{\min}^{s}, V_{\min}^{s-1}\right), \quad V_{\max}^{down} = \max_{down}\left(V_{\max}^{s}, V_{\max}^{s-1}\right) \tag{7.4}$$

7.2.2 Decision maker module:

Once $V_{\min}^{down}$ and $V_{\max}^{down}$ are determined, the decision maker find the change of the voltage profile ΔV_{state} compared with the previous state and decide whether to *inform* the upstream control agent or not. If $\Delta V_{state} \geq \Delta V_{band}$, the control agent will send an i*nform* message for the upstream control agent contains $V_{\min}^{down}$ and $V_{\max}^{down}$; where ΔV_{band} is the bandwidth of voltage change at which the LTC control agent will not take an action.

7.3 The Proposed Voltage Control for LTC Control Agent

In this section, the detailed interior structure of the proposed LTC control agent is presented.

7.3.1 Percepts (from the bidirectional interface and the communicator):

The LTC control agent receives data from the local sensors and informing messages from the first downstream DG control agents that are connected in each feeder. As shown in the previous section, the

local real-time measurements represent the sending end voltage of the substation *Vs* and the output power from the substation to each feeder (P_o^f, Q_o^f). Informing messages contains the DG voltage magnitude, real and reactive power at the end-node of the first segment in each feeder ($P_n^{f,}$, $Q_n^{f,1}$ and $V_n^{f,1}$)

7.3.2 Beliefs module:

This module receives the percepts then:

1- *It determines the minimum and maximum voltages in the system*: using the estimation algorithm in the previous section, the beliefs module of the LTC control agent can find the overall minimum and maximum voltages along each feeder. Then the overall minimum and maximum voltages of the system can be obtained using:

$$V_{\min}^{sys} = \min_F \left(V_{\min}^f\right), \quad V_{\max}^{sys} = \max_F \left(V_{\max}^f\right) \tag{7.5}$$

where, *F* is the number of feeders in the distribution system.

2- *It checks the condition for infeasible solution:* once the system minimum and maximum voltages are determined, the *beliefs* module will check the condition for infeasible solution using (7.1).

3- *It predicts the tap operation*: to avoid excessive tap operation it is assumed that the beliefs module has the capability to predict the expected daily tap operation. This prediction could be determined through carrying out offline simulations by having the forecasted load and generation pattern. This task could be done by estimating the change of the overall minimum and maximum voltages in the system with the change of the forecasted load distribution and generated power using the cooperative algorithm in section 7.2 and by considering the LTC as the only device responsible for voltage control.

7.3.3 Decision Maker:

The beliefs module sends two binary inputs to its decision maker. These inputs are *FS* (the status of infeasible solution) and *ET* (the status of daily expected tap operation). The decision maker has two binary outputs. These outputs are *VR* (regulate the voltage) and *cooperate* (start cooperation with other control agents). The decision maker performs a mapping between inputs and outputs to achieve the desires of the LTC agent by minimizing the voltage deviation and reduce the tap operation.

Table 7.1: Logic rules of the LTC decision maker

inputs		Outputs	
FS	*ET*	*VR*	*Cooperate*
0	0	1	0
0	1	1	1
1	0	0	1
1	1	0	1

At each specific time, the decision maker selects one of the desires: 1) do voltage control by itself or 2) relieve the stress of tap operation via cooperation with other control agents. In a general case a best compromise solution cannot be determined in a satisfying way purely by mathematical means and typically, a human decision maker (*DM*) who can be considered as expert of underlying problem, is used to determine sub-objectively this best compromise. The task of the *DM* is to find a balance between conflicting objectives, and this can be obtained by finding favorable trade-off between objectives. Table 7.1 shows a logic-based mapping between the inputs and the outputs of the LTC decision maker.

7.3.4 Control algorithm:

The control strategies module receives the output from the decision maker and executes this decision. When the control agent decides to regulate the voltage (the flag of *VR* is raised), the control strategies module solves the integer optimization problem shown in (7.6)-(7.10). As shown in (7.6), the objective function aims to find the tap setting *T* that minimizes the voltage deviation of both the minimum and maximum voltages along the multiple feeders with respect to the nominal value [136]. The control strategies module will send a *request* message when the flag of *ET* or *FS* is raised.

$$Min_T\ J = \sum_{f=1}^{F} \left(\begin{array}{l} \left(V_{nom} - V_{\min}^{f} \left(1 + \left(T - T^{old} \right) \right) \right)^2 + \\ \left(V_{\max}^{f} \left(1 + \left(T - T^{old} \right) \right) - V_{nom} \right)^2 \end{array} \right) \tag{7.6}$$

subject to:

$$V_s = V_p + T \times \Delta V_{tap} \tag{7.7}$$

$$V_{\min}^{f} \geq V_{\min} \tag{7.8}$$

$$V_{\max}^{f} \leq V_{\max} \tag{7.9}$$

$$T_{\min} \le T \le T_{\max} \tag{7.10}$$

where, T^{old} is the current tap position, V_p is the substation primary voltage and ΔV_{tap} is the step voltage of each tap. In order to avoid unnecessary tap operation due to small dynamic voltage variations, the improvement of the voltage regulation in (7.6) considering the optimal tap setting T^{new} is compared with the same objective function considering the current tap setting T^{old} using:

$$\varepsilon_{imp} = \frac{J(T^{new}) - J(T^{old})}{J(T^{old})} \times 100 \tag{7.11}$$

If the improvement in (7.11) is less than a certain tolerance δ, the tap changing operation is delayed or sustained; where δ is equivalent to the dead band of the conventional LDC control [136].

7.4 The Proposed Coordinated Voltage Control Scheme between DG Control Agents:

Currently all DG units are assumed to operate at the maximum power point tracking (*MPPT*) and do not share in voltage control. Based on Table 7.1, if the LTC control agent requests sharing in voltage control, it works as *initiator* and it sends a request message for all DG control agents, as shown in Figure 7.3. Once DG control agents (*Participants*) receive a request for voltage control from LTC control agent, they will assess the request based on a pre-defined regulation between the utility and DG owners i.e. each DG control agent has the right to agree or refuse the request message based on its assessment. Mathematically, at each time step the objective function of each DG control agent can be defined as follows:

$$\min_{Q_g, P_g} J = w_g^{curtail}(P_g^{MPPT} - P_g) + J^R \tag{7.12}$$

where, $w_g^{curtail}$ is the weight of the active power curtailment, P_g^{MPPT} is the current maximum power, P_g is the controlled injected active power and Q_g is the controlled injected reactive power; J^R is the voltage regulation function that is activated when the DG control agent receives a request message from the LTC control agent. J^R can be defined for each DG control agent as follows:

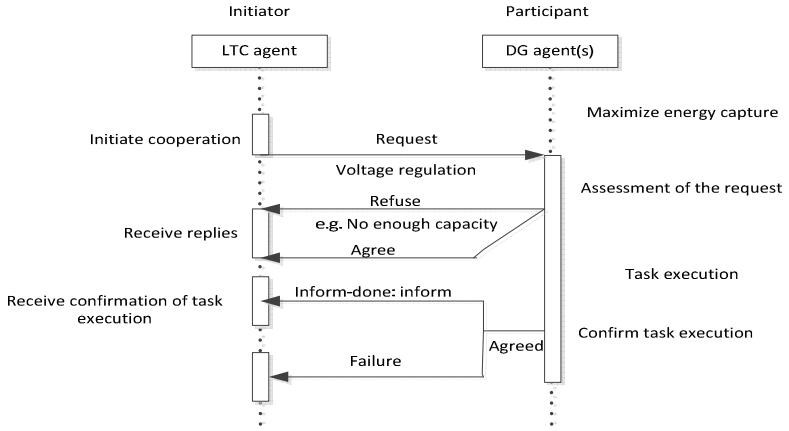

Figure 7.3: FIPA *request* protocol between LTC and DG control agents.

$$J^R = w_g^R \sum_{s=1}^{S} \left(\left(V_{nom} - V_{\min}^s\right)^2 + \left(V_{\max}^s - V_{nom}\right)^2 + \left(V_{\max}^s - V_{\min}^s\right)^2 \right) \tag{7.13}$$

where, w_g^R is the weight for voltage support. As shown in (7.13), when a DG control agent shares in voltage support, it will minimize the voltage deviation from the nominal value and the voltage drop between the minimum and maximum values in each segment *s* of the feeder to improve voltage regulation and avoid the increase in the losses along the feeder, respectively. The self- constraints of the optimization problem for each DG control agent are:

$$|Q_g| \leq Q_g^{\lim}\ ,\ Q_g^{\lim} = \sqrt{S_{g\max}^2 - P_g^2} \tag{7.14}$$

$$V_{\min}^s = V_{\min}^{s,old} - L_{\min}^s \Delta P_g - H_{\min}^s \Delta Q_g \tag{7.15}$$

$$V_{\max}^s = V_{\max}^{s,old} - L_{\max}^s \Delta P_g - H_{\max}^s \Delta Q_g \tag{7.16}$$

where, S_{gmax} is the rating power, ΔP_g and ΔQ_g are the change of the real and reactive power of the DG unit i.e. (P_g^{MPPT}-P_g), (Q_g^{old}-Q_g) respectively; L and H are the sensitivity factors for the change of voltages with respect to the change of real and reactive power, respectively.

To calculate the sensitivity factors, consider a single DG unit is connected between LTC and the end of a feeder, the feeder will be divided into two segments. The change of the voltage profile at node *i* in the upstream segment due to the change of the DG real and reactive power can be obtained using (7.17) as follows

$$\Delta V_i^{2^{s=1}} = \Delta V_o^{2^{s=1}} + 2\left(\left(\sum_{k=0}^{i-1} r_k^{s=1}\right)\Delta P_g + \left(\sum_{k=0}^{i-1} x_k^{s=1}\right)\Delta Q_g\right) \tag{7.17}$$

where, $\Delta V_o^{2^{s=1}}$ is the change in the substation voltage and it is calculated based on the transformer impedance and the system input impedance at the primary side of the substation. The detailed derivation of (7.17) can be found in Appendix B. If the change of the substation voltage is very small, the sensitivity factors at each node *i* in the upstream segment can be obtained as follows:

$$L_i^{s=1} = \sum_{k=0}^{i-1} r_k^{s=1} \ , \ H_i^{s=1} = \sum_{k=0}^{i-1} x_k^{s=1} \tag{7.18}$$

While, the change in the voltage profile at any node *i* downstream the DG unit equals the change of the voltage profile at the location of the DG unit. Thus, the sensitivity factors at each node *i* in the downstream segment can be given as follows:

$$L_i^{s=2} = \sum_{k=0}^{n+1} r_k^{s=1} \ , \ H_i^{s=2} = \sum_{k=0}^{n+1} x_k^{s=1} \tag{7.19}$$

Equations (7.18) and (7.19) can be generalized for any node *i* at segment *s* upstream or downstream a certain DG unit when multiple DG units are connected.

For all participants (DG control agents), the optimization problem in (7.12) can be distributed into two sequential problems; they are coordinated reactive power control and real power curtailment for voltage support.

7.4.1 First problem: coordinated reactive power control

The first problem aims to determine the reactive power control scheme between DG control agents for voltage support. First, for each DG unit lets minimize (J^R/w_g^R) using the available reactive power Q_g and by setting P_g=P_g^{MPPT}. Hence Q_g will be the only control variable in this problem. Therefore, for each DG unit the optimum change of Q_g can be obtained by differentiating the quadratic equation in (7.13) with respect to ΔQ_g . The optimal change of reactive power is found to be:

$$\Delta Q_g^{new} = \frac{1}{2}\frac{\sum_{s=1}^{S} V_{nom}\left(H_{\min}^s + H_{\max}^s\right) + V_{\min}^{s,old} h_{\min}^s + V_{\max}^{s,old} h_{\max}^s}{\sum_{s=1}^{S}\left(H_{\min}^{s\ 2} + H_{\max}^{s\ 2} - H_{\min}^s H_{\max}^s\right)} \tag{7.20}$$

where

$$h^s_{\min} = H^s_{\max} - 2H^s_{\min}\ , h^s_{\max} = H^s_{\min} - 2H^s_{\max} \tag{7.21}$$

When Q_g^{new} is larger than the available reactive power, it will be set at Q_g^{lim} and the new minimum and maximum voltages at each segment are estimated using (7.15) and (7.16).Thus each DG control agent is capable of determining the optimum setting of its reactive power and the improvement of voltage regulation.

Second, using (7.20), the first problem can be formulated to minimize the cost of reactive power control for all participants to regulate the voltage within acceptable bandwidth. The problem of reactive power control for N_{DG} control agents can be formulated as follows:

$$\min_{Q_g} J = \sum_{n_{DG}=1}^{N_{DG}} w_{n_{DG}}^{Q_g} \min\left(Q_{g,n_{DG}}^{new}, Q_{g,n_{DG}}^{\lim}\right) \tag{7.22}$$

subject to

$$V^f_{\min} \geq V^{band}_{\min}\ , V^f_{\max} \leq V^{band}_{\max} \tag{7.23}$$

where, $w_{n_{DG}}^{Q_g}$ is the weight of reactive power control for voltage support; V_{min}^{band} and V_{max}^{band} are the acceptable limits of bandwidth for voltage regulation using DG control agents. In this work, it is assumed that all DG units have equal weights of reactive power control for voltage support. Therefore, the prioritization of the reactive power settings for DG agents is determined based on the sensitivity factors using the following coordinated reactive power control scheme:

1- If the DG control agents receive a voltage regulation request message, a backward sweep coordinated reactive power control scheme is initiated, where:

2- The last downstream DG unit (most sensitive DG) calculates the new reactive power setting using (7.20) and the improvement in voltage regulation using (7.11).

3- If the improvement is acceptable, it updates the reference of its reactive power and it compares the new minimum and maximum voltages with the specified regulation bandwidth.

4- If the new minimum and/or maximum voltages out of the bandwidth, it sends them to its upstream DG unit.

5- Steps 2-4 are repeated for each DG control agent until the regulation bandwidth is achieved or the first DG unit (closet DG to LTC) is reached.

6- If the first DG unit is reached and the flag of *FS* or *ET* is still raised, a coordinated real power curtailment control scheme is initiated.

7- It is worth noting that the above procedures are applicable for FSC control agents. Equation (6.16) is applied to determine the number of capacitor banks that will change their status.

7.4.2 Second problem: coordinated real power curtailment

The second problem aims to minimize the cost of real power curtailment for all participants that is required to satisfy the feeder voltage constraints. This problem is activated when the feeder voltage constraints are not satisfied in the coordinated reactive power control and the flag of *FS* or *ET* is still raised. The second problem can be defined as follows:

$$\min_{P_g} J = \sum_{n_{DG}=1}^{N_{DG}} w_{n_{DG}}^{curtail} \left(P_{g,n_{DG}}^{MPPT} - P_{g,n_{DG}} \right) \tag{7.24}$$

subject to:

$$V_{\max} - V_{\max}^{f,old} + \sum_{n_{DG}=1}^{N_{DG}} L_{\max,n_{DG}}^{f} \left(P_{g,n_{DG}}^{MPPT} - P_{g,n_{DG}} \right) = 0 \tag{7.25}$$

Based on the location and value of the maximum voltage, the sensitivity factors, the maximum power extracted for each DG unit and the cost of curtailment, the real power setting for voltage support at each DG unit can be obtained as follows:

$$P_{g,n_{DG}}^{new} = P_{g,n_{DG}}^{MPPT} - \frac{V_{\max}^{f,old} - V_{\max}}{L_{\max,n_{DG}}^{f}} \left(\frac{w_{n_{DG}}^{curtail} L_{\max,n_{DG}}^{f} P_{g,n_{DG}}^{MPPT}}{\sum_{n_{DG}=1}^{N_{DG}} w_{n_{DG}}^{curtail} L_{\max,n_{DG}}^{f} P_{g,n_{DG}}^{MPPT}} \right) \tag{7.26}$$

Equation (7.26) provides a reasonable sharing of real power curtailment for voltage support between DG units depending not only on how much each DG unit is sensitive to the location of the maximum voltage, but also on the cost of curtailments and ratio of its maximum extracted power compared to the total extracted power from the DG units in the feeder. The FIPA contact net protocol (*CNP*) is

Table 7.2: Logics of the DG decision maker

Inputs		outputs	
LTC	*Mode*	*Reply*	*Mode*
ET	MPPT	agree	Q-control
FS	MPPT	agree	Q-control
ET	Q-control	reject	Q-control
FS	Q-control	accept	P-curtail

proposed to coordinate the real power curtailment between DG units. The proposed *CNP* can be summarized as follows [127]:

1- LTC control agent (manager) sends a *call for proposal (CPF)* message for voltage support to the DG control agents connected in the feeder at which maximum voltage violates the specified limits. The message contains the location of the maximum voltage.

2- Each DG control agent (participant) sends a *propose* message contains $P_{g,n_{DG}}^{MPPT}$, $L_{\max,n_{DG}}^{f}$ and $w_{n_{DG}}^{curtail}$.

3- Based on (7.26), the LTC control agent determines the required real power curtailment of each DG unit and sends *accept for proposal* message to each participant. The message contains the real power curtailment of each DG unit.

7.4.3 Decision maker and control strategies modules:

The beliefs module of each DG agent receives the *percepts* and it passes two inputs to the decision maker for voltage control; they are the mode of operation of the DG unit (measurement) and the current state of the LTC control agent (messages). The decision maker has two outputs; *Mode* and *Reply*. Table 7.2 shows the logics of a DG decision maker that maps the inputs and outputs. The logics have been extracted based on the DG preferences and LTC current states. The control strategies module executes the proposed coordinated reactive control and real power curtailment schemes using (7.20)-(7.26).

7.5 The Combined Distributed Voltage Estimation and Control

The distributed voltage estimation in section 7.2 and the distributed voltage control schemes in sections 7.3 and 7.4 have been combined in the flowchart shown in Figure 7.4 to present the detailed interior structure and exchanging messages of LTC and DG control agents.

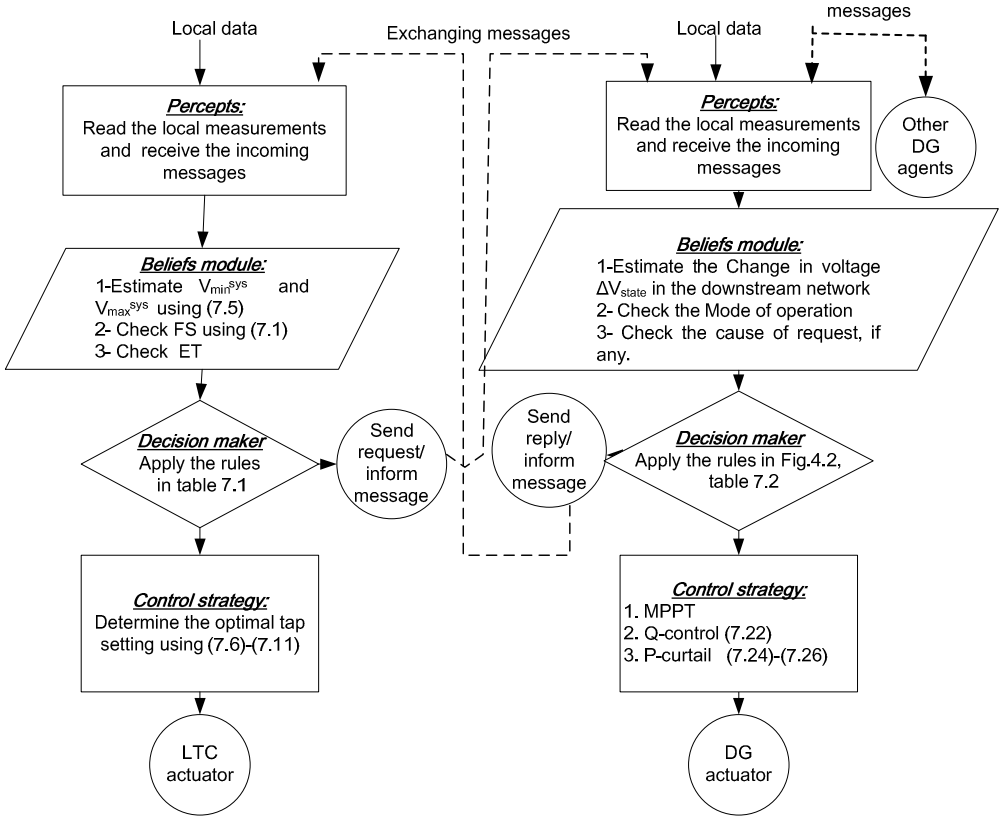

Figure 7.4: A detailed schematic diagram of the proposed cooperative protocol between the LTC and DG control agents

7.6 Simulation Studies

In this section simulation studies have been carried out in MATLAB/SIMULINK to show the validity of the proposed control structure. Figure A.7 shows the distribution system under study [137]. The test system consists of four feeders; the feeders have different lengths, ratings and load types. Variable power sources with different characteristics have been installed at different locations along the feeders to simulate the expected unbalance in load/generation diversity between the feeders. Table A.14 shows a summary of the generation and load profiles along the feeders. Figure 7.5 shows a typical load profile for residential, commercial and industrial loads for the two days under study (weekend and weekday), respectively. Figure 7.6 shows the generation profile for wind and photovoltaic (PV) for the two days under study. The error of the pseudo measurements has been assumed to be 50% and the error of the real-time measurement is neglected.

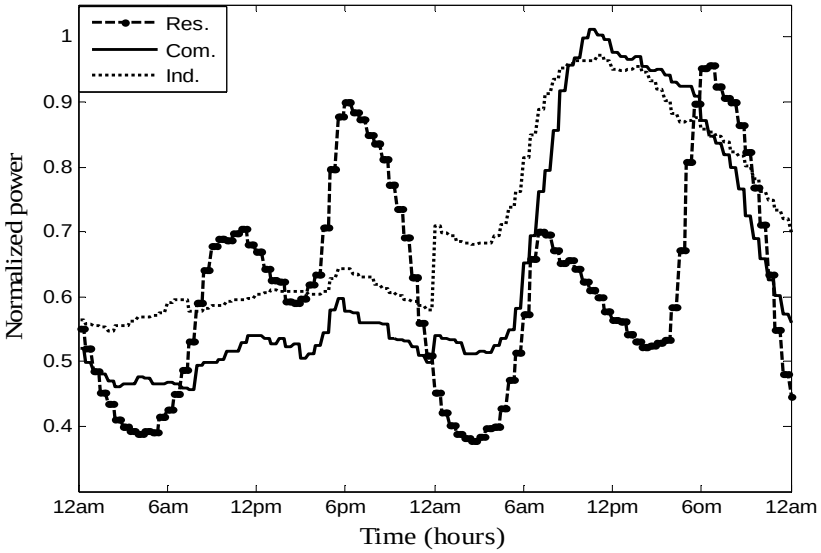

Figure 7.5: Different Load profiles for a weekend and weekday

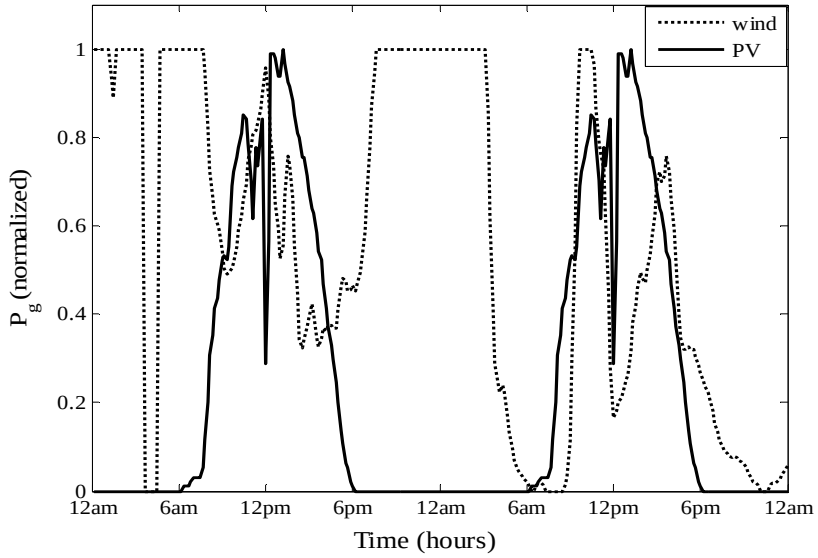

Figure 7.6: Different generation profiles for a weekend and weekday

The minimum improvement for the regulation function to accept the new tap setting is selected to be 5%. The regulation bandwidth of DG units is chosen to be 2% of the nominal voltages when the coordinated reactive power control is activated.

7.6.1 Impacts of proper estimation and reactive power control

Figure 7.7 shows the estimated $V_{\min}^{sys}$ and $V_{\max}^{sys}$ during the studied period at different control schemes. As shown in the figure, undervoltages occur when the local control scheme in [137] is applied due to the improper voltage estimation, improper tap settings and infeasible solutions. When the developed distributed state estimation is used and the DG units operate in MPPT without reactive power control, the LTC has proper voltage estimation, which has a negligible error of 1×10^{-4} compared with the results obtained from power flow algorithms. However, it could not solve the areas of infeasible solution. When the proposed coordinated reactive power control scheme is activated via request protocol, the areas of infeasible solution are mitigated. Figure 7.8 shows the change of tap operations during the studied period with and without applying the reactive power control scheme. As shown in the figure, the coordinated reactive power control relieves the stress on tap operation and it is reduced from 36 to 22 taps.

Figure 7.9 shows the settings of the reactive power for the wind DG units in feeder #1 and the PV DG unit connected at node 8 in feeder #2 during the studied period when the coordinated reactive power control is activated. As shown in the figure, the proposed reactive power control scheme compensates the changes of the generated power and therefore it is capable of reducing the dynamic changes in the voltage profile and hence the number of taps operation. Figure 7.10 shows the total system losses with and without the reactive power control scheme. As shown in the figure, the proposed scheme does not cause an increase in the total system losses due to considering the minimization of voltage deviation between the minimum and maximum voltage in the voltage regulation function in (7.13).

7.6.2 Impacts of LTC regulation dead-band:

It is noticed that widening the regulation dead-band δ of LTC will result in reducing the number of tap operation significantly. However, overvoltages, undervoltages or infeasible solution are expected with widening the regulation dead-band due to the improper settings of taps. When δ increased from 5% to 15% the number of taps reduced from 22 taps to 12 taps. However, as shown in Figure 7.11, widening the LTC regulation dead-band causes undervoltages.

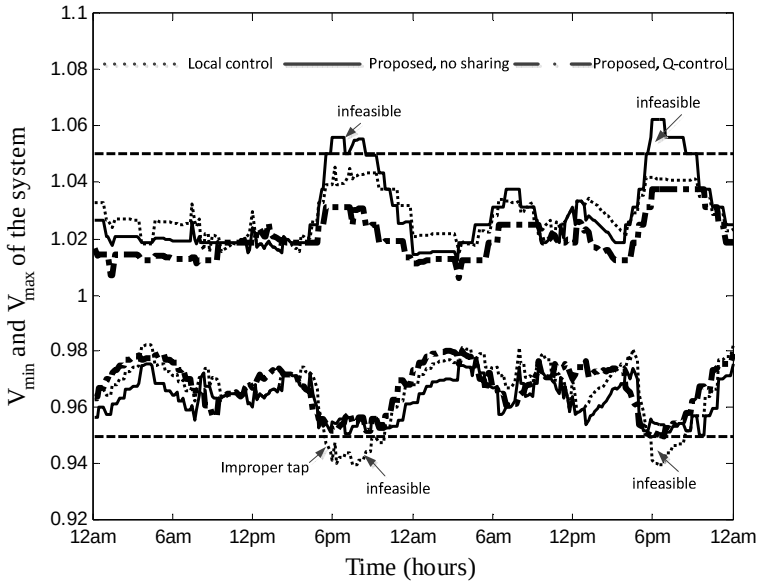

Figure 7.7: The per unit minimum and maximum voltage profile over the studied period at different control schemes

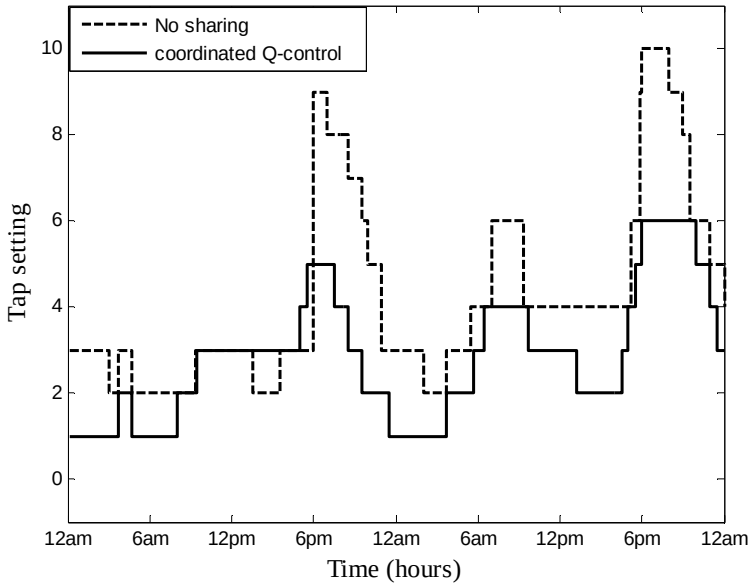

Figure 7.8: The change of the tap operation at different control schemes

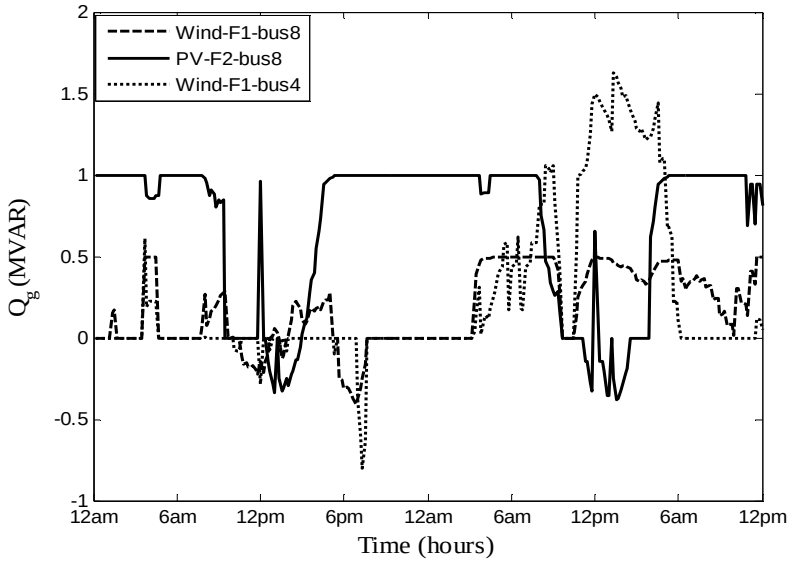

Figure 7.9: The reactive power settings between DG units

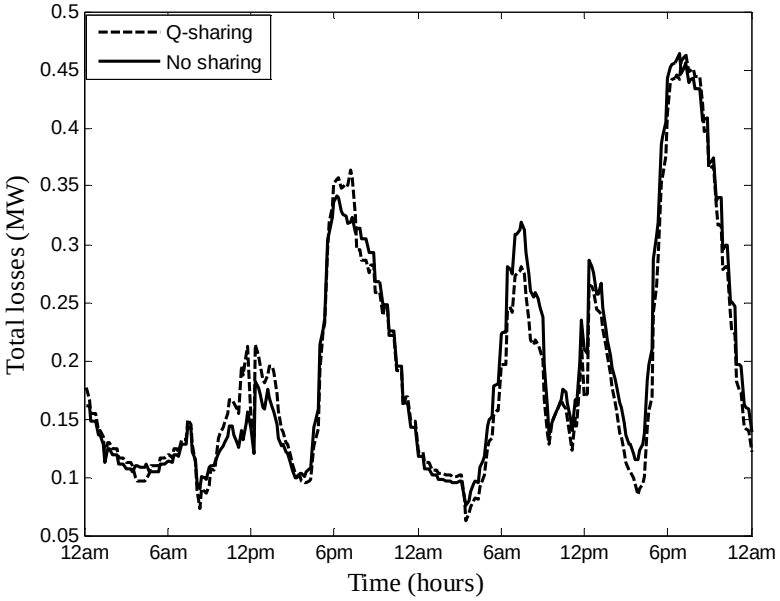

Figure 7.10: The total system losses with and without reactive power control

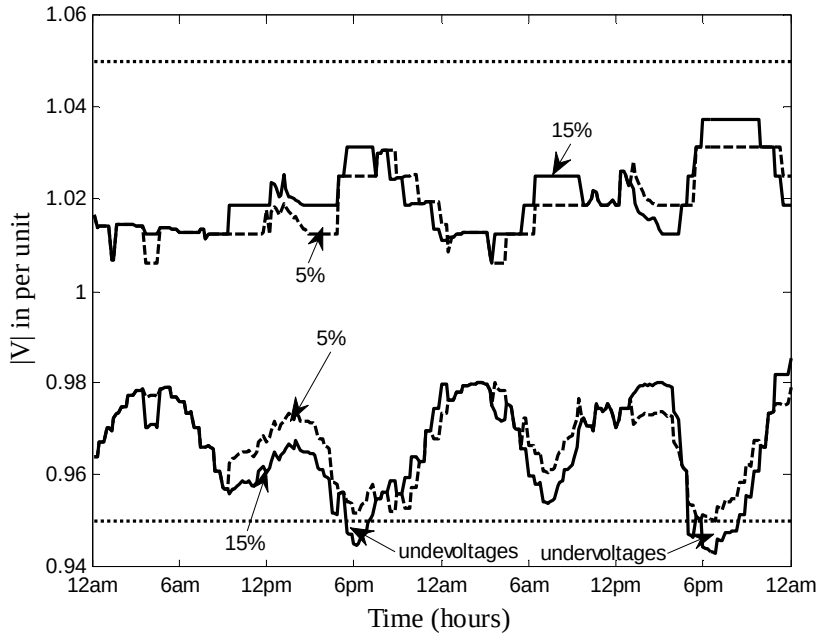

Figure 7.11: The per unit minimum and maximum voltage profile over the studied period at different δ.

Table 7.3: Real power curtailments

Feeder	DG location	P_g^{MPPT} (MW)	$L^f_{\max,n_{DG}}$	$P_g^{curtail}$ (MW)
1	4	2	0.7871	0.86
1	8	0.5	0.7871	0.22
3	3	0.5	0.5904	0.21
3	6	2.5	1.1807	1.05

7.6.3 Impacts of real power coordinated control scheme

Figure 7.12 shows the voltage profile along the feeders when the wind DG units operate at their rated power (there is no available reactive power) in feeders # 1 and 3, while the PV units are out of service and the residential load is 88% of its nominal. As shown in the figure, when DG units operate at maximum power, an infeasible solution occurs at node 4 in feeder#1 and node 6 in feeder #3. When the proposed real power curtailment scheme for voltage support is activated via call for proposal protocol, the problem of infeasible solution has been mitigated. Table 7.3 gives the maximum power, sensitivity for each DG unit to the location of the maximum voltages and the new power settings based on (7.26) when the DG units have equal cost of curtailment.

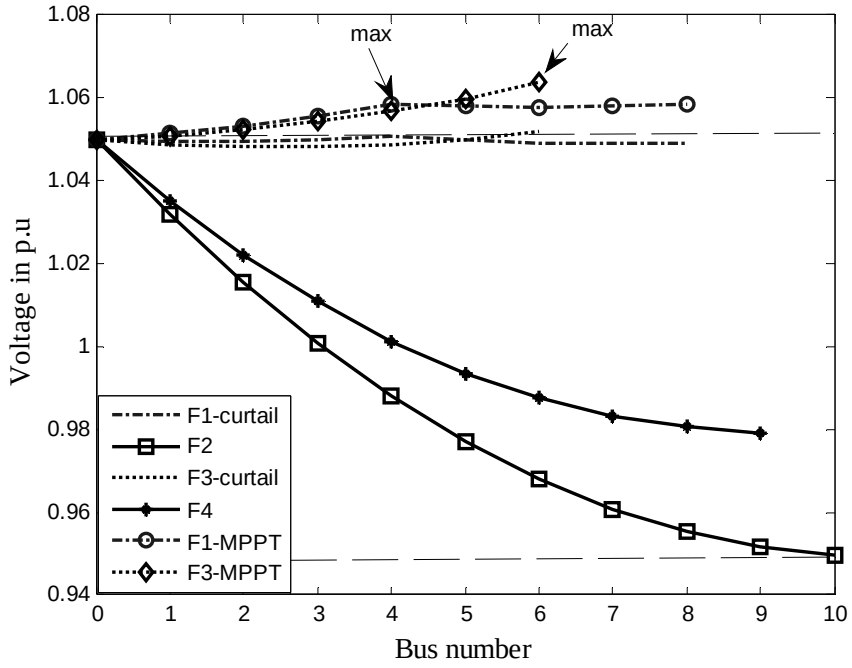

Figure 7.12: The per unit voltage profile without and with real power curtailment

7.7 Discussion

The problem of voltage and reactive power control for multiple feeders with multiple DG units and a LTC has been formulated in a distributed control scheme consisting of LTC and DG control agents. Each control agent has a global and a self-objective. A cooperative protocol scheme consists of a distributed voltage estimation and decision making has been designed to achieve the best compromise for global and self-objectives of the control agents. The interior structure of the control agents has been defined based on the BDI theory and the exchanging messages follow the FIPA communication acts. A logic-based decision making has been defined for each control agent to find a favorable trade-off between objectives. New coordinated reactive power control and real power curtailment schemes have been proposed when DG units share the voltage support. The proposed coordinated control schemes aim to minimize voltage deviation and prevent any voltage violation when LTC decides to reduce the tap operation or faces infeasible solution. The proposed cooperative control scheme has the capability to properly regulate the voltage in all operating conditions, relieve the stress on tap operation and avoid unnecessary real power curtailment from DG units.

The main differences and advantages of the proposed cooperative protocol presented in this chapter compared with centralized control schemes are:

1- The concept of distributed state estimation and decision making is in line with the current trend of ADNs structure, which is mainly clustered or distributed in the form of microgrids with many DG owners having different preferences. Using distributed control it will be easier to modify and upgrade ADNs control without disturbing other parts of the control process. In addition, it will be easier to implement expansion and provide local operator interface and control for DG owners.

2- The proposed distributed control breakdown the centralized voltage and reactive power control optimization problem into small sub-problems that can be solved simultaneously via exchanging messages between agents (the control agents do parallel computing). Therefore, the proposed control requires less computational burden. Furthermore, it mitigates the numerical instability and convergence problems that are accompanied with the centralized control that run the power flow algorithms in each time step; especially in the case of high *R/X* networks.

3- It reduces the communication burden (network traffic); where status information concerning the local process of each control agent is transmitted to other control agents but time-critical data used for real-time control does not need to be sent over the network (e.g. fast settings of DG power). Furthermore, distributed control has the options to select the time at which inform messages are sent to other control agents. For instance, inform messages will be sent only when such messages affects the action of other control agents.

Chapter 8
Conclusions

8.1 Summary and Conclusions

The research in this thesis presents new algorithms to address and mitigate the voltage and reactive power aspects in ADNs considering islanded microgrids under SG paradigm. Three stages are presented in the thesis; they are assessment (chapters 3 and 4), planning (chapter 5) and control (chapters 6 and 7).

In chapter 3, conventional voltage and reactive power control schemes in ADNs with high penetration of DG units have been assessed. A generic power flow algorithm for ADNs has been developed to validate the assessment. The assessment shows that with the existence of high DG penetration potential conflicts between the DG units and conventional voltage and reactive power control devices are expected. It is concluded in this chapter that there is a need for the evolution of voltage and reactive power control techniques from their passive control structure (without communication links) to an active (communication-based) control.

In chapter 4, the successful operation of islanded microgrids considering voltage and reactive power constraints has been assessed. An islanded droop-based microgrid simulation model that takes the special operational characteristic of islanded microgrid has been adapted to validate the assessment. A probabilistic model for the microgrids components (loads and generation) has been developed. Supply adequacy indices have been modified to consider the voltage and reactive power constraints. It is concluded in this chapter that voltage and reactive power constraints have significant impacts on the microgrid islanding success. Therefore, the issue of voltage and reactive power constraints must be considered in the design, planning and operation of ADNs.

The problem of capacitor planning in ADNs considering islanded microgrids has been presented in chapter 5. A probabilistic formulation that takes into account the operation of islanded microgrids and the stochastic nature of loads and generations has been developed. The simulation results show that proper capacitor planning considering islanded microgrids will facilitate a successful implementation for the concept of microgrids in ADNs.

In chapter 6, a two ways communication-based distributed control structure has been proposed for voltage regulation in active distribution feeders. An expert-based cooperation mechanism via communication acts has been proposed to avoid interference between the autonomous operations of DG units and conventional voltage and reactive power control devices. A TCP/IP interface between

Simulink^{TM} and Java Agent Development Framework (JADE) has been developed to build a continuous time simulation model for the proposed distributed control scheme.

The distributed control framework presented in chapter 6 has been extended in chapter 7 to provide a proper distributed voltage profile state estimation and decision making for the problem of voltage and reactive power control of multiple feeders with multiple DG units and a LTC. New coordinated reactive power control and real power curtailment schemes have been proposed when DG units share in voltage support.

It is concluded in chapters 6 and 7 that proper coordination via two ways communication is a simple and efficient solution to avoid conflicts between devices. This control structure and its implementation could facilitate the applications of SG technologies for autonomous control in future distribution systems.

8.2 Contributions

The main contributions in this thesis can be highlighted as follows:

1- ***The idea of using the element incidence matrix has been applied to develop a simple, efficient and generalized three phase power flow algorithm for ADNs.*** Unlike previous works, the algorithm is simple because it depends mainly on the bus incidence matrix which represents the relation between bus–injection currents to branch currents. It is also efficient as it shows good convergence characteristics in all operating conditions. Furthermore, it is generalized because it incorporates the three phase model of feeders, unbalance due to both loads and different type of phases, exact load modeling, SVR model, and DG model in its different operation modes.

2- ***Assessment of the drawbacks of conventional voltage and reactive power control schemes and the necessities of their evolution in ADNs***. The main contribution in this assessment is that the study takes into consideration the most salient feature of distribution systems which is being unbalanced and it is performed on practical IEEE test feeders. The previous studies show that overvoltages are the main issue in the integration of DG units. Unlike previous studies, the assessment in this work shows that the conflict between the regulators and the DG units will cause overvoltages, undervoltages, voltage fluctuation, excessive wear and tear of voltage regulators and increase in the total systems losses.

3- ***The development of analytical assessment approach to Study the impacts of reactive power and voltage regulation aspects on the successful operation of islanded microgrids***. To

facilitate the study, the steady-state and dynamic microgrid models that reflect the special characteristics of islanded microgrid operation have been integrated in the probabilistic analytical assessment approach, which takes into consideration the operational characteristics of dispatchable and wind DG units.

4- ***Supply adequacy and reliability indices have been modified to account for the voltage and reactive power constraints and the dynamic stability for ADNs with different microgrid configurations.*** The indices provide an accurate evaluation for the anticipated benefits that the microgrid may bring to customers, DG owners and utilities.

5- ***The conventional problem of shunt capacitor planning in distribution networks has been reformulated for ADNs considering the design of different microgrid configurations***. The new formulation takes into account the probabilistic nature of DG units and the special philosophy of islanded microgrids. The new formulation aims to maximize the saving of 1) the cost of power and energy losses in ADNs during normal parallel conditions, 2) the cost of interruption when islanded microgrids fail to support the load due to a shortage of reactive power and voltage regulation aspects and 3) the cost of the capital investment of the installed capacitors. It is worth noting that the framework of the planning approach developed in this work is a generic framework that can be easily adapted for other planning studies in ADNs considering microgrids.

6- ***The development of a new multiagent control scheme for voltage regulation in active distribution feeders.*** The control scheme consists of three types of control agents; namely LTC/SVR, DG and FSC control agents. The distributed control scheme is capable of mitigating the interference issues between DG units and conventional voltage and reactive power control devices. The key contribution in this work is the well definition of the organization paradigm between the control agents, the detailed internal structure and operation mechanism to be implemented in each control agent, the proper coordination and communication protocols among the control agents and the implementation of the control scheme in a continuous time simulation model.

7- ***The development of a novel cooperative control scheme consisting of distributed state estimation and decision making for voltage and reactive power control in multiple feeders with a LTC , unbalanced load diversity and multiple DG units.*** The distributed state estimation algorithm has been designed to provide the control agents with the proper

knowledge of the current state of affairs. The distributed decision making has been designed to achieve the best compromise between the system and device objectives of each control agent. The developed cooperative scheme can regulate the voltage properly in all operating conditions, relieve the stress on tap operation, avoid the increase in total system losses and prevent unrequired curtailment of DG injected real power.

8.3 Directions for Future Work

In continuation of this work, the following subjects are suggested for future studies:

1- Incorporating line voltage regulators in islanded microgrid power flow algorithm and evaluating their conflicts with DG units.

2- Optimal allocation for line voltage regulators in ADNs considering islanded microgrids.

3- Development of a multiagent voltage and reactive power control scheme for islanded microgrids.

4- Development of a new self-healing mechanism for ADNs considering microgrids.

Appendix A

Figures and Data of the Distribution Test Systems

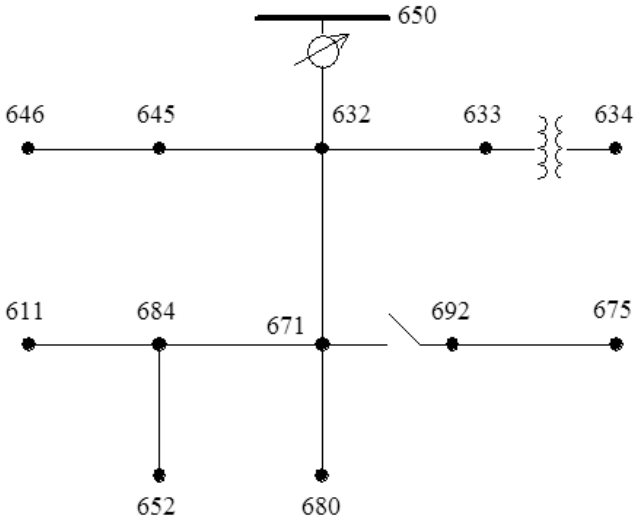

Figure A.1: IEEE 13 bus test feeder

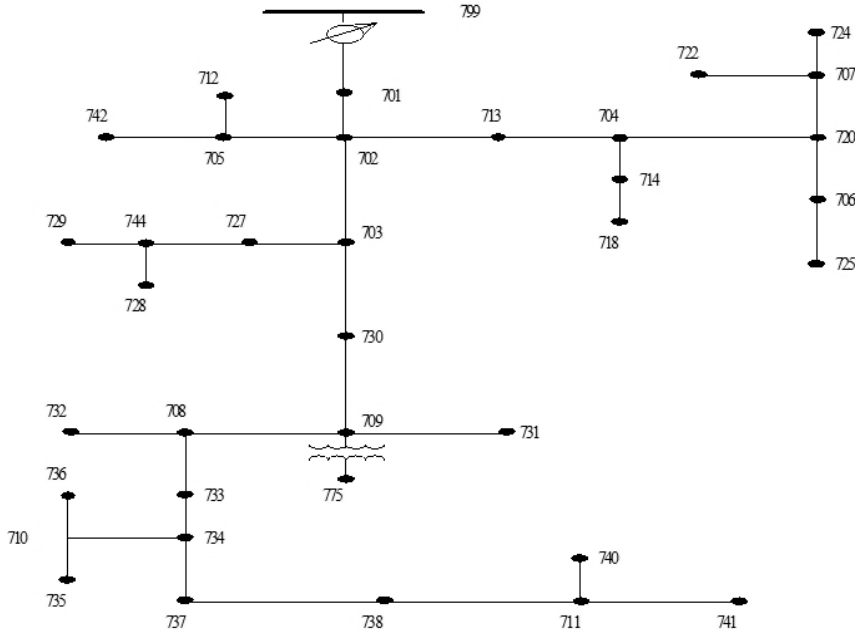

Figure A.2: IEEE 37 bus test feeder

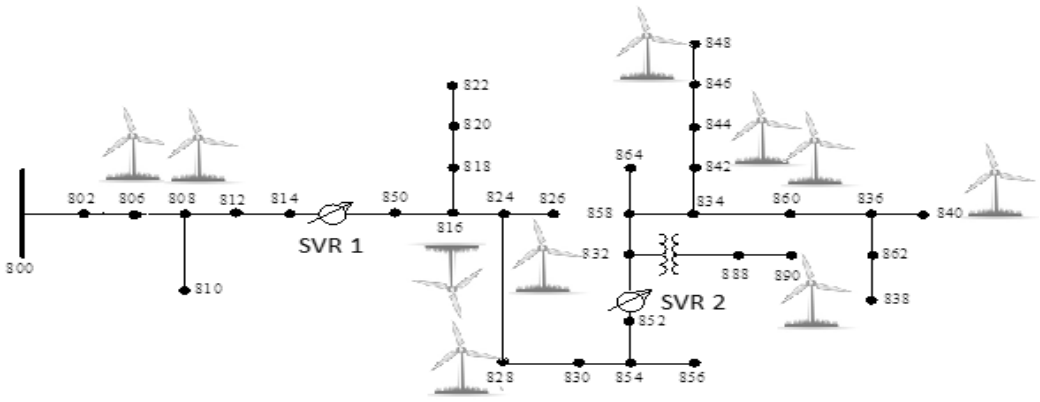

Figure A.3: IEEE 34 bus test feeder with ten wind turbines at different locations

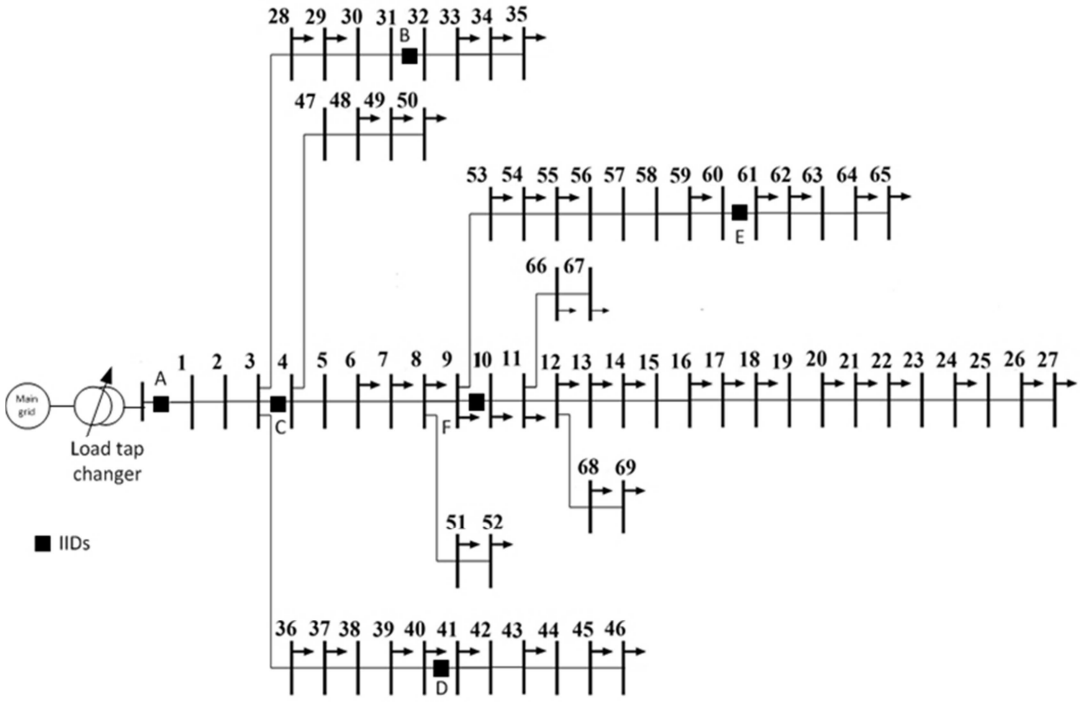

Figure A.4: The 69-bus balanced distribution system

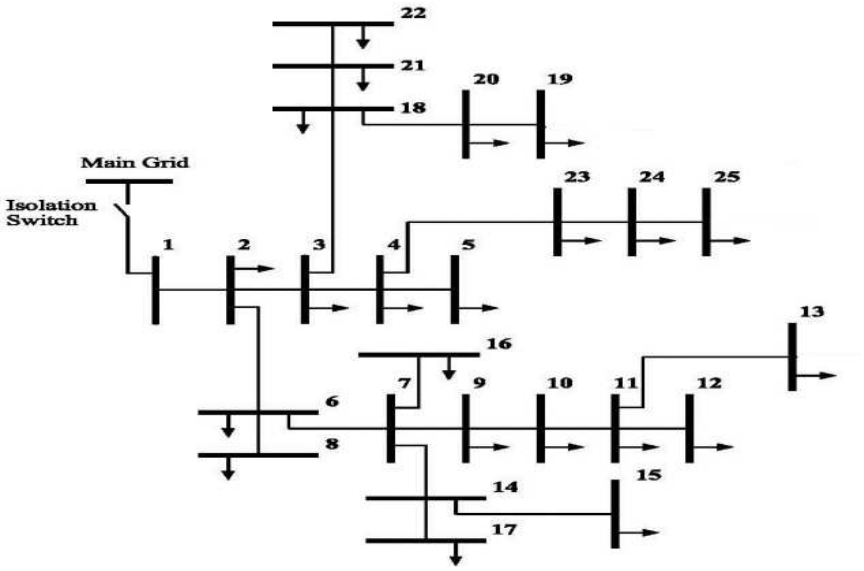

Figure A.5: The 25-bus distribution test system

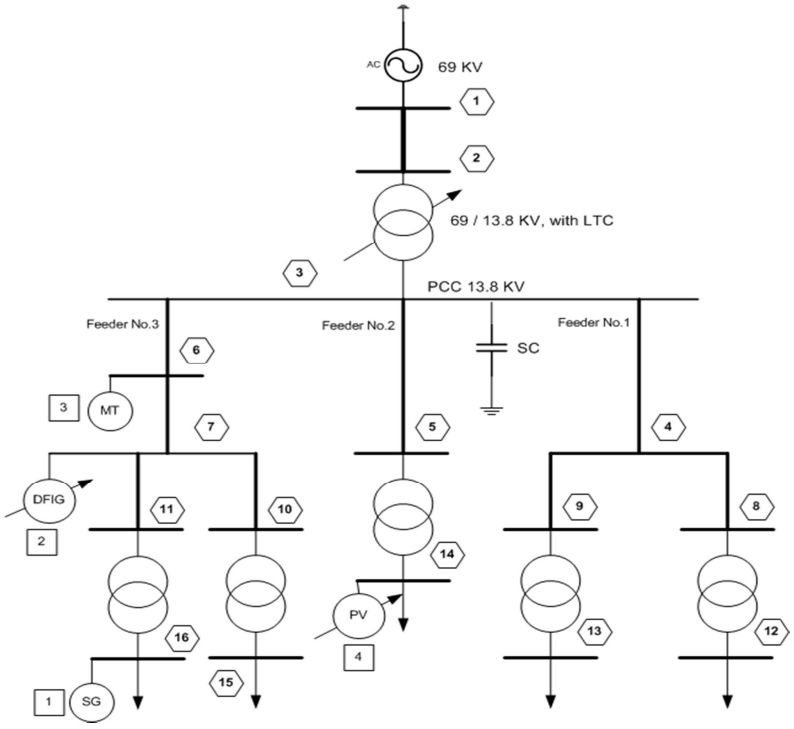

Figure A.6: The 16-bus distribution test system

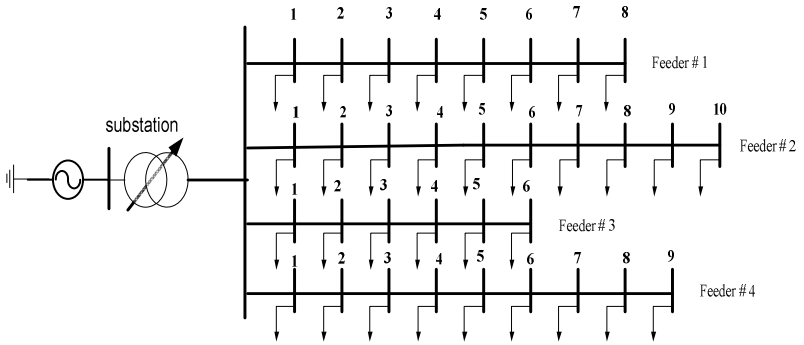

Figure A.7: Four feeders' distribution test system

Table A.1: The locations, types and ratings of the DG units in the IEEE 37 bus test feeder

DG #	Location	P_{gmax} (KW)	Type	PF
1	701	600	3-phase	Controllable
2	703	450	3-phase	0.9 lag
3	775	450	3-phase	Controllable
4	742	200	3-phase	Controllable
5	722	200	3-phase	Controllable
6	725	200	3-phase	Controllable
7	710	250	3-phase	Controllable
8	741	150	1-phase	0.9 lag

Table A.2: Loads and line data of the 69-bus distribution system

Branch #	***Sending***	***Receiving***	***R (ohm)***	***X (ohm)***	***PL (KW) Receiving***	***QL (Kvar) Receiving***	***Load type***
1	1	2	0.0005	0.0012	0	0	
2	2	3	0.0005	0.0012	0	0	
3	3	4	0.0015	0.0036	0	0	
4	4	5	0.0251	0.0294	0.06	0	R
5	5	6	0.366	0.1864	2.6	2.2	R
6	6	7	0.3811	0.1941	40.4	30	R
7	7	8	0.0922	0.047	75	54	C
8	8	9	0.0493	0.0251	30	22	R
9	9	10	0.819	0.2707	28	19	R
10	10	11	0.1872	0.0619	145	104	C
11	11	12	0.7114	0.2351	145	104	C
12	12	13	1.03	0.34	8	5	R
13	13	14	1.044	0.345	8	5.5	R
14	14	15	1.058	0.3496	0	0	
15	15	16	0.1966	0.065	45	30	R
16	16	17	0.3744	0.1238	60	35	C
17	17	18	0.0047	0.0016	60	35	C
18	18	19	0.3276	0.1083	0	0	0
19	19	20	0.2106	0.069	1	0.6	R
20	20	21	0.3416	0.1129	114	81	C
21	21	22	0.014	0.0046	5	3.5	R
22	22	23	0.1591	0.0526	0	0	

Table A.2 Cont.

23	23	24	0.3463	0.1145	28	20	R
24	24	25	0.7488	0.2475	0	0	
25	25	26	0.3089	0.1021	14	10	R
26	26	27	0.1732	0.0572	14	10	R
27	3	28	0.0044	0.0108	26	18.6	R
28	28	29	0.064	0.01565	26	18.6	R
29	29	30	0.3978	0.1315	0	0	
30	30	31	0.0702	0.0232	0	0	
31	31	32	0.351	0.116	0	0	
32	32	33	0.839	0.2816	14	10	R
33	33	34	1.708	0.5646	19.5	14	R
34	34	35	1.474	0.4873	6	4	R
35	3	36	0.0044	0.0108	26	18.55	R
36	36	37	0.064	0.1565	26	18.55	R
37	37	38	0.1053	0.123	0	0	
38	38	39	0.00304	0.0355	24	17	R
39	39	40	0.0018	0.0021	24	17	R
40	40	41	0.7283	0.8509	1.2	1	R
41	41	42	0.31	0.3623	0	0	
42	42	43	0.041	0.0478	6	4.3	R
43	43	44	0.0092	0.0116	0	0	
44	44	45	0.1089	0.1373	39.22	26.3	R
45	45	46	0.0009	0.0012	39.22	26.3	R
46	4	47	0.0034	0.0084	0	0	
47	47	48	0.0851	0.2083	79	56.4	C
48	48	49	0.2898	0.7091	384.7	274.5	I
49	49	50	0.0822	0.2011	384.7	274.5	I
50	8	51	0.0928	0.0473	40.5	28.3	R
51	51	52	0.3319	0.1114	3.6	2.7	R
52	9	53	0.174	0.0886	4.35	3.5	R
53	53	54	0.203	0.1034	26.4	19	R
54	54	55	0.2842	0.1447	24	17.2	R
55	55	56	0.2813	0.1433	0	0	
56	56	57	1.59	0.5337	0	0	
57	57	58	0.7837	0.263	0	0	
58	58	59	0.3042	0.1006	100	72	I
59	59	60	0.3861	0.1172	0	0	
60	60	61	0.5075	0.2585	1244	888	I
61	61	62	0.0974	0.0496	32	23	C
62	62	63	0.145	0.0738	0	0	
63	63	64	0.7105	0.3619	227	162	C
64	64	65	1.041	0.5302	59	42	C
65	11	66	0.2012	0.0611	18	13	R
66	66	67	0.0047	0.0014	18	13	R
67	12	68	0.7394	0.2444	28	20	R
68	68	69	0.0047	0.0016	28	20	R

Table A.3: The DGs types, parameters and ratings for the 69-bus

Type	***Mode***	***Kp (p.u.)***	***Kq (p.u.)***	***S_{Gmax} (MVA)***	***FOR***
Dispatchable	Droop	0.004	0.083	1.5	0.0975
Wind	PQ - 0.9 PF Lead	-	-	1.0	0.04

Table A.4: ρ_{up} and $\rho_{uncreated}$ for different microgrids in the 69-bus system

Microgrid #	***Isolation Switch (IID)#***	ρ_{up}	$\rho_{uncreated}$
1	A	1.3E-4	54.7E-4
2	B	2.83E-4	10.08E-4
3	C	2.83E-4	38.8E-4
4	D	2.83E-4	2.97E-4
5	E	15.09E-4	5.79E-4
6	F	15.09E-4	17.92E-4

Table A.5: Load states model for 69-bus system

Peak load (%)	***Load level (MVA)***	***Probability***
100	6.5230	0.01
85.3	5.5641	0.056
77.4	5.0488	0.1057
71.3	4.6509	0.1654
65	4.2399	0.1654
58.5	3.8159	0.163
51	3.3267	0.163
45.1	2.9418	0.0912
40.6	2.6483	0.0473
35.1	2.2896	0.033

Table A.6: Wind generation power states for 2 MW DG unit

Wind speed limits m/s	***Hours***	***Power level (KW)***	***Probability FOR=0.04***
0 to 4	1804	0	0.073
4 to 5	579	99.96	0.024
5 to 6	984	299.7	0.032
6 to 7	908	399.87	0.044
7 to 8	983	699.77	0.046
8 to 9	799	899.73	0.075
9 to 10	677	1099.64	0.089
10 to 11	439	1299.58	0.109
11 to 12	395	1499.2	0.101
12 to 13	286	1699.45	0.109
13 to 14	219	1899.4	0.062
14 to 25	687	2000	0.236

Table A.7: Part I of the line data for the 25 bus test system

Branch #	Send. Bus	Recev. Bus	raa ohm	xaa ohm	rab ohm	xab ohm	rac ohm	xac ohm
1	1	2	0.0698	0.1298	0.0032	0.0287	0.0029	0.0208
2	2	3	0.0349	0.0649	0.0016	0.0143	0.0015	0.0104
3	2	6	0.0924	0.0825	0.0016	0.0161	0.0014	0.0120
4	3	4	0.0349	0.0649	0.0016	0.0143	0.0015	0.0104
5	3	18	0.0924	0.0825	0.0016	0.0161	0.0014	0.0120
6	4	5	0.0924	0.0825	0.0016	0.0161	0.0014	0.0120
7	4	23	0.0739	0.0660	0.0013	0.0129	0.0012	0.0096
8	6	7	0.0924	0.0825	0.0016	0.0161	0.0014	0.0120
9	6	8	0.1848	0.1651	0.0032	0.0321	0.0029	0.0239
10	7	9	0.0924	0.0825	0.0016	0.0161	0.0014	0.0120
11	7	14	0.0924	0.0825	0.0016	0.0161	0.0014	0.0120
12	7	16	0.0924	0.0825	0.0016	0.0161	0.0014	0.0120
13	9	10	0.0924	0.0825	0.0016	0.0161	0.0014	0.0120
14	10	11	0.0554	0.0495	0.0009	0.0096	0.0009	0.0072
15	11	12	0.0730	0.0538	0.0006	0.0045	0.0006	0.0045
16	11	13	0.0730	0.0538	0.0006	0.0045	0.0006	0.0045
17	14	15	0.0554	0.0495	0.0009	0.0096	0.0009	0.0072
18	14	17	0.1095	0.0806	0.0009	0.0067	0.0009	0.0067
19	18	20	0.0924	0.0825	0.0016	0.0161	0.0014	0.0120
20	18	21	0.1461	0.1075	0.0012	0.0090	0.0012	0.0090
21	20	19	0.1461	0.1075	0.0012	0.0090	0.0012	0.0090
22	21	22	0.1461	0.1075	0.0012	0.0090	0.0012	0.0090
23	23	24	0.0739	0.0660	0.0013	0.0129	0.0012	0.0096
24	24	25	0.1461	0.1075	0.0012	0.0090	0.0012	0.0090

Table A.8: Part II of the line data for the 25 bus test systems

Branch #	***Sending Bus***	***Recev. Bus***	r_{bb} ***ohm***	x_{bb} ***ohm***	r_{bc} ***ohm***	x_{bc} ***ohm***	r_{cc} ***ohm***	x_{cc} ***ohm***
1	1	2	0.0712	0.1272	0.0036	0.0392	0.0705	0.1284
2	2	3	0.0356	0.0636	0.0018	0.0196	0.0353	0.0642
3	2	6	0.0932	0.0820	0.0018	0.0215	0.0929	0.0819
4	3	4	0.0356	0.0636	0.0018	0.0196	0.0353	0.0642
5	3	18	0.0932	0.0820	0.0018	0.0215	0.0929	0.0819
6	4	5	0.0932	0.0820	0.0018	0.0215	0.0929	0.0819
7	4	23	0.0746	0.0656	0.0014	0.0172	0.0743	0.0655
8	6	7	0.0932	0.0820	0.0018	0.0215	0.0929	0.0819
9	6	8	0.1864	0.1639	0.0035	0.0431	0.1858	0.1638
10	7	9	0.0932	0.0820	0.0018	0.0215	0.0929	0.0819
11	7	14	0.0932	0.0820	0.0018	0.0215	0.0929	0.0819
12	7	16	0.0932	0.0820	0.0018	0.0215	0.0929	0.0819
13	9	10	0.0932	0.0820	0.0018	0.0215	0.0929	0.0819
14	10	11	0.0559	0.0492	0.0011	0.0129	0.0557	0.0491
15	11	12	0.0731	0.0538	0.0006	0.0045	0.0732	0.0539
16	11	13	0.0731	0.0538	0.0006	0.0045	0.0732	0.0539
17	14	15	0.0559	0.0492	0.0011	0.0129	0.0557	0.0491
18	14	17	0.1097	0.0808	0.0009	0.0067	0.1099	0.0809
19	18	20	0.0932	0.0820	0.0018	0.0215	0.0929	0.0819
20	18	21	0.1463	0.1077	0.0012	0.0090	0.1465	0.1078
21	20	19	0.1463	0.1077	0.0012	0.0090	0.1465	0.1078
22	21	22	0.1463	0.1077	0.0012	0.0090	0.1465	0.1078
23	23	24	0.0746	0.0656	0.0014	0.0172	0.0743	0.0655
24	24	25	0.1463	0.1077	0.0012	0.0090	0.1465	0.1078

Table A.9: Bus data of the 25 bus test system

Branch #	P_a ***KW***	Q_a ***KVar***	P_b ***KW***	Q_b ***KVar***	P_c ***KW***	Q_c ***KVar***	***Length feet***
1	0	0	0	0	0	0	1000
2	35	25	40	30	45	32	500
3	50	40	60	45	50	35	500
4	40	30	40	30	40	30	500
5	40	30	45	32	35	25	500
6	0	0	0	0	0	0	500
7	40	30	40	30	40	30	400
8	60	45	50	40	50	35	500
9	35	25	40	30	45	32	1000
10	45	32	35	25	40	30	500
11	50	35	60	45	50	40	500
12	35	25	45	32	40	30	500
13	50	35	50	40	60	45	500
14	133.3	100	133.3	100	133.3	100	300
15	40	30	40	30	40	30	200
16	40	30	35	25	45	32	200
17	40	30	40	30	40	30	300
18	60	45	50	35	50	40	300
19	35	25	40	30	45	32	500
20	40	30	35	25	45	32	400
21	50	35	60	45	50	40	400
22	60	45	50	40	50	35	400
23	35	25	45	32	40	30	400
24	60	45	50	30	50	35	400

Table A.10: the DGs types, parameters and ratings (25-bus system)

Type	***Mode***	***Kp (p.u.)***	***Kq (p.u.)***	S_{Gmax} ***(MVA)***	***FOR***
Dispatchable	Droop	0.0135	0.025	2	0.0975
Wind	PQ - 0.9 PF Lead	-	-	0.25	0.04

Table A.11: Types, locations, parameters and ratings of DG units

Type	***Locations***	***Mode***	***Kp (p.u.)***	***Kq (p.u.)***	S_{Gmax} ***(MVA)***
Dispatchable	3,27,29,46,48,61	Droop: (PDR)	0.005	0.05	1.5
Wind	19,52,65	PQ: (NPDR)	-	-	1.5

Table A.12: Data of the 16-bus test system, V_{base}=13.8 KV & S_{base}=10 MVA

Branch #	***Sending***	***Receiving***	***R (pu %)***	***X (pu %)***	***PL (MW) Receiving***	***QL (Mvar) Receiving***	***Length km***
1	1	2	0.151	0.296	0	0	3.05
2	2	3	0667	5.33	0	0	-
3	3	4	3.976	5.127	0	0	2.06
4	3	5	3.564	2.661			0.976
5	3	6	3.0325	5.075			2.415
6	4	8	0.104	0.135			0.148
7	4	9	0.732	0.095			0.104
8	8	12	8.21	57.5	0.8	0.47	-
9	9	13	3.29	2.3	1.5	1.0	-
10	5	14	2.44	14.8	3.2	1.9	-
11	6	7	3.0325	5.075			-
12	7	10	2.56	0.332			0.362
13	7	11	0.423	0.154			0.189
14	10	15	5.6	48	0.9	0.6	-
15	11	16	6.48	38.3	0.9	0	-

Table A.13: Distributed generators data

DG #	**Location**	**Type**	**S_{Gmax} (MVA)**	**PF_{max} (Lag)**	**PF_{min} (Lead)**
1	16	Synchronous SG	1.5	0.9	0.95
2	7	Wind-DFIG	8.75	0.9	0.95
3	6	Micro-turbine MT	1.37	0.9	0.9
4	14	Solar-PV	3	0.9	0.95

Table A.14: Data of load and generation

Feeder number	*Generation profile*			*Load profile*	
	Locations	Types	Ratings (MVA)	Type	Total peak (MVA)
1	4,8	Wind	2,0.5	Com.	4
2	2,5,8	PV	5,2,1	Res.	5
3	3,6	Wind	0.5,2.5	Ind.	3
4	5,8	PV, wind	0.5,0.5	Res.	4.5

Appendix B

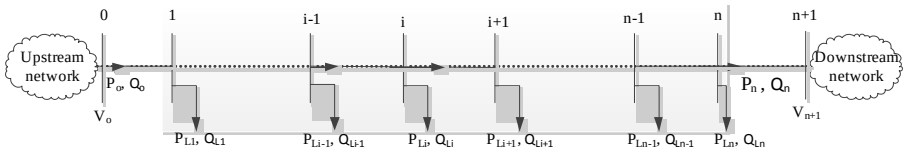

Figure B.1: A radial distribution feeder in ADNs

Figure B.1: A radial distribution feeder in ADNsshows a typical structure of radial distribution feeder in ADNs. Generally, a set of recursive equations can be used to model the power flow in the segment between the upstream and downstream networks of the radial feeder shown in the figure. The branch active and reactive powers at branch *i* and the voltage at node *i* are given as follows [138]:

$$P_i = P_{i-1} - r_{i-1}\frac{P_{i-1}^{\ 2} + Q_{i-1}^{\ 2}}{V_{i-1}^{\ 2}} - P_{Li} \tag{B.1}$$

$$Q_i = Q_{i-1} - x_{i-1}\frac{P_{i-1}^{\ 2} + Q_{i-1}^{\ 2}}{V_{i-1}^{\ 2}} - Q_{Li} \tag{B.2}$$

$$V_i^2 = V_{i-1}^{\ 2} - 2\left(r_{i-1}P_{i-1} + x_{i-1}Q_{i-1}\right) + (r_{i-1}^2 + Q_{i-1}^2)\frac{P_{i-1}^{\ 2} + Q_{i-1}^{\ 2}}{V_{i-1}^{\ 2}} \tag{B.3}$$

where, P_{Li} and Q_{Li} are the load active and reactive power at node i ; r_{i-1} and x_{i-1} are the impedance parameters at branch *i-1*. Also, it is noticed that the quadratic terms in the equations is much smaller than the branch power [138]. Thus (B.1)-(B.3) can be simplified by dropping the second order terms as follow:

$$P_i = P_{i-1} - P_{Li} \tag{B.4}$$

$$Q_i = Q_{i-1} - Q_{Li} \tag{B.5}$$

$$V_i^2 = V_{i-1}^{\ 2} - 2\left(r_{i-1}P_{i-1} + x_{i-1}Q_{i-1}\right) \tag{B.6}$$

Therefore the branch active and reactive powers at branch *i* and the voltage magnitude at node *i* can be given as follows:

$$P_i = P_n + \sum_{k=i+1}^{n} P_{Lk} \tag{B.7}$$

$$Q_i = Q_n + \sum_{k=i+1}^{n} Q_{Lk} \tag{B.8}$$

$$V_i^2 = V_o^2 - 2\sum_{k=0}^{i-1}\left(r_k P_k + x_k Q_k\right) \tag{B.9}$$

where P_n and Q_n are the active and reactive power of the branch downstream the segment respectively. Equations (B.7)-(B.9) show that the change of the power flow direction and consequently the change of the voltage profile along the segment depend on the change of the load distribution along the segment, the active and reactive power flow of the branch downstream the segment (P_n , Q_n) and the voltage magnitude at the upstream node of the segment (V_o).

Consider the change in the voltage profile as a result of the change of power flow at the downstream network i.e. $\Delta P_n, \Delta Q_n$ at node *n* of the segment. A good estimate can be obtained by using (B.7)-(B.9). From (B.7), the changes in branch power at a branch *i* within the segment will be:

$$\Delta P_i = P_i^{new} - P_i^{old} = \Delta P_n \quad , \; \Delta Q_i = Q_i^{new} - Q_i^{old} = \Delta Q_n \tag{B.10}$$

Thus the change in voltage magnitude at node *i* of the segment can be obtained using:

$$\Delta V_i^2 = V_i^{2}{}_{new} - V_i^{2}{}_{old} = \Delta V_o^2 - 2\left(\Delta P_n \sum_{k=0}^{i-1} r_k + \Delta Q_n \sum_{k=0}^{i-1} x_k\right) \tag{B.11}$$

Bibliography

[1] K. Moslehi and R. Kumar, "A reliability perspective of the smart grid," *IEEE Trans. Smart Grid,* vol. 1, pp. 57-64, 2010.

[2] J. A. Momoh, "Smart grid design for efficient and flexible power networks operation and control," in *Power Systems Conference and Exposition, 2009. PSCE'09. IEEE/PES,* 2009, pp. 1-8.

[3] A. Ipakchi and F. Albuyeh, "Grid of the future," *IEEE Power and Energy Magazine,* vol. 7, pp. 52-62, 2009.

[4] L. F. Ochoa, C. J. Dent and G. P. Harrison, "Distribution network capacity assessment: Variable DG and active networks," *IEEE Trans. Power Syst.,* vol. 25, pp. 87-95, 2010.

[5] G. Venkataramanan and C. Marnay, "A larger role for microgrids," *IEEE Power and Energy Magazine,* vol. 6, pp. 78-82, 2008.

[6] C. Marnay, G. Venkataramanan, M. Stadler, A. S. Siddiqui, R. Firestone and B. Chandran, "Optimal technology selection and operation of commercial-building microgrids," *IEEE Trans. Power Syst.,* vol. 23, pp. 975-982, 2008.

[7] H. Jiayi, J. Chuanwen and X. Rong, "A review on distributed energy resources and MicroGrid," *Renewable and Sustainable Energy Reviews,* vol. 12, pp. 2472-2483, 2008.

[8] P. Chiradeja and R. Ramakumar, "An approach to quantify the technical benefits of distributed generation," *IEEE Trans. Energ. Conv.,* vol. 19, pp. 764-773, 2004.

[9] C. L. T. Borges and D. M. Falcao, "Optimal distributed generation allocation for reliability, losses, and voltage improvement," *International Journal of Electrical Power & Energy Systems,* vol. 28, pp. 413-420, 2006.

[10] J. J. Paserba, D. J. Leonard, N. W. Miller, S. T. Naumann, M. G. Lauby and F. P. Sener, "Coordination of a distribution level continuously controlled compensation device with existing substation equipment for long term VAr management," *IEEE Trans. Power Del.,* vol. 9, pp. 1034-1040, 1994.

[11] American national standard for electric power systems and equipment-voltage ratings (60 hertz), ANSI Standard C84.1, Dec. 2006.

[12] F. C. Lu and Y. Y. Hsu, "Reactive power/voltage control in a distribution substation using dynamic programming," in *Generation, Transmission and Distribution, IEE Proceedings-,* 1995, pp. 639-645.

[13] F. A. Viawan and D. Karlsson, "Combined local and remote voltage and reactive power control in the presence of induction machine distributed generation," *IEEE Trans. Power Syst.,* vol. 22, pp. 2003-2012, 2007.

[14] W. H. Kersting, *Distribution System Modeling and Analysis.* CRC press, 2002.

[15] P. Brady, C. Dai and Y. Baghzouz, "Need to revise switched capacitor controls on feeders with distributed generation," in *Transmission and Distribution Conference and Exposition, 2003 IEEE PES*, 2003, pp. 590-594.

[16] Y. Y. Hsu and C. C. Yang, "A hybrid artificial neural network-dynamic programming approach for feeder capacitor scheduling," *IEEE Trans. Power Syst.,* vol. 9, pp. 1069-1075, 1994.

[17] Y. Y. Hsu and H. C. Kuo, "Dispatch of capacitors on distribution system using dynamic programming," in *Generation, Transmission and Distribution, IEE Proceedings C,* 1993, pp. 433-438.

[18] F. C. Lu and Y. Y. Hsu, "Fuzzy dynamic programming approach to reactive power/voltage control in a distribution substation," *IEEE Trans. Power Syst.,* vol. 12, pp. 681-688, 1997.

[19] Y. Y. Hsu and F. C. Lu, "A combined artificial neural network-fuzzy dynamic programming approach to reactive power/voltage control in a distribution substation," *IEEE Trans. Power Syst.,* vol. 13, pp. 1265-1271, 1998.

[20] M. Liu, C. A. Cañizares and W. Huang, "Reactive power and voltage control in distribution systems with limited switching operations," *IEEE Trans. Power Syst.,* vol. 24, pp. 889-899, 2009.

[21] Y. Liu, P. Zhang and X. Qiu, "Optimal volt/var control in distribution systems," *International Journal of Electrical Power & Energy Systems,* vol. 24, pp. 271-276, 2002.

[22] IEEE Guide for Design, Operation, and Integration of Distributed Resource Island Systems with Electric Power Systems, IEEE standard 1547.4, July 2011.

[23] C. Masters, "Voltage rise: the big issue when connecting embedded generation to long 11 kV overhead lines," *Power Eng J,* vol. 16, pp. 5-12, 2002.

[24] S. Repo, H. Laaksonen, P. Jarventausta, O. Huhtala and M. Mickelsson, "A case study of a voltage rise problem due to a large amount of distributed generation on a weak distribution network," in *Power Tech Conference Proceedings, 2003 IEEE Bologna,* 2003, pp. 6 pp. Vol. 4.

[25] H. E. Farag and E. El-Saadany, "Voltage regulation in distribution feeders with high DG penetration: From traditional to smart," in *Power and Energy Society General Meeting, 2011 IEEE,* 2011, pp. 1-8.

[26] L. Kojovic, "Impact of DG and voltage regulator interaction on distribution system voltage regulation," *CIRED, Barcellona,* 2003.

[27] P. P. Barker and R. De Mello, "Determining the impact of distributed generation on power systems. I. radial distribution systems," in *Power Engineering Society Summer Meeting, 2000. IEEE,* 2000, pp. 1645-1656.

[28] R. Walling, R. Saint, R. C. Dugan, J. Burke and L. A. Kojovic, "Summary of distributed resources impact on power delivery systems," *IEEE Trans. Power Del.,* vol. 23, pp. 1636-1644, 2008.

[29] N. Pogaku, M. Prodanovic and T. C. Green, "Modeling, analysis and testing of autonomous operation of an inverter-based microgrid," *IEEE Trans. Power Electron.,* vol. 22, pp. 613-625, 2007.

[30] Y. Mohamed and E. F. El-Saadany, "Adaptive decentralized droop controller to preserve power sharing stability of paralleled inverters in distributed generation microgrids," *IEEE Trans. Power Electron.,* vol. 23, pp. 2806-2816, 2008.

[31] F. Katiraei and M. Iravani, "Power management strategies for a microgrid with multiple distributed generation units," *IEEE Trans. Power Syst.,* vol. 21, pp. 1821-1831, 2006.

[32] C. K. Sao and P. W. Lehn, "Autonomous load sharing of voltage source converters," *IEEE Trans. Power Del.,* vol. 20, pp. 1009-1016, 2005.

[33] P. M. Costa and M. A. Matos, "Assessing the contribution of microgrids to the reliability of distribution networks," *Electr. Power Syst. Res.,* vol. 79, pp. 382-389, 2009.

[34] P. M. Costa, M. A. Matos and J. Peças Lopes, "Regulation of microgeneration and microgrids," *Energy Policy,* vol. 36, pp. 3893-3904, 2008.

[35] Y. Atwa, E. El-Saadany, M. Salama, R. Seethapathy, M. Assam and S. Conti, "Adequacy evaluation of distribution system including wind/solar DG during different modes of operation," *IEEE Trans. Power Syst.,* vol. 26, pp. 1945-1952, 2011.

[36] Y. M. Atwa and E. F. El-Saadany, "Reliability evaluation for distribution system with renewable distributed generation during islanded mode of operation," *IEEE Trans. Power Syst.,* vol. 24, pp. 572-581, 2009.

[37] P. Noferi and L. Paris, "Effects of voltage and reactive power constraints on power system reliability," *IEEE Trans. Power App. and Syst.,* vol. 94, pp. 482-490, 1975.

[38] W. Qin, P. Wang, X. Han and X. Du, "Reactive power aspects in reliability assessment of power systems," *IEEE Trans. Power Syst.,* vol. 26, pp. 85-92, 2011.

[39] W. Li, *Reliability Assessment of Electrical Power Systems using Monte Carlo Methods.* Springer, 1994.

[40] J. Grainger and S. Lee, "Capacity release by shunt capacitor placement on distribution feeders: a new voltage-dependent model," *IEEE Trans. Power App. and Syst.,* pp. 1236-1244, 1982.

[41] H. Ng, M. Salama and A. Chikhani, "Classification of capacitor allocation techniques," *IEEE Trans. Power Del.*, vol. 15, pp. 387-392, 2000.

[42] I. C. da Silva, S. Carneiro, E. J. de Oliveira, J. de Souza Costa, J. Rezende Pereira and P. A. N. Garcia, "A heuristic constructive algorithm for capacitor placement on distribution systems," *IEEE Trans. Power Syst.*, vol. 23, pp. 1619-1626, 2008.

[43] M. Ladjavardi and M. A. S. Masoum, "Genetically optimized fuzzy placement and sizing of capacitor banks in distorted distribution networks," *IEEE Trans. Power Del.*, vol. 23, pp. 449-456, 2008.

[44] M. Delfanti, G. P. Granelli, P. Marannino and M. Montagna, "Optimal capacitor placement using deterministic and genetic algorithms," *IEEE Trans. Power Syst.*, vol. 15, pp. 1041-1046, 2000.

[45] G. Levitin, A. Kalyuzhny, A. Shenkman and M. Chertkov, "Optimal capacitor allocation in distribution systems using a genetic algorithm and a fast energy loss computation technique," *IEEE Trans. Power Del.*, vol. 15, pp. 623-628, 2000.

[46] Y. C. Huang, H. T. Yang and C. L. Huang, "Solving the capacitor placement problem in a radial distribution system using tabu search approach," *IEEE Trans. Power Syst.*, vol. 11, pp. 1868-1873, 1996.

[47] A. Dukpa, B. Venkatesh and L. Chang, "Fuzzy Stochastic Programming Method: Capacitor Planning in Distribution Systems With Wind Generators," *IEEE Trans. Power Syst.*, vol. 26, pp. 1971-1979, 2011.

[48] P. Hrisheekesha and J. Sharma, "AI Applications to Distribution System with Distributed Generation," *International Journal of Computer Applications IJCA*, vol. 1, pp. 42-46, 2010.

[49] F. A. Viawan and D. Karlsson, "Voltage and reactive power control in systems with synchronous machine-based distributed generation," *IEEE Trans. Power Del.*, vol. 23, pp. 1079-1087, 2008.

[50] T. S. Basso and R. DeBlasio, "IEEE 1547 series of standards: interconnection issues," *IEEE Trans. Power Electron.*, vol. 19, pp. 1159-1162, 2004.

[51] P. M. S. Carvalho, P. F. Correia and L. Ferreira, "Distributed reactive power generation control for voltage rise mitigation in distribution networks," *IEEE Trans. Power Syst.*, vol. 23, pp. 766-772, 2008.

[52] R. Tonkoski, L. A. C. Lopes and T. H. M. El-Fouly, "Coordinated active power curtailment of grid connected PV inverters for overvoltage prevention," *IEEE Trans. Sustainable Energy*, vol. 2, pp. 139-147, 2011.

[53] A. Kiprakis and A. Wallace, "Maximising energy capture from distributed generators in weak networks," in *Generation, Transmission and Distribution, IEE Proceedings-*, 2004, pp. 611-618.

[54] M. Kashem and G. Ledwich, "Multiple distributed generators for distribution feeder voltage support," *IEEE Trans. Energ. Conv.*, vol. 20, pp. 676-684, 2005.

[55] S. Paudyal, C. A. Canizares and K. Bhattacharya, "Optimal operation of distribution feeders in smart grids," *IEEE Trans. Ind. Electron.*, vol. 58, pp. 4495-4503, 2011.

[56] J. H. Choi and J. C. Kim, "Advanced voltage regulation method of power distribution systems interconnected with dispersed storage and generation systems," *IEEE Trans. Power Del.*, vol. 16, pp. 329-334, 2001.

[57] A. Borghetti, M. Bosetti, S. Grillo, S. Massucco, C. A. Nucci, M. Paolone and F. Silvestro, "Short-term scheduling and control of active distribution systems with high penetration of renewable resources," *IEEE Systems Journal*, vol. 4, pp. 313-322, 2010.

[58] J. M. Vidal, "Fundamentals of multiagent systems," 2007.

[59] T. Nagata and H. Sasaki, "A multi-agent approach to power system restoration," *IEEE Trans. Power Syst.*, vol. 17, pp. 457-462, 2002.

[60] H. Wang, "Multi-agent co-ordination for the secondary voltage control in power-system contingencies," in *Generation, Transmission and Distribution, IEE Proceedings-*, 2001, pp. 61-66.

[61] L. Cristaldi, A. Monti, R. Ottoboni and F. Ponci, "Multiagent based power systems monitoring platform: A prototype," in *Power Tech Conference Proceedings, 2003 IEEE Bologna*, 2003, pp. 5 pp. Vol. 2.

[62] S. D. J. McArthur, E. M. Davidson, V. M. Catterson, A. L. Dimeas, N. D. Hatziargyriou, F. Ponci and T. Funabashi, "Multi-agent systems for power engineering applications—Part II: technologies, standards, and tools for building multi-agent systems," *IEEE Trans. Power Syst.*, vol. 22, pp. 1753-1759, 2007.

[63] P. H. Nguyen, W. L. Kling and J. M. A. Myrzik, "Promising concepts and technologies for future power delivery systems," in *Universities Power Engineering Conference, 2007. UPEC 2007. 42nd International*, 2007, pp. 47-52.

[64] P. Lund, "The danish cell project-part 1: Background and general approach," in *Power Engineering Society General Meeting, 2007. IEEE*, 2007, pp. 1-6.

[65] H. E. Farag, E. El-Saadany and L. El Chaar, "A multilayer control framework for distribution systems with high DG penetration," in *Innovations in Information Technology (IIT), 2011 International Conference On*, 2011, pp. 94-99.

[66] Z. Jiang, "Agent-based control framework for distributed energy resources microgrids," in *Intelligent Agent Technology, 2006. IAT'06. IEEE/WIC/ACM International Conference On*, 2006, pp. 646-652.

[67] T. Logenthiran, D. Srinivasan and D. Wong, "Multi-agent coordination for DER in MicroGrid," in *Sustainable Energy Technologies, 2008. ICSET 2008. IEEE International Conference On*, 2008, pp. 77-82.

[68] M. Pipattanasomporn, H. Feroze and S. Rahman, "Multi-agent systems in a distributed smart grid: Design and implementation," in *Power Systems Conference and Exposition, 2009. PSCE'09. IEEE/PES*, 2009, pp. 1-8.

[69] M. E. Baran and I. M. El-Markabi, "A multiagent-based dispatching scheme for distributed generators for voltage support on distribution feeders," *IEEE Trans. Power Syst.*, vol. 22, pp. 52-59, 2007.

[70] M. E. Elkhatib, R. El-Shatshat and M. M. A. Salama, "Novel coordinated voltage control for smart distribution networks with DG," *IEEE Trans. Smart Grid*, vol. 2, pp. 598-605, 2011.

[71] J. H. Teng, "A direct approach for distribution system load flow solutions," *IEEE Trans. Power Del.*, vol. 18, pp. 882-887, 2003.

[72] A. Zidan, H. Farag and E. El-saadany, "Network reconfiguration for balanced and unbalanced distribution systems with high DG penetration," in *Power and Energy Society General Meeting, 2011 IEEE*, 2011, pp. 1-8.

[73] Y. Zhu and K. Tomsovic, "Adaptive power flow method for distribution systems with dispersed generation," *IEEE Trans. Power Del.*, vol. 17, pp. 822-827, 2002.

[74] W. Wu and B. Zhang, "A three-phase power flow algorithm for distribution system power flow based on loop-analysis method," *International Journal of Electrical Power & Energy Systems*, vol. 30, pp. 8-15, 2008.

[75] A. Garcia and M. Zago, "Three-phase fast decoupled power flow for distribution networks," in *Generation, Transmission and Distribution, IEE Proceedings-*, 1996, pp. 188-192.

[76] P. A. N. Garcia, J. L. R. Pereira, S. Carneiro Jr, V. M. da Costa and N. Martins, "Three-phase power flow calculations using the current injection method," *IEEE Trans. Power Syst.*, vol. 15, pp. 508-514, 2000.

[77] J. H. Teng and C. Y. Chang, "A novel and fast three-phase load flow for unbalanced radial distribution systems," *IEEE Trans. Power Syst.*, vol. 17, pp. 1238-1244, 2002.

[78] A. Bhutad, S. Kulkarni and S. Khaparde, "Three-phase load flow methods for radial distribution networks," in *TENCON 2003. Conference on Convergent Technologies for Asia-Pacific Region*, 2003, pp. 781-785.

[79] T. H. Chen, M. S. Chen, K. J. Hwang, P. Kotas and E. A. Chebli, "Distribution system power flow analysis-a rigid approach," *IEEE Trans. Power Del.*, vol. 6, pp. 1146-1152, 1991.

[80] D. Thukaram, H. Wijekoon Banda and J. Jerome, "A robust three phase power flow algorithm for radial distribution systems," *Electr. Power Syst. Res.*, vol. 50, pp. 227-236, 1999.

[81] J. H. Teng, "A modified Gauss–Seidel algorithm of three-phase power flow analysis in distribution networks," *International Journal of Electrical Power & Energy Systems,* vol. 24, pp. 97-102, 2002.

[82] S. Moghaddas-Tafreshi and E. Mashhour, "Distributed generation modeling for power flow studies and a three-phase unbalanced power flow solution for radial distribution systems considering distributed generation," *Electr. Power Syst. Res.,* vol. 79, pp. 680-686, 2009.

[83] M. Ding, X. Guo and Z. Zhang, "Three phase power flow for weakly meshed distribution network with distributed generation," in *Power and Energy Engineering Conference, 2009. APPEEC 2009. Asia-Pacific*, 2009, pp. 1-7.

[84] S. Naka, T. Genji and Y. Fukuyama, "Practical equipment models for fast distribution power flow considering interconnection of distributed generators," in *Power Engineering Society Summer Meeting, 2001,* 2001, pp. 1007-1012.

[85] T. Oomori, T. Genji, T. Yura, T. Watanabe, S. Takayama and Y. Fukuyama, "Development of equipment models for fast distribution three-phase unbalanced load flow calculation," *Electrical Engineering in Japan,* vol. 142, pp. 8-19, 2003.

[86] J. H. Teng, "Modelling distributed generations in three-phase distribution load flow," *Generation, Transmission & Distribution, IET,* vol. 2, pp. 330-340, 2008.

[87] S. Khushalani, J. M. Solanki and N. N. Schulz, "Development of three-phase unbalanced power flow using PV and PQ models for distributed generation and study of the impact of DG models," *IEEE Trans. Power Syst.,* vol. 22, pp. 1019-1025, 2007.

[88] W. Kersting, "Radial distribution test feeders," in *Power Engineering Society Winter Meeting, 2001. IEEE,* 2001, pp. 908-912.

[89] H. E. Farag, E. El-Saadany, R. El Shatshat and A. Zidan, "A generalized power flow analysis for distribution systems with high penetration of distributed generation," *Electr. Power Syst. Res.,* vol. 81, pp. 1499-1506, 2011.

[90] H. Zeineldin and J. Kirtley, "Islanding operation of inverter based distributed generation with static load models," in *Power and Energy Society General Meeting-Conversion and Delivery of Electrical Energy in the 21st Century, 2008 IEEE,* 2008, pp. 1-6.

[91] H. E. Farag, E. F. El-Saadany and R. Seethapathy, "The Evolution for Voltage and Reactive Power Control in Smart Distribution Systems," *International Journal of Emerging Electric Power Systems,* vol. 13, 2012.

[92] S. Segura, L. Da Silva and R. Romero, "Generalised single-equation load flow method for unbalanced distribution systems," *Generation, Transmission & Distribution, IET,* vol. 5, pp. 347-355, 2011.

[93] R. M. S. Danaraj, S. F. Kodad and T. R. Das, "An algorithm for radial distribution power flow in Complex mode including voltage controlled buses," *Indian Journal of Science and Technology,* vol. 1, pp. 1-5, 2007.

[94] IEEE PES Distribution System Analysis Subcommittee, "IEEE PES distribution test feeders," 22 May 2012, 2012. Available: http://ewh.ieee.org/soc/pes/dsacom/testfeeders/index.html

[95] http://www.polarisamerica.com/turbines/small-models/50kw.html.

[96] H. E. Farag, M. M. A. Abdelaziz and E. F. El-Saadany, "Voltage and reactive power impacts on successful operation of islanded microgrids," *IEEE Trans. Power Syst.,* to be published.

[97] M. M. A. Abdelaziz, H. E. Farag, E. F. El-Saadany and Y. A. R. I. Mohamed, "A Novel and Generalized Three-Phase Power Flow Algorithm for Islanded Microgrids Using a Newton Trust Region Method," *IEEE Trans. Power Syst.,* to be published .

[98] F. Blaabjerg, R. Teodorescu, M. Liserre and A. V. Timbus, "Overview of control and grid synchronization for distributed power generation systems," *IEEE Trans. Ind. Electron.,* vol. 53, pp. 1398-1409, 2006.

[99] M. Hassan and M. Abido, "Optimal design of microgrids in autonomous and grid-connected modes using particle swarm optimization," *IEEE Trans. Power Electron.,* vol. 26, pp. 755-769, 2011.

[100] G. Díaz, C. González-Morán, J. Gómez-Aleixandre and A. Diez, "Composite loads in stand-alone inverter-based microgrids—Modeling procedure and effects on load margin," *IEEE Trans. Power Syst.,* vol. 25, pp. 894-905, 2010.

[101] M. I. Marei, E. F. El-Saadany and M. M. A. Salama, "A novel control algorithm for the DG interface to mitigate power quality problems," *IEEE Trans. Power Del.,* vol. 19, pp. 1384-1392, 2004.

[102] D. Issicaba, J. A. P. Lopes and M. A. da Rosa, "Adequacy and Security Evaluation of Distribution Systems With Distributed Generation," *IEEE Trans. Power Syst.,* vol. 27, pp. 1681-1689, 2012.

[103] A. R. Conn, N. I. M. Gould and P. L. Toint, *Trust Region Methods.* Society for Industrial Mathematics, 1987.

[104] C. A. Hernandez-Aramburo, T. C. Green and N. Mugniot, "Fuel consumption minimization of a microgrid," *IEEE Trans. Ind. Appl.,* vol. 41, pp. 673-681, 2005.

[105] J. Savier and D. Das, "Impact of network reconfiguration on loss allocation of radial distribution systems," *IEEE Trans. Power Del.,* vol. 22, pp. 2473-2480, 2007.

[106] H. Hamedi and M. Gandomkar, "Evaluation of reliability, losses and power quality considering time variations of load in presence of distributed generation sources," *International Journal of Academic Research,* vol. 3, 2011.

[107] D. L. Duan, X. Y. Wu and H. Z. Deng, "Reliability Evaluation in Substations Considering Operating Conditions and Failure Modes," *IEEE Trans. Power Del.*, vol. 27, pp. 309-316, 2012.

[108] J. Pinheiro, C. Dornellas, M. T. Schilling, A. Melo and J. Mello, "Probing the new IEEE reliability test system (RTS-96): HL-II assessment," *IEEE Trans. Power Syst.*, vol. 13, pp. 171-176, 1998.

[109] C. Singh and Y. Kim, "An efficient technique for reliability analysis of power systems including time dependent sources," *IEEE Trans. Power Syst.*, vol. 3, pp. 1090-1096, 1988.

[110] A. Micallef, M. Apap, C. Spiteri-Staines and J. Guerrero, "Secondary control for reactive power sharing in droop-controlled islanded microgrids," in *Industrial Electronics (ISIE), 2012 IEEE International Symposium On*, 2012, pp. 1627-1633.

[111] G. K. V. Raju and P. Bijwe, "Efficient reconfiguration of balanced and unbalanced distribution systems for loss minimisation," *Generation, Transmission & Distribution, IET*, vol. 2, pp. 7-12, 2008.

[112] A. A. Chowdhury, T. Mielnik, L. Lawton, M. Sullivan, A. Katz and D. O. Koval, "System reliability worth assessment using the customer survey approach," *IEEE Trans. Ind. Appl.*, vol. 45, pp. 317-322, 2009.

[113] H. Farag, E. F. El-Saadany and R. Seethapathy, "A two ways communication-based distributed control for voltage regulation in smart distribution feeders," *IEEE Trans. Smart Grid*, vol. 3, pp. 271-281, 2012.

[114] M. Wooldridge, *Reasoning about Rational Agents*. MIT press, 2000.

[115] W. Shen, D. H. Norrie and J. P. Barthès, *Multi-Agent Systems for Concurrent Intelligent Design and Manufacturing*. CRC, 2000.

[116] T. Finin, D. McKay and R. Fritzson, *An Overview of KQML: A Knowledge Query and Manipulation Language*, 1992.

[117] F. L. Bellifemine, G. Caire and D. Greenwood, "Developing multi-agent systems with jade (wiley series in agent technology)," 2007.

[118] F. Bellifemine, A. Poggi and G. Rimassa, "JADE–A FIPA-compliant agent framework," in *Proceedings of PAAM*, 1999, pp. 33.

[119] S. Galli, A. Scaglione and Z. Wang, "For the grid and through the grid: The role of power line communications in the smart grid," *Proc IEEE*, vol. 99, pp. 998-1027, 2011.

[120] T. V. Ramabadran and S. S. Gaitonde, "A tutorial on CRC computations," *Micro, IEEE*, vol. 8, pp. 62-75, 1988.

[121] R. Johannesson and K. S. Zigangirov, *Fundamentals of Convolutional Coding*. Wiley-IEEE press, 1999.

[122] G. Bumiller and L. Lampe, "Fast burst synchronization for power line communication systems," *EURASIP Journal on Advances in Signal Processing,* vol. 2007, 2007.

[123] G. Bumiller, L. Lampe and H. Hrasnica, "Power line communication networks for large-scale control and automation systems," *IEEE Communications Magazine,* vol. 48, pp. 106-113, 2010.

[124] B. Bassan and M. Scarsini, "On the value of information in multi-agent decision theory," *J. Math. Econ.,* vol. 24, pp. 557-576, 1995.

[125] A. Sajadi, H. Farag, P. Biczel and E. El-Saadany, "Voltage regulation based on fuzzy multi-agent control scheme in smart grids," in *Energytech, 2012 IEEE,* 2012, pp. 1-5.

[126] P. Nguyen, J. Myrzik and W. Kling, "Coordination of voltage regulation in active networks," in *Transmission and Distribution Conference and Exposition, 2008. T&# x00026; D. IEEE/PES,* 2008, pp. 1-6.

[127] F. Bellifemine, A. Poggi and G. Rimassa, "Developing multi-agent systems with JADE," *Intelligent Agents VII Agent Theories Architectures and Languages,* pp. 42-47, 2001.

[128] D. E. Comer, "Internetworking with TCP IP, volume 3 client/server programming and applications (BSD socket version)," *Recherche,* vol. 67, pp. 02, 1996.

[129] F. Katiraei, M. R. Iravani and P. Lehn, "Micro-grid autonomous operation during and subsequent to islanding process," *IEEE Trans. Power Del.,* vol. 20, pp. 248-257, 2005.

[130] J. H. Choi and J. C. Kim, "The online voltage control of ULTC transformer for distribution voltage regulation," *International Journal of Electrical Power & Energy Systems,* vol. 23, pp. 91-98, 2001.

[131] M. E. Baran and A. W. Kelley, "State estimation for real-time monitoring of distribution systems," *IEEE Trans. Power Syst.,* vol. 9, pp. 1601-1609, 1994.

[132] K. Li, "State estimation for power distribution system and measurement impacts," *IEEE Trans. Power Syst.,* vol. 11, pp. 911-916, 1996.

[133] H. Farag and E. F. El-Saadany, "A novel cooperative protocol for distributed voltage control in active distribution systems," *IEEE Trans. Power Syst.,* to be published.

[134] A. K. Ghosh, D. L. Lubkeman and R. H. Jones, "Load modeling for distribution circuit state estimation," in *Transmission and Distribution Conference, 1996. Proceedings., 1996 IEEE,* 1996, pp. 13-19.

[135] Y. Deng, Y. He and B. Zhang, "A branch-estimation-based state estimation method for radial distribution systems," *IEEE Trans. Power Del.,* vol. 17, pp. 1057-1062, 2002.

[136] J. H. Choi and S. I. Moon, "The Dead Band Control of LTC Transformer at Distribution Substation," *IEEE Trans. Power Syst.,* vol. 24, pp. 319-326, 2009.

[137] M. E. Elkhatib, R. El Shatshat and M. M. A. Salama, "Optimal Control of Voltage Regulators for Multiple Feeders," *IEEE Trans. Power Del.*, vol. 25, pp. 2670-2675, 2010.

[138] M. E. Baran and F. F. Wu, "Network reconfiguration in distribution systems for loss reduction and load balancing," *IEEE Trans. Power Del.*, vol. 4, pp. 1401-1407, 1989.